The importance of domain-domain interactions in the regulation and activity of neuronal nitric oxide synthase

Andrew David Welland

Doctor of Philosophy

University of Edinburgh

2008

Declaration

I declare that the work presented in this thesis is the original work of the author, except where specific reference is made to other sources. It has not been submitted in part, or in whole, for any other degree.

Andrew David Welland
June 2008

Acknowledgements

I would firstly like to thank my family, in particular my parents, without the support of whom I wouldn't even have started this project, let alone finished it. On the scientific side of things, the experimental and technical expertise of the following people has been invaluable; Drs. Pierre-Emmanuel Garnaud, Caroline Miles, Jon Clark, Ross Anderson, Chris Mowat, and soon-to-be-Drs. Sally Atkinson and Davide Papale. Some of the research was carried out with Emma Bruce as a BSc.(Hons) project and my thanks go to her and also to everyone from the past and present in lab N2.6 for making the experience of day-to-day life an enjoyable one; this extends to the Yellowlees group who introduced me to the wonderful Miss Sarah Dodds.

Secondly I would like to mention all those in the department who have kept me (reasonably) sane over the past three and a half years; especially Ross and Dot for making my fits of rage feel relatively normal. Euan, Pekka, Gordon, Augo, Keri, and wee Ross were always available for a chat about the beautiful game and were my fellow members of the Vikings - undefeated 2007 ChemSoc football league champions. Thanks also to the original version; Michele, Emiliano, Alex, Mike, Sidong, and the current members of the rebranded Vikings; Luccy, Phil, Kev and everyone else who was persuaded to play in the dank and freezing cold on a Monday night at two hours notice. One more group worthy of a mention is the crazy runners who did the KB Dash every month come rain, hail or shine.

Last but not least, of course, my supervisors Dr. Simon Daff and Prof. Steve Chapman. Thanks very much for a wonderful opportunity, about 2000 cups of tea and coffee, and guidance and direction when I needed it. All the very best for the future.

Cheers!

Abstract

Nitric oxide synthases (NOSs) catalyse the production of the physiological messenger molecule NO from L-arginine in a unique two step oxygenation reaction. Constitutive forms of NOS are activated by the binding of calmodulin (CaM) to a 20-amino-acid inter-domain region in the presence of calcium ions, causing inter-domain electron transfer to occur from FAD to heme via FMN. This electron transfer step involves a large scale movement of the FMN-binding domain and is influenced by a number of structural features unique to NOS which include an autoinhibitory loop, a C-terminal extension, a number of phosphorylation sites, and the hinge region that connects the FAD- and FMN- binding domains. X-ray crystallographic data indicate that all of these regulatory elements lie at the interface between the two domains, restricting their motion relative to each other. The importance of this interface region in the CaM-dependent activation mechanism of neuronal NOS (nNOS) was investigated by site-directed mutagenesis of interface residues in the isolated reductase domain (nNOSrd). A range of kinetic and thermodynamic analytical techniques were employed in order to determine which catalytic steps are affected by changes in domain mobility.

The rate-limiting step in the turnover of nNOSrd has been speculated to be one of three catalytic events; the hydride transfer from NADPH to FAD, the electron transfer between the bound flavin cofactors, or the electron transfer between FMN and external electron acceptors such as cytochrome *c*. In each case, the binding of CaM enhances the rate of reduction. In wild-type nNOSrd, NADPH reduced the FAD by hydride transfer in what should have been a simple 1-step reaction but was in fact a biphasic process. Isotope effects and the use of differing ionic strength indicated that different conformations of enzyme have different rates of reaction with NADPH. The redox state of the FMN cofactor also influenced the rate of reduction of FAD, through the interaction with the peptide backbone in the interface region.

A putative proton transfer pathway exists between the bound FAD cofactor and solvent, involving Ser1176, Asp1393, His1032 and Arg1229. Mutation of the former three residues diminished the catalytic activity, specifically focused on the rate of hydride transfer, while the R1229E mutation had a much more dramatic effect. Arg1229 forms one of only two electrostatic contacts between the FAD and FMN-

binding domains in the interface region and the charge reversal substitution introduced a likely inter-domain repulsion. This was expected to cause the two domains to separate, favouring a hinged-open conformation. The hydride transfer step from NADPH to FAD was activated in the CaM-free enzyme, while FAD to FMN electron transfer was inhibited. Electron transfer from reduced FMN to the artificial electron acceptor horse-heart cytochrome *c* was also activated in the CaM-free state. The effect on the three catalytic events meant that during steady-state turnover with cytochrome *c*, CaM deactivated the enzyme and caused cytochrome *c*-dependent inhibition. Evidently, domain-domain separation was large enough in the mutant to accommodate cytochrome *c*, a 12 kDa protein, in the space between the cofactors at the interface.

The effects of this single charge-reversal on the three distinct catalytic events illustrated how each is differently dependent on the enzyme conformation. FAD to FMN electron transfer was shown to occur exclusively in the hinged-closed form, consistent with the crystal structure of nNOSrd. The remaining two events, hydride transfer from NADPH to FAD, and electron transfer from FMN to cytochrome *c*, occur in the hinged-open state.

In the wild-type enzyme, the hinged-open and hinged-closed states are tightly regulated by a conformational equilibrium which is affected by CaM binding. It appears that CaM activates the enzyme by shifting this equilibrium to an open form.

Abbreviations

Amino Acids

Alanine	Ala	A	Leucine	Leu	L
Arginine	Arg	R	Lysine	Lys	K
Asparagine	Asn	N	Methionine	Met	M
Aspartatic acid	Asp	D	Phenylalanine	Phe	F
Cysteine	Cys	C	Proline	Pro	P
Gluatmic acid	Glu	E	Serine	Ser	S
Glutamine	Gln	Q	Threonine	Thr	T
Glycine	Gly	G	Tryptophan	Trp	W
Histidine	His	H	Tyrosine	Tyr	Y
Isoleucine	Ile	I	Valine	Val	V

Mutations

Amino acid mutations are represented as a code/number/code, where the first code and number represents the original residue and its position on the polypeptide chain, and the second code represents the corresponding residue in the mutant enzyme. For example, the mutation of an arginine, residue number 1229, to a glutamate is represented by Arg1229Glu, thus generating the mutant R1229E.

Kinetic parameters

K_m	Michaelis constant
K_d	Dissociation constant
K_i	Inhibition constant
k_{cat}	Rate constant at saturation
k_{obs}	Observed rate constant
$k_{1,2}$	Rate constants for the first or second phase of a multi-phase reaction
t	Time

Standard units

Å	angstrom
^{o}C	degrees Celsius
g	gram
h	hour
l	litre
m	metre
M	molar
S	second
V	volt

Textual abbreviations

A	Absorbance
ACAD	Acyl-CoA dehydrogenase
ADP	Adenosine diphosphate
AI	Autoinhibitory loop
ATP	Adenosine triphosphate
CaM	Calmodulin
cAMP	Cyclic adenosine monophosphate
cGMP	Cyclic guanosine monophosphate
cNOS	Constitutive NOS
CO	Carbon monoxide
CPR	Cytochrome P450 reductase
CT	C-terminal tail
Da	Dalton
DEAE	Diethylaminoethyl
DMSO	Dimethyl sulfoxide
DNA	Deoxyribonucleic acid
DTT	Dithiothreitol
ε	Molar extinction coefficient
EDRF	Endothelium-derived relaxation factor

EDTA	Ethylenediaminetetraacetic acid
EGTA	Ethyleneglycoltetraacetic acid
E_m	Midpoint reduction potential
ETF	Electron transfer flavoprotein
eNOS	Endothelial NOS
FAD	Flavin adenine dinucleotide
FMN	Flavin mononucleotide
FNR	Ferredoxin-$NADP^+$ reductase
FPLC	Fast protein liquid chromotography
G-cyclase	Guanylate cyclase
GTP	Guanosine triphosphate
Hb	Hemoglobin
H_4B	Tetrahydrobiopterin
I	Ionic strength
iNOS	Inducible NOS
IPTG	Isopropyl-β-D-thiogalactoside
L-arg	L-arginine
LB	Luria bertani
MAO	Monoamine oxidase
MB	Methylene blue
NADPH	Nicotinamide adenine dinucleotide phosphate
NAO	Nitroalkane oxidase
NMN	Nicotine mononucleotide
nNOS	neuronal NOS
NO	Nitric oxide
NOHA	N-hydroxy-L-Arginine
NOS	Nitric oxide synthase
NOSoxy	NOS oxygenase domain
NOSrd	NOS reductase domain
OTTLE	Optically transparent thin layer electrode
PAGE	Polyacrylamide gel electrophoresis
PDB	Protein data bank
PDZ	Postsynaptic density-95 discs large / ZO-1

PHBH	p-hydroxybenzoate hydroxylase
PMSF	Phenylmethylsulfonyl fluoride
SOC	Super optimal catabolite
SOD	Superoxide dismutase
SDS	Sodium dodecyl sulphate
SHE	Standard hydrogen electrode
SI	Small insertion
TB	Terrific broth
Tris	Tris (hydroxymethyl) aminomethane
UV	Ultraviolet
Vis	Visible
WT	Wild type

Table of contents

List of Figures

List of Tables

Chapter 1
Introduction

1.1 Nitric Oxide

"Nitric oxide as a signalling molecule in the cardiovascular system" was the title of the 1998 Nobel Prize in Physiology or Medicine awarded to Furchgott, Ignarro and Murad [1]. Their work, both before the award and subsequently, has led to a field of research resulting in over 200,000 published papers on nitric oxide (NO) and its effects.

Furchgott's work initially involved studying the drugs affecting blood vessels, where muscarinic agonists gave differing effects depending on the experimental preparation [2]. This was found to depend on whether the surface of the blood vessel (the endothelium) was intact, with acetylcholine shown to cause dilation only if it was. The production of an unknown relaxing substance was thought to cause this, and it was later referred to as endothelial-derived-relaxation-factor (EDRF). It was also observed that a rise in cyclic guanosine monophosphate (cGMP) accompanied the acetylcholine-induced relaxation.

Ignarro's early research concerned cGMP and the related molecule cAMP (cyclic adenosine monophosphate) which were known to mediate opposite effects on cellular function [3]. After the discovery that NO and nitro-compounds might cause NO-stimulated cGMP production in tissues [4], experiments were performed to confirm that nitroglycerin and related organic nitrate and nitrite esters could release NO in aqueous solution. These chemicals required an interaction with thiols to generate S-nitrosothiols that decompose to liberate NO. In addition to this, Ignarro reported that NO caused smooth muscle relaxation and activated guanylate-cyclase (G-cyclase), the enzyme that produces cGMP, isolated from the same tissue [5].

NO was identified as a potent inhibitor of platelet aggregation, mediated by cGMP, while the anti-platelet action of nitroprusside appeared to involve the action of S-nitrosothiols. NO activated G-cyclase from platelets by heme-dependent mechanisms, which was followed by G-cyclase being found to contain heme [6]. Studies then revealed that binding of NO to the heme breaks the bond with the axial histidine ligand and causes a conformational change near to the catalytic site that increases the affinity for substrate (GTP) and increases production of cGMP [7].

Murad worked on G-cyclase and cGMP in the early stages of research in this area, where experiments with azide, hydroxylamine and nitrite activated many, but not all,

preparations of G-cyclase [8]. The activation by azide required oxygen and was enhanced by the addition of thiols. Other smooth muscle relaxants such as nitroprusside and hydrazines increased cGMP levels and caused smooth-muscle relaxation that didn't require catalase for activation and was inhibited by hemoglobin (Hb) and myoglobin. This led to the suggestion that NO was the activator and this was proven by the direct action of the gas on G-cyclase [4]. L-arginine (L-arg) had been identified as activating G-cyclase, the action of which was blocked by Hb or methylhydroxylamine (that also blocked nitrovasodilators) [9]. This discovery would lead to the finding that NO is produced from L-arg. The cytotoxic effects of macrophages on tumour cells could be correlated with accumulation of nitrite and nitrate, were increased with the addition of L-arg and were blocked by an analogue of it [10].

Hemoglobin and methylene blue (MB) were identified as inhibitors of endothelium-dependent relaxation, with Hb inhibiting G-cyclase and relaxation of smooth muscle [11]. It was originally proposed that Hb binding to EDRF inhibited relaxation but when EDRF was identified as NO it was clear that HbO_2 reacts with NO to produce nitrate. MB was found to inhibit stimulation of G-cyclase by nitrovasodilators extremely quickly when added immediately after endothelium-dependent relaxation. This was eventually pinpointed as being caused by superoxide anions generated by MB in tissue [12]. Further evidence linking EDRF to NO was provided by superoxide dismutase (SOD) which stabilised EDRF released from endothelial cells or arteries [13].

The key piece of research from Furchgott's laboratory was the use of acidified, rather than neutral, sodium nitrite which produced transient relaxations of the aorta. NO gas gave the same results as this acidified nitrite and the similarity between these and acetylcholine-induced EDRF led to the proposal that they were the same thing [14]. Experiments by Ignarro and colleagues revealed that EDRF activated G-cyclase by mechanisms inhibited by MB and enhanced by antioxidants. The activation of G-cyclase by EDRF was then found to be heme-dependent and this linked it to NO [15].

Since those two independent discoveries, NO has been found to be involved in the central nervous system, the immune system, the gastrointestinal tract, the kidneys, the lungs along with the circulatory system and the heart [16]. It can function as a messenger due to its small size and free radical nature. However, in all of the locations in which it is found, the effects of NO can be both harmful as well as

protective; for example, in the immune system the anti-microbial and anti-tumour actions can lead to septic shock and tissue damage. In the blood vessels it is primarily anti-thrombotic and vasoprotective, but it can also lead to reperfusion injuries and inflammation. The central nervous system uses NO for memory formation and neuro-endocrine secretion but it can cause migraine and convulsions. In all cases the production of NO must be tightly regulated [17].

1.2 Nitric Oxide Synthases

The pathway to the production of NO from L-arginine was discovered in 1988 and it was the first example of biological hydroxylation of the L-arg guanidinium moiety [18]. The family of enzymes responsible for carrying out this reaction in mammals are the Nitric Oxide Synthases (NOSs), which perform the sequential oxidation of L-arg using nicotinamide adenine dinucleotide phosphate (NADPH) and molecular oxygen as substrates [19]. NOSs firstly catalyse the mono-oxygenation of L-arg to N-hydroxy-arginine (NOHA) and in a second oxidation step produce NO and L-citrulline from NOHA [20], as shown in Figure 1.1.

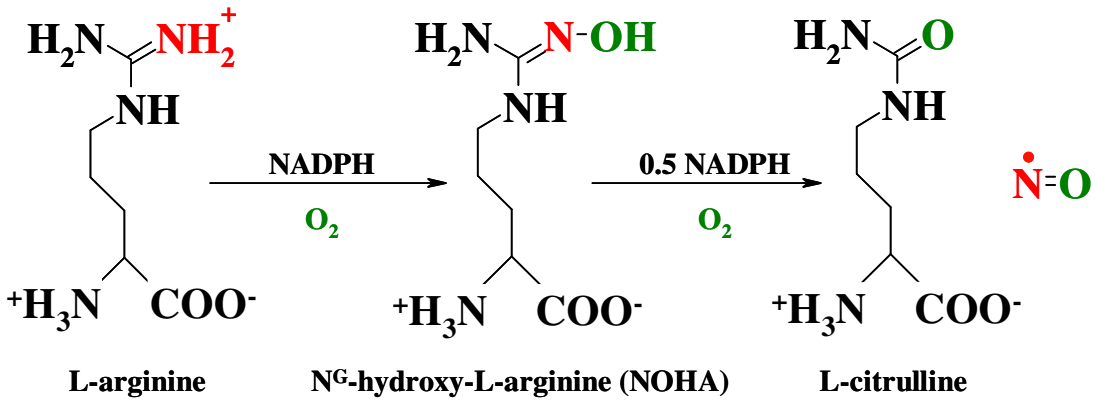

Figure 1.1 Production of nitric oxide from L-arginine via N-hydroxy-arginine

1.2.1 Function and locality

There are three isoforms of NOS found in mammalian systems, which carry out distinct functional roles. Neuronal NOS (nNOS) was originally discovered in rat neurons [21, 22], endothelial NOS (eNOS) was first identified from bovine endothelial cells [23], and inducible NOS (iNOS) is synthesised in a wide range of cells and tissues in response to inflammatory or pro-inflammatory mediators [24]. Both iNOS and nNOS are cytosolic enzymes while eNOS is membrane bound. eNOS is also unique in that it is targeted to the caveolae of vascular endothelial cells, where it is dynamically regulated by interactions with caveolin [25].

The genes encoding the NOS isoforms are located on 3 different chromosomes but have a similar genomic structure, suggesting a common ancestral NOS gene. The overall sequence homology across the NOS family is approximately 50-60% [26].

Two of the isoforms, nNOS and eNOS, are constitutively expressed and synthesise NO in response to increased calcium (Ca^{2+}) concentration, or occasionally in response to Ca^{2+}-independent stimuli such as shear stress. These constitutive NOSs (cNOSs) are also indirectly regulated by tetrahydrobiopterin (H_4B) synthesis and by other proteins through direct binding, subcellular localisation and phosphorylation. nNOS and eNOS directly link changes in the level of intracellular Ca^{2+} to NO production, activating G-cyclase. iNOS, on the other hand, is transcriptionally activated by endotoxins and cytokines in macrophages, hepatocytes and vascular smooth muscle [27].

The sensitivity to Ca^{2+} concentration in the cNOSs is achieved by the binding of the protein calmodulin (CaM). nNOS and eNOS are activated by CaM binding, and indeed iNOS does not fold properly without CaM and is always found with it tightly bound [28].

1.2.2 Structure and arrangement

Although the length of the polypeptide chain of each NOS isoform varies, they all share the same basic structure, being split into an N-terminal oxygenase domain and a

C-terminal reductase domain, and represented in Figure 1.2. The two domains are linked by a short (approximately 20 amino acids long) region that forms the binding site for CaM. The oxygenase domain binds a cysteine-thiol ligated heme, tetrahydrobiopterin (H_4B) and L-arginine. It is structurally unique and forms the active site where NO synthesis takes place [29].

The reductase domain binds flavin mononucleotide (FMN), flavin adenine dinucleotide (FAD), and NADPH, acquiring electrons from the nicotinamide moiety and transferring them through FAD and FMN and on to the heme iron [30]. It is structurally similar to cytochrome P450 reductase (CPR) [31], with two important differences marked on Figure 1.2; one loop within the FMN-binding domain of the cNOSs and the C-terminal residues of all three isoforms. These form autoinhibitory features that are important in the regulation of electron transfer. The di-flavin reductase arrangement allows the shuttling of electrons from a two-electron donor (in this case NADPH) to a one-electron acceptor (heme iron). In the constitutive NOSs, flavin to heme electron transfer is triggered by the binding of CaM, and it is this step that couples the level of calcium to the production of NO [30].

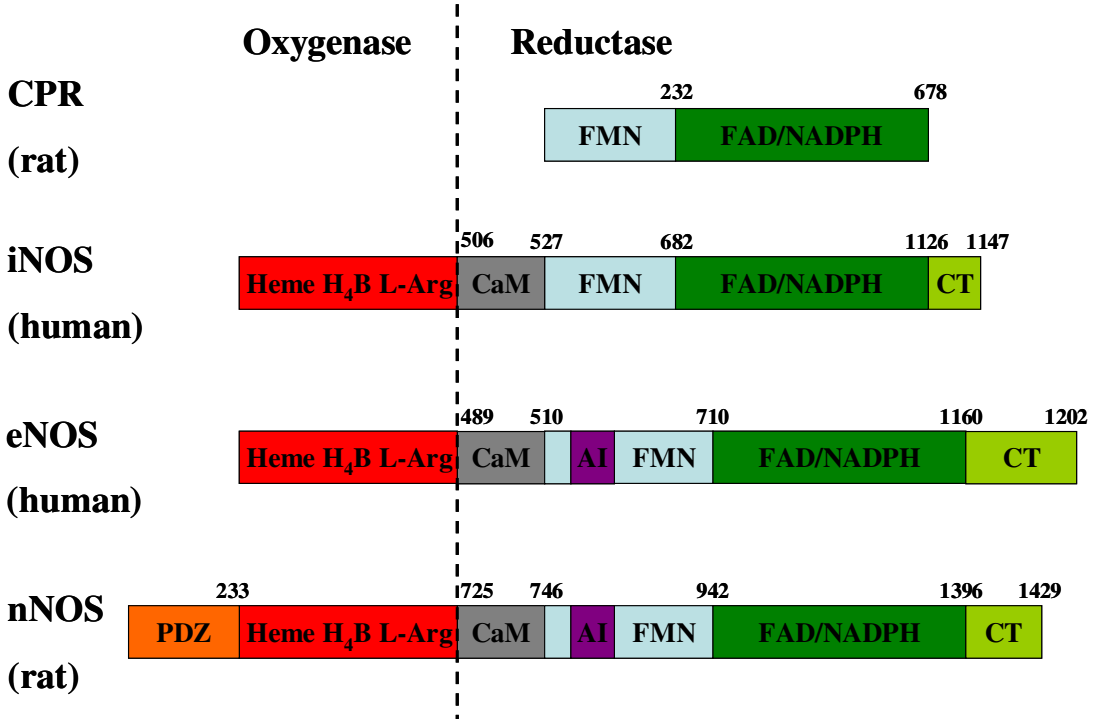

Figure 1.2 Schematic representation of the sequence alignment of CPR, iNOS, eNOS and nNOS. AI = autoinhibitory loop, CT = C-terminal tail.

The first 220 residues of nNOS are not found in the other isoforms and are known as the PDZ domain. PDZ stands for PSD-95 discs large/ZO-1 homology domain, and PSD is post synaptic density protein. This domain targets nNOS to synaptic sites in the brain and in skeletal muscle (where it is responsible for mediation of the binding of nNOS to the skeletal muscle protein syntrophin), and mediates the membrane association of nNOS in neurones [32].

All of the NOS isoforms are functional homodimers, with the dimer interface formed between the two oxygenase domains [33]. The presence of a Zn^{2+} ion stabilises the dimer by binding to two cysteines from each subunit, while each of the hemes functions independently in a NOS dimer and receives electrons from the reductase domain of the adjacent monomer [34, 35]. A representation of the possible dimeric structure of nNOS is shown in Appendix I.

The differing localisation of the isoforms of NOS means that they are required to produce NO at different rates. iNOS produces NO fastest because of the most urgent need for NO production at the site of infection, nNOS is intermediate, and eNOS is the slowest with longer lasting effects on the cardiovascular system [36]. Chimeras of the different isoforms showed that the reductase domains can still transfer electrons to oxygenase domains of a differing isoform; however these chimeras had activities characteristic of the isoform of the reductase domain in the chimera, indicating that the production of NO is regulated through the transfer of electrons in the reductase domain [37].

1.2.3 Catalysis of NO synthesis

In both reaction steps of the NOS pathway, the hydroxylation of L-arg to NOHA and the oxidation of NOHA to L-citrulline and NO (from Figure 1.1), the active site of the enzyme proceeds through a similar cycle, as illustrated in Figure 1.3 [38]. The resting state of the heme iron is the ferric form, with H_4B bound to the enzyme (species I). The binding of substrate (Arg or NOHA) in iNOS affects the reduction potential of the heme cofactor, shifting it to a more positive potential that is analogous to the effect in cytochrome P450s [39]. In the constitutive NOSs the effect is to ensure that all of the heme is in a five-coordinate state. The ferric heme is then able to accept an

electron from the FMN hydroquinone in the reductase domain, to become the ferrous species (II). This can bind oxygen to form an oxyferrous complex (III), which can also be represented as its canonical form, the ferric superoxide species (IV) [40].

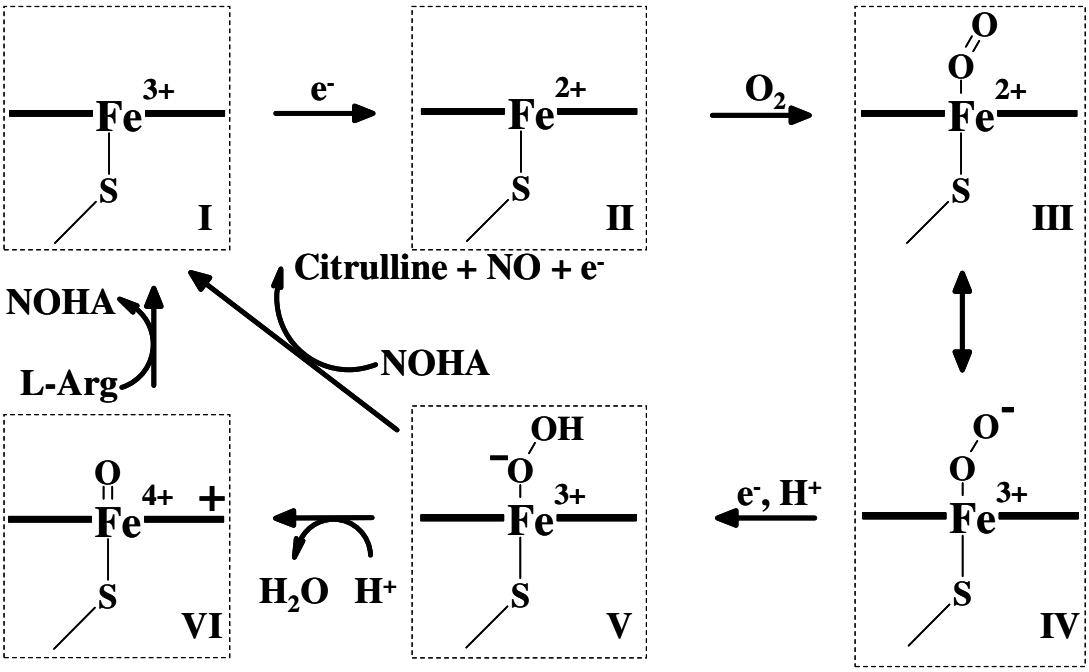

Figure 1.3 Schematic representation of the catalytic cycle of the heme cofactor in nNOS. Adapted from ref. 40

The stability of the oxyferrous complex (III) is a crucial factor in the catalytic cycle, and in the role that H_4B plays. In solution studies, the presence of L-arg or NOHA has been found to stabilise the oxyferrous complex, while the addition of H_4B destabilises it [41]. The first role of H_4B in the catalytic cycle, therefore, is to activate the oxyferrous complex by donating an electron and possibly a proton to form the hydroperoxy species (V). The pterin is re-reduced by the reductase domain, and it is believed that the reduction of the superoxide species by H_4B and not directly by the reductase domain leads to more efficient reduction [42]. Furthermore, it decreases the possibility of the release of cytotoxic superoxide into the cellular environment, and thereby increases the coupling efficiency of the reaction. The O-O bond in the hydroperoxy species is then cleaved which leads to a ferryl species with a π-cation radical on the porphyrin ring (VI) that is the active oxygen intermediate. This goes on to hydroxylate L-arg, via a P450-like oxygen insertion reaction, producing NOHA (as shown in Figure 1.1) and the ferric enzyme (I).

The second mono-oxygenation reaction was thought to proceed via a different mechanism, as it only requires one electron which is insufficient to produce the ferryl species (VI) present in the first reaction. However, it has recently been shown that the enzyme goes through the same cycle from (I)-(V) in Figure 1.3 [40]. The peroxy intermediate in this case does not undergo cleavage of the O-O bond; instead it undergoes a nucleophilic attack on NOHA to form L-citrulline, NO and a water molecule. In this final step in the catalytic cycle H_4B has a second role to play. Following on from the production of L-citrulline and radical NO, the NO will be bound to the ferrous form of the enzyme. This ferrous nitrosyl complex is particularly stable and the NO would not readily dissociate. In this scenario, a high potential electron acceptor would be required to form the ferric nitrosyl complex that is labile and able to release NO. The H_4B radical that is formed during catalysis is able to perform this role and complete the catalytic cycle [43].

The dissociation of NO is in competition with a non-productive pathway in the final step. This "futile cycle" involves the re-reduction of the heme by the reductase domain, and subsequent reaction with oxygen to produce nitrate. These conflicting cycles are presented in Figure 1.4, where k_r represents the rate of heme reduction by the flavoprotein. Increasing the magnitude of k_r will increase the rate of formation of heme-NO complex but will also cause more of it to proceed through the unproductive cycle [44].

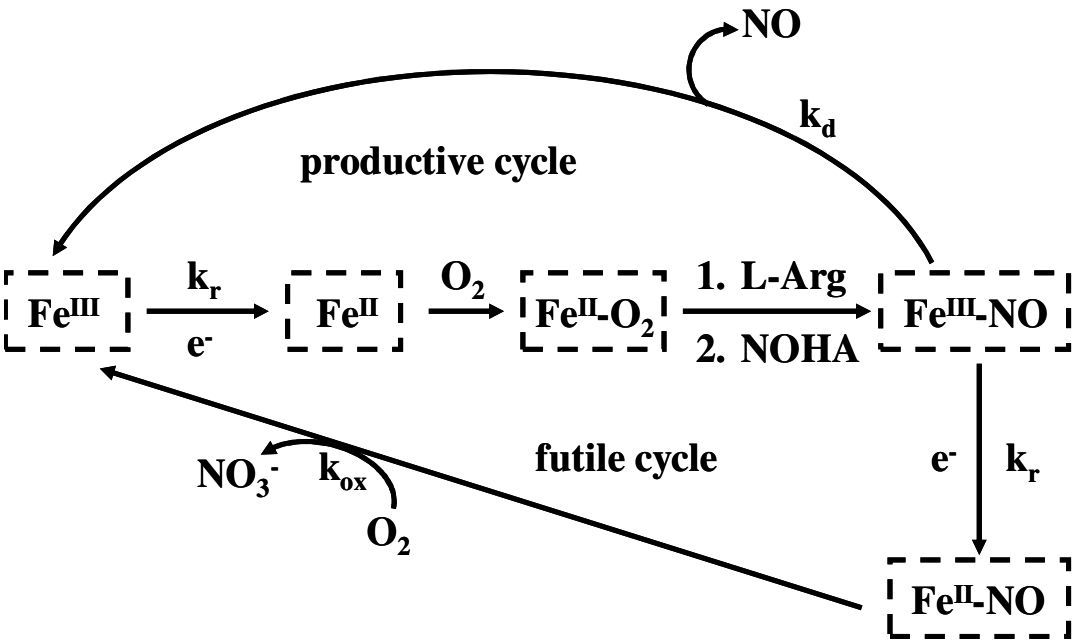

Figure 1.4 Schematic representation of the catalytic cycle of NOS

In comparison to the other isoforms, nNOS has a near-optimal k_r, whereby any increase in the rate of heme reduction will limit the rate of NO release [45]. This was observed for an nNOS mutant that had an increased rate of electron transfer from the reductase domain. Initially it was thought that the increase in electron flux would lead to an increase in NO synthesis, however this was not the case. The rate of NADPH oxidation by the mutant was greater than wild-type nNOS, as was heme reduction in the pre-steady state, but the rate of NO synthesis was slower. The rate of heme reduction was modified by the use of CaM from soybean sources rather than mammalian cells. In wild-type nNOS all of the CaM variants slowed down the rate of heme reduction and also the rate of NO synthesis, while in the S1412D mutant, the decreased rate of heme reduction by certain CaM isoforms caused an increase in the rate of NO synthesis. This correlated with the near-optimal heme reduction rate observed in wild-type nNOS [46].

1.3 NOS oxygenase domain

The X-ray crystal structure of full-length holo-NOS has yet to be solved. However, considerable insight has been gained from the publication of the structures of the isolated oxygenase domains (NOSoxy) of all three isoforms; mouse iNOS, human eNOS and rat nNOS [47 – 49]. Each of these is dimeric (Figure 1.5 shows nNOSoxy) and has a similar structure, with the domain being made up of one continuous α-β fold consisting of several winged β-sheets. The distal pocket that forms the active site of the enzyme is present in related cytochrome P450s, peroxidases and catalases, all of which have a largely α-helical structure. The β-sheet structure of the distal pocket in NOS makes it unique among these related systems. Heme is present in each subunit of NOSoxy as iron protoporphyrin IX and is cysteine-thiol ligated by Cys415 (rat nNOS numbering). Substrate binding channels are formed in each monomer of nNOSoxy, near to the binding site for heme, which allow access to L-arginine and the release of L-citrulline.

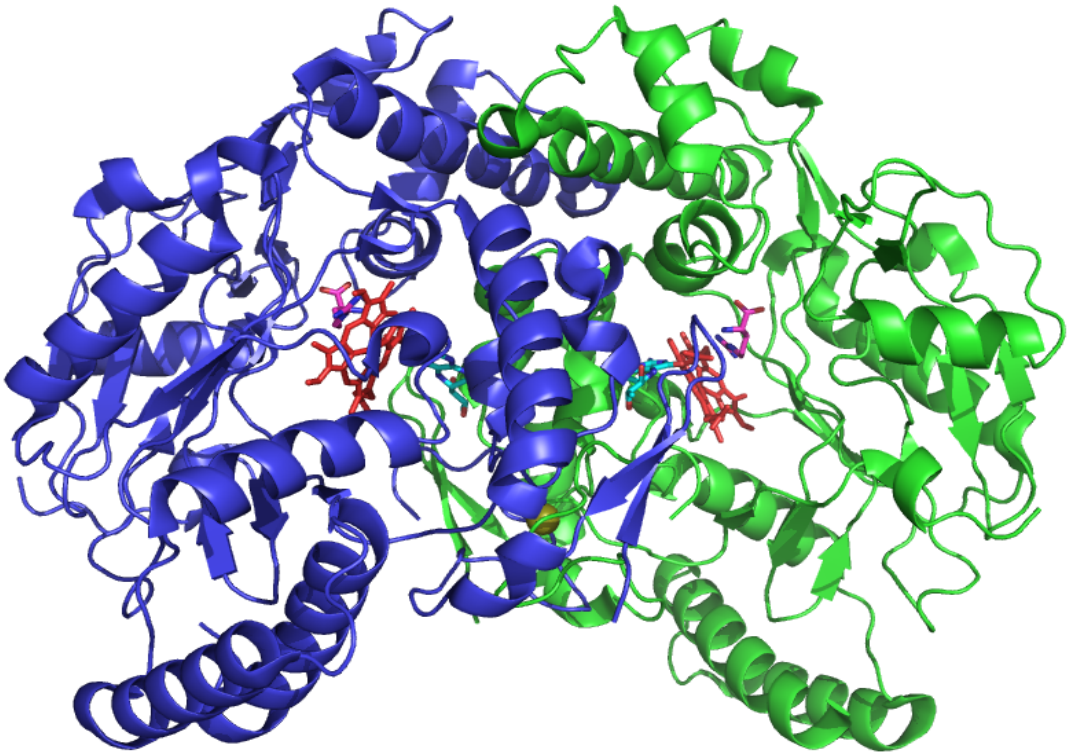

Figure 1.5 Dimeric structure of nNOSoxy (PDB code 1OM4). The monomers are coloured blue and green, the bound heme cofactors in red, L-arginine in magenta, H_4B in cyan, and the zinc ion in yellow.

L-arg binds with its side-chain tightly bound in the channel (Figure 1.6), with one carboxylate oxygen H-bonding with Tyr588 and Gln478 and the other carboxylate oxygen within H-bonding distance of Asp597. The α-amino nitrogen forms H-bonds bridging Glu592 and one heme propionate, and the specificity in this amino-acid binding region is such that the L-enantiomer is favoured; the H-bonding contacts could not accommodate the D-enantiomer. The guanidine group of L-arg is held above the heme plane by further H-bonding interactions with Glu592 and the backbone carbonyl oxygen of Trp587.

The structure of nNOSoxy with NOHA bound has also been published [50], and it shows NOHA bound with the same interactions as L-arg, in both the main amino-acid section and the guanidine group. The hydroxyl group of NOHA is present over the heme plane and does not coordinate, but instead points toward the backbone amide of Gly586 to form a weak H-bond or a non-bonded contact.

The binding of H_4B occurs within the dimer interface and is anchored by protein structural elements that are involved in the dimeric interaction (Figure 1.6). The

pterin makes H-bond contacts with Ser334 from its own subunit and Phe691 from the other subunit. The positioning of H_4B is such that its rings are positioned to the side of the heme, almost perpendicular to the plane, and it π-stacks with a conserved tryptophan, Trp678. This residue is crucial for stabilisation of the pterin radical formed during catalysis. Substitution by phenylalanine or alanine in full-length nNOS decreased the rate of NO synthesis and caused uncoupled NADPH oxidation, due to the inability of H_4B to reduce the oxyferrous complex [51].

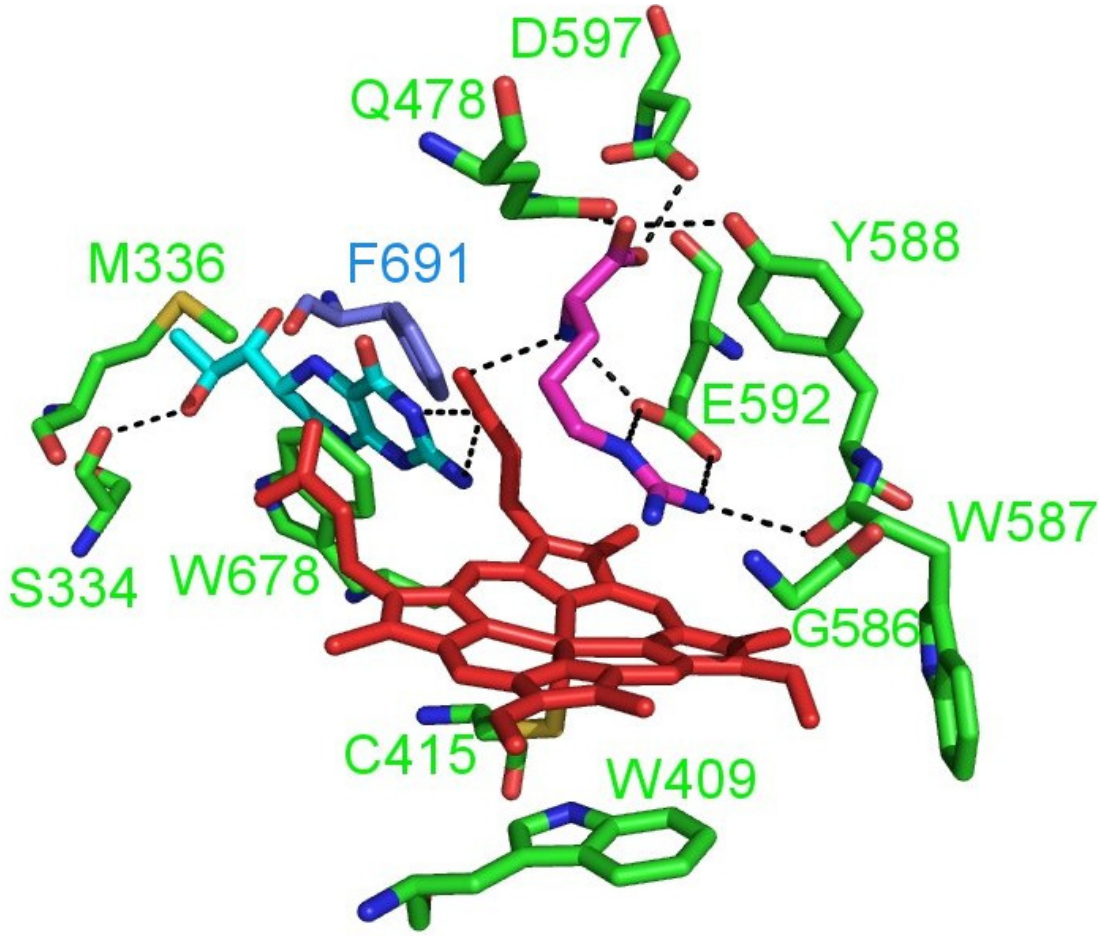

Figure 1.6 Active site of nNOSoxy (PDB code 1OM4). Backbone residues are coloured green and blue from the two subunits, the bound heme cofactor in red, L-arginine in magenta, and H_4B in cyan. Interactions between named residues and the cofactors are presented as black dashed lines

Further structural information about nNOSoxy has been provided in the form of the crystal structures of the CO- and NO- bound ferrous forms [52]. The only difference in structure in the distal heme pocket between the ferrous and the ferric forms is the presence of an additional water molecule. This is within H-bonding distance of the guanidine nitrogen of L-arg and a second water molecule, present in the original ferric

structure. The binding of CO and NO to the heme pull the iron into the porphyrin plane as expected, without altering the distortion of the plane itself, and both diatomic ligands H-bond to the active site water. It is speculated that this water may H-bond to bound oxygen in the active site, and ultimately act as a proton source for the O-O bond cleavage step. There are instances of other P450-oxy and heme oxygenase structures where water is the direct proton donor to the oxygen [53, 54].

Another important structural feature of the NOS oxygenase domain is its interaction with the reductase domain. In P450s, the protein surface near to the heme group contains cationic patches made up of arginines and lysines that form a docking site for anionic surface patches of CPR, specifically on the FMN domain close to where the cofactor is bound [55]. The ionic interaction between the two domains allows the electron transfer to the heme that is required for catalysis. As the anionic residues from CPR are conserved in the NOS reductase domain, it is thought that the delivery of electrons in NOS occurs in the same manner. Lys423 is a well conserved residue in the constitutive NOSs, solvent exposed in the crystal structure of nNOSoxy (Figure 1.7). Charge-reversal substitution of this residue by glutamate in full-length nNOS yielded an enzyme that was markedly slower in terms of NO synthesis, heme reduction and NADPH oxidation. The interaction between the electron-delivering reductase domain and the heme domain was disrupted to the extent that efficient catalysis could not take place [56].

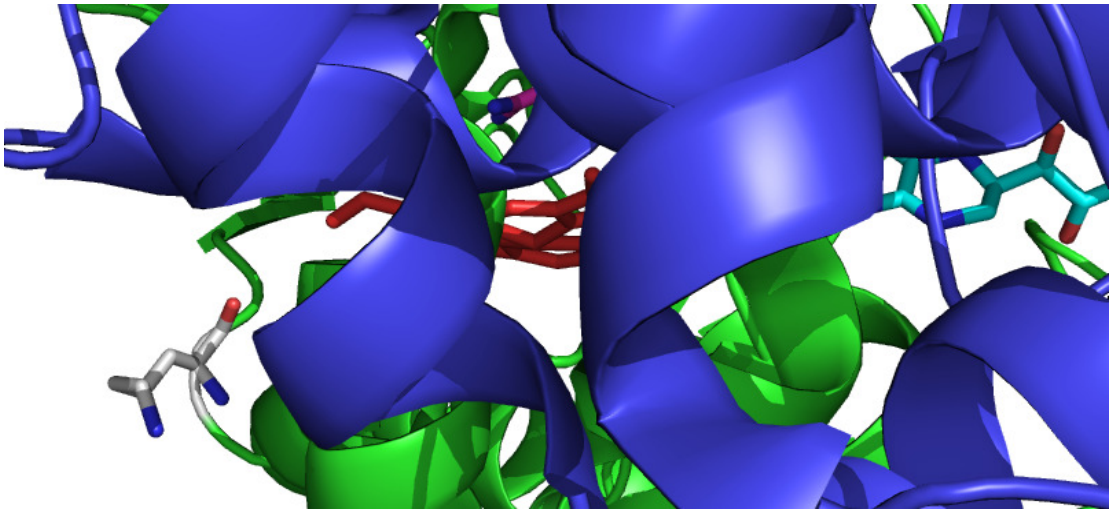

Figure 1.7 Surface exposed residue Lys423 of nNOSoxy (PDB code 1OM4). The two subunits are coloured blue and green, the bound heme cofactor in red, L-Arginine in magenta, H_4B in cyan, Lys423 in grey.

1.4 Flavins and flavoproteins

FMN and FAD are generated from riboflavin (vitamin B_2) which can be synthesised by plants, bacteria and fungi but not by animals, which must obtain it from the diet [57]. The structure of FAD, FMN and riboflavin are shown in Figure 1.8, with the numbering system of the isoalloxazine ring highlighted. This ring system consisting of fused benzene, pyrimidine and piperizine rings can exist in three oxidation states – fully oxidised (quinone), one-electron reduced (semiquinone) and two-electron reduced (hydroquinone). These are also depicted in Figure 1.8.

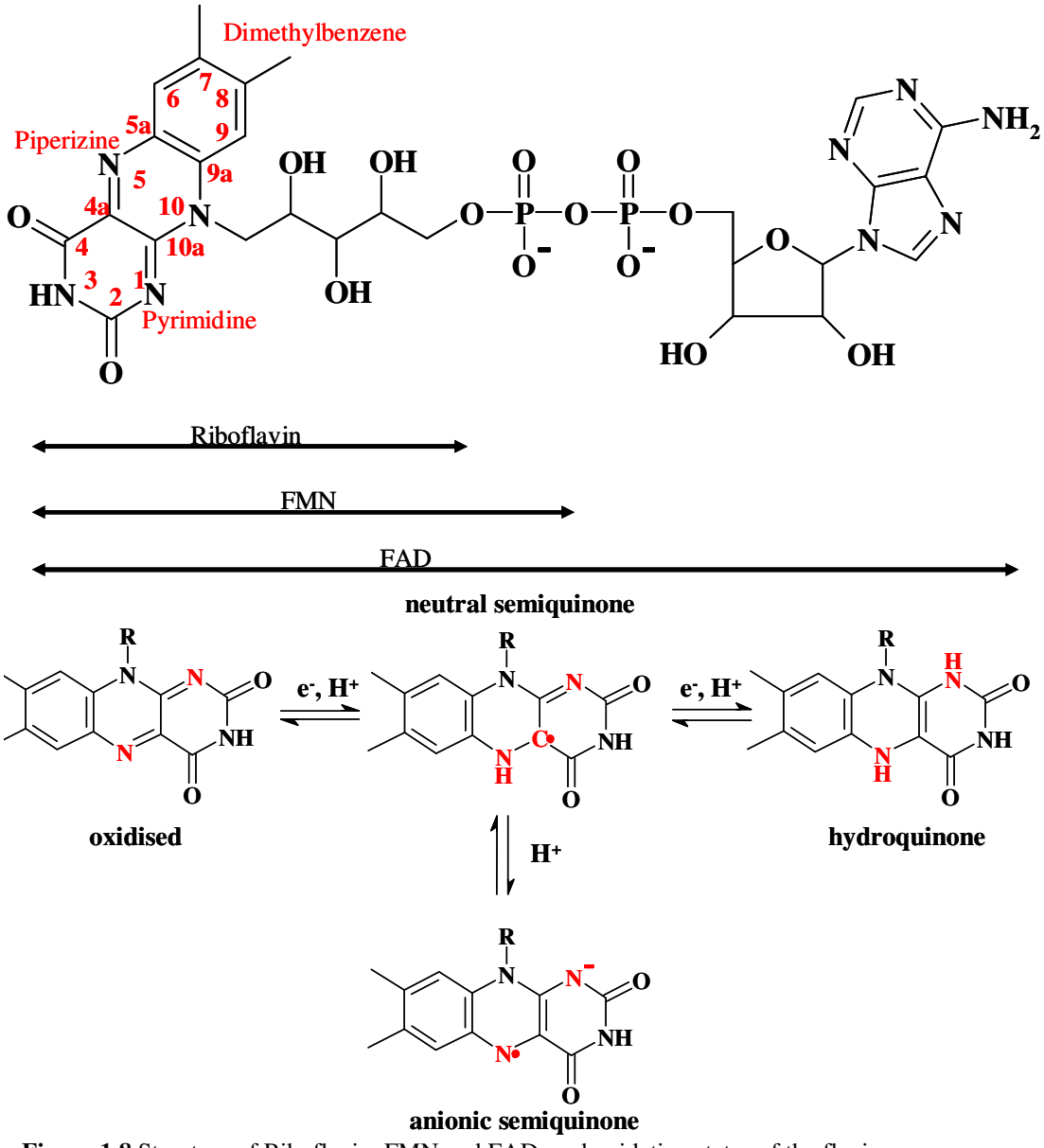

Figure 1.8 Structure of Riboflavin, FMN and FAD, and oxidation states of the flavin group

Flavin-binding proteins are estimated to be encoded for by 1-3% of genes in eukaryotic and bacterial genomes. Each of the redox, ionic, and electronic states of the flavin group has distinct chemical properties that can be modified by a protein environment, and this allows the protein-bound flavin to perform a huge variety of enzymatic reactions. Simple flavoproteins are classified by the reactivity of the reduced enzyme with molecular oxygen. The oxidases react with dioxygen rapidly, using it as an electron acceptor to produce hydrogen peroxide and oxidised flavoprotein. Examples of this class include D-amino acid oxidase, glucose oxidase and glycolate oxidase. Common properties of these enzymes include; stabilisation of the anionic red flavin semiquinone rather than the neutral blue version, formation of flavin N5-sulfite adducts, and production of the benzoquinoid anion form of substituted flavin. These properties all mean that a positive region of the protein is interacting with the pyrimidine ring of the flavin [57].

Monoamine oxidase (MAO) is an unusual flavoprotein oxidase, as the flavin is covalently linked to the protein via the 8-methyl substituent, meaning the prosthetic group is an 8-α-S-cysteinyl-FAD. Two forms of MAO, A and B, exist in the outer mitochondrial membrane and, while sharing around 70% amino acid identity, they differ greatly in their specificity and biological function [58]. Generally speaking, they catalyse the oxidative deamination of amines that is an extremely thermodynamically unfavourable reaction. The redox potential of the normally high-potential amines is lowered and that of the low-potential flavin is raised by protein environment to allow the reaction to proceed. MAO B mostly acts on small exogenous amines, whereas MAO A carries out degradation of bulkier endogenous neurotransmitters such as serotonin. For this reason they are a pharmacological target and inhibitors of MAO A and B have been used in the treatment of neurological disorders [59].

The flavin mono-oxygenases use dioxygen to insert an oxygen atom into their substrate. The reduced enzyme reacts with O_2 to form a C(4a)-hydroperoxide intermediate, and the physiological reductant in this case is always NADH or NADPH [57]. In the absence of a further substrate the flavin-hydroperoxide decays to H_2O_2 and oxidised flavin. In the presence of such a substrate the flavin-hydroperoxide transfers an oxygen atom to the substrate which results in a C(4a)-hydroxyflavin, which dehydrates to the oxidised flavin for the next catalytic cycle. An advantage of

the flavin hydroperoxide is that solvent elimination of peroxide is mostly prevented so the hydroperoxy species is able to react with a wide variety of electron-rich groups.

An example of this class is p-hydroxybenzoate hydroxylase (PHBH), which is involved in the pathway of aromatic degradation. The aromatic substrate is hydroxylated at the position ortho to the activating para-substituent, and the enzyme exhibits a high degree of specificity for its one substrate [60]. An unusual property of PHBH is the kinetic stability of the complex between substrate and reduced flavin, in this case FAD. The flavin actually moves in the active site to allow exchange of substrate with solvent and in a second conformation it tightly binds to the substrate, ensuring rapid hydroxylation. The movement of the flavin is also important in the interaction with NADPH that produces reduced FAD in the first part of catalysis, as the enzyme has no discernable NADPH-binding domain [61].

The electron transferases are a class of flavoproteins that react very slowly with dioxygen, producing the superoxide anion and flavin semiquinone, in a reaction that represents decoupling of their actual function. They are involved in physiological single-electron transfers and include flavodoxin, ferredoxin-$NADP^+$-reductase and cytochrome P450 reductase [57]. The semiquinone state of the flavin is thermodynamically stabilised as the blue neutral species, and there is no production of sulfite adducts or stabilised benzoquinoid formation. Solution studies show that typically the benzene ring is the only part of the flavin accessible to solvent.

Some families of flavoproteins are not as easy to classify under one of the three headings, for example Acyl-CoA dehydrogenases (ACADs) react with acyl-CoA substrates by proton-abstraction from the α-carbon by an enzyme base and subsequent hydride transfer from the β-carbon to the flavin [62]. The catalytic reaction cycle is completed by sequential electron transfers to the electron-transferring flavoprotein (ETF), which channels the reducing equivalents from the reduced flavin of ACAD into the mitochondrial respiratory chain. The related enzyme nitroalkane oxidase (NAO) exhibits flavin-dependent covalent catalysis, by performing the oxidative degradation of nitroalkanes to generate nitrite, hydrogen peroxide and an aldehyde or ketone [63]. An active-site aspartate residue acts as the base that abstracts a proton from the substrate at the start of the catalytic cycle. Following on from the formation of the covalent intermediate between the substrate and the N5 flavin atom, a

hydrophobic channel that extends from the protein surface to the flavin ring provides a binding site for the adduct.

Flavoproteins are also found coupled to other redox centres. Bacterial enzymes that are involved in the degradation of unactivated aromatic compounds, such as benzene and catechol, involve iron-containing dioxygenases and flavoproteins that mediate reduction of the dioxygenase by NADPH. An example of this is phthalate dioxygenase reductase which contains FAD and an iron-sulfur centre [57].

Flavocytochromes contain heme groups in addition to flavins, the most studied of which is yeast L-lactate dehydrogenase, or flavocytochrome b_2 [64]. This contains a b-type cytochrome domain along with an FMN group. Similarly, flavocytochrome c_3 from *Shewanella* is a fumarate reductase that contains four heme groups in a c_3 domain, as well as FAD that forms the active site in catalysis [65]. Among the cytochromes P450, flavocytochrome P450-BM3 from *Bacillus megaterium* is a fusion of a cytochrome P450 domain and an NADPH-cytochrome P450 reductase that contains FAD and FMN. This is very similar to the domain arrangement in NOS [66].

1.5 Cytochrome P450 reductase

The cytochrome P450 super-family of enzymes typically catalyse the mono-oxygenation of hydrophobic compounds for example long-chain fatty acids, inserting one atom of dioxygen into the organic substrate while the other atom is reduced to water [67]. Electrons are provided by NADPH in eukaryotes and NADH in prokaryotes. The provision of the electrons is in the form of a hydride (H^-) and leads to two differing modes of electron transfer; through an FAD-containing reductase and a diffusible electron carrier such as an iron-sulfur protein, or through an FAD- and FMN-containing reductase, cytochrome P450 reductase (CPR).

The sequence homology among CPR found in different species is very high, indicating an evolutionary importance for the enzyme. There are many similarities between nNOSrd and CPR; it is a 78 kDa membrane-bound protein which accepts a hydride from NADPH, passes an electron through FAD then FMN and onto a heme acceptor. Furthermore it cycles between the one- and three-electron reduced states

and contains a stable semiquinone on FMN. However, it has a small N-terminal hydrophobic anchor section unlike NOS, attached to the C-terminal hydrophilic catalytic domain. The anchor attaches CPR to the endoplasmic reticulum and allows interaction with cytochromes P450. Proteolytic removal of this domain leaves the solubilised catalytic domain which can transfer electrons to cytochrome *c* but not to cytochromes P450 [68].

Figure 1.9(A) presents the crystal structure of the catalytic domain of rat liver CPR with its four component domains highlighted [69]. Seven residues at the N-terminus are disordered, indicating flexibility and motion relative to the membrane bound domain. The next 170 residues, coloured red, form the FMN-binding domain which is similar in structure to flavodoxin [70], a bacterial electron carrier. The green connecting domain is linked to the FMN-binding domain by a disordered section which is flexible and involved in the motion of the FMN-binding domain relative to the other sections. The connecting domain is largely α-helical, in contrast to the other domains which bind cofactors through β-sheet interactions. Adjacent to the C-terminal end of the connecting domain is the FAD-binding domain, coloured blue, with the FAD cofactor bound close to NADPH and on the edge of its binding domain such that it is end-on to the FMN cofactor. The structure of the enzyme appears to be poised for FAD to FMN electron transfer.

The interface between the connecting and FMN-binding domains is mostly hydrophilic so the interaction between them is electrostatic. On the other hand the interfaces between the FAD-binding and connecting domains, and the NADPH- and FAD-binding domains, are mostly hydrophobic and these three domains are interlinked indicating that they cannot be separated easily. They also appear to have a bacterial ancestor, being similar in sequence and structure to Ferredoxin-$NADP^+$ reductase (FNR) [71]. This enzyme works in the reverse direction to CPR, reducing $NADP^+$ rather than oxidising NADPH, but the protein fold appears largely unchanged between the two.

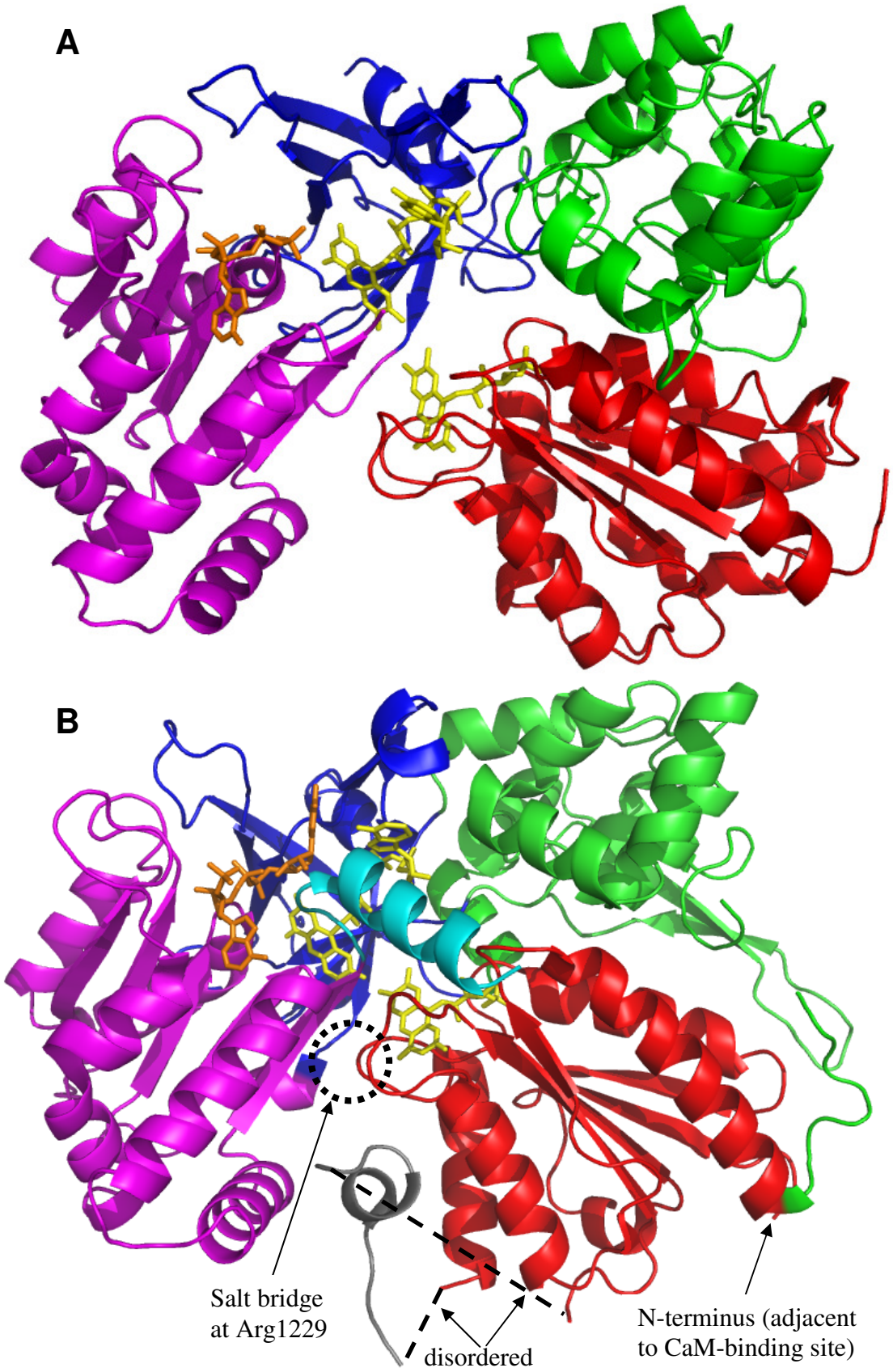

Figure 1.9 X-Ray crystal structures of (A) CPR (PDB code 1AMO), and (B) nNOSrd (1TLL). Bound flavin cofactors are coloured yellow, NADPH orange, domains from N- to C-terminus red (FMN-binding), green (connecting), blue (FAD-binding), magenta (NADPH-binding). Additional features on nNOSrd coloured cyan (CT) and grey (AI).

1.6 NOS reductase domain

The C-terminal di-flavin reductase is the larger of the two NOS domains; in rat nNOS it is comprised of residues 695-1429, which includes the CaM-binding region. Sequence analysis was the first indication that it was structurally homologous to other di-flavin reductases, sharing 36% identity and 58% close homology with CPR [72]. This is represented in Figure 1.10, where the sequences of the three NOS isoforms and CPR are simplified into binding-domain blocks and compared. From N- to C-terminal ends the basic arrangement is the same throughout, with the additional features on the NOSs being primarily the extension at the C-terminus (CT) and for the cNOSs the autoinhibitory loop within the FMN-binding domain (AI).

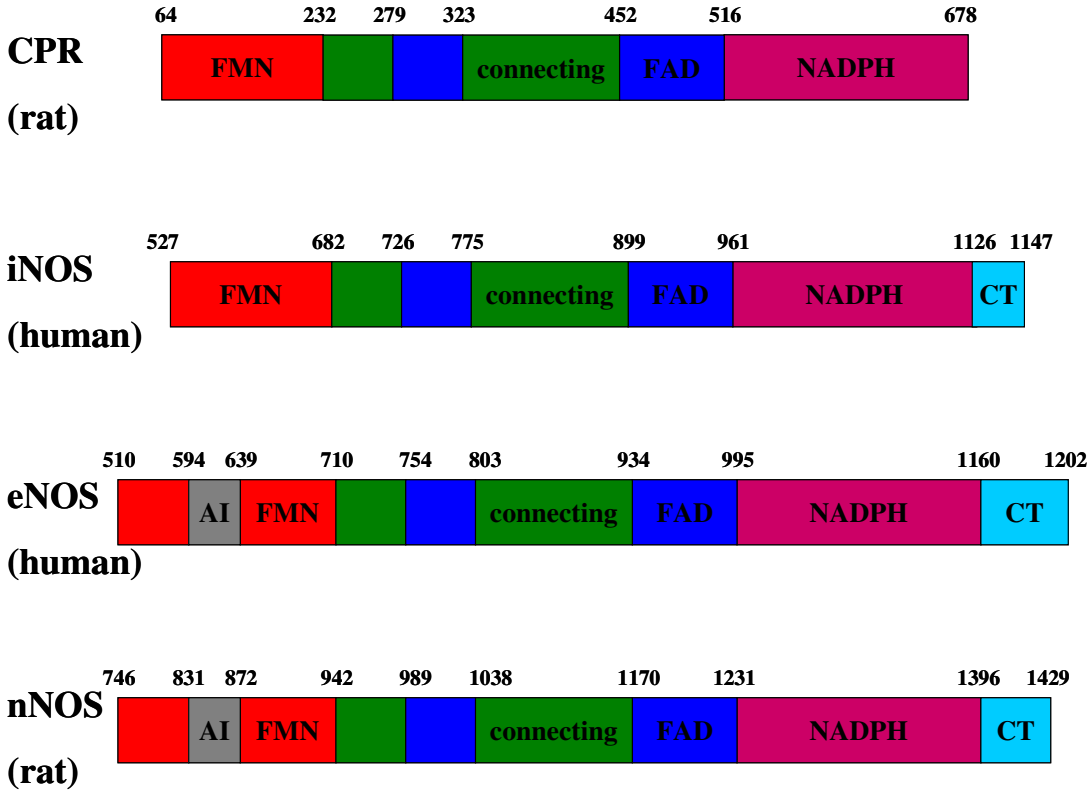

Figure 1.10 Schematic representation of the sequence alignment of the reductase domains of CPR, iNOS, eNOS and nNOS, expanded from Figure 1.2. Colouring of domains is the same as for the X-ray crystal structures, Figure 1.9.

The crystal structure of rat nNOSrd was first published using a proteolysed version that contained only the C-terminal sections of the enzyme, the FAD- and NADPH-binding domains [73]. As expected, this was very similar in structure to FNR and the

corresponding parts of CPR. A more complete structure, containing all of the constituent parts of nNOSrd without the CaM-binding region, is represented in Figure 1.9(B), in comparison to its homologue CPR. Clearly the arrangement and protein fold of the two enzymes are very similar, with the domains laid out in the same manner and the cofactors in the same relative positions. Interestingly, the structure of nNOSrd was found to be dimeric and further investigation revealed that this was the case in solution [74]. This revelation has implications for the overall arrangement of holo-nNOS, where the dimer interface in the oxygenase domain was presumed to be the only such interaction.

There are many conserved features between the structures of CPR and nNOSrd; the π-stacking interaction between FAD and an aromatic residue (Trp677 in CPR, Phe1395 in nNOSrd) is one of them, and is important in the regulation of catalytic activity. Also conserved is the network of residues around the FAD cofactor which form important H-bonding interactions. The binding of NADPH is mainly through the adenosine moiety, with the nicotinamide moiety held unproductively relative to FAD. Furthermore, at the interface between the two flavin cofactors and their binding domains is a salt-bridging interaction, in CPR it is a single interaction between an arginine and an aspartate while in nNOSrd it is a double-bridge between the conserved arginine and one of three glutamates. The additional features of nNOSrd, however, may be the most important in the structure. The two autoinhibitory features, coloured cyan, are the focus of much research on the activation of electron transfer through the enzyme. The flavin cofactors in nNOSrd are positioned only 4.8 Å apart, suggesting that this enzyme is also poised for interflavin electron transfer. For FMN to heme electron transfer to occur, it is clear to see that large-scale motion of the FMN-binding domain would be required.

1.6.1 Function and activity

Isolated nNOSrd can transfer electrons to acceptors such as cytochrome *c* or ferricyanide, just as CPR can [75]. The electron transfer activity of isolated nNOSrd, and within holo-nNOS, is summarised in Table 1.1, where it can be seen that the

binding of CaM activates the reductase domain to the same extent as it does the reductase activity of the nNOS holoenzyme [76]. This activation by CaM can be regarded as a de-repression of function, as the activity of CaM-free nNOSrd is severely down-regulated compared to other di-flavin reductases and iNOSrd [77]. It is only upon binding CaM that the electron transfer activity of nNOSrd is comparable with its homologues.

Table 1.1 Summary of activation of electron transfer through nNOSrd

Study	Enzyme	-CaM / s^{-1}	+CaM / s^{-1}	CaM-effect
Cytochrome *c* reduction				
78	nNOS	4	47	11.8-fold
	iNOS	n/a	42	
76	nNOSrd	4	48	12-fold
	CPR	n/a	38	
77	nNOSrd	6	52	8.7-fold
	iNOSrd	n/a	50	
79	nNOS	7	83	11.9-fold
80	nNOSrd	7.6	66	8.7-fold
81	nNOS	10	97	9.7-fold
Ferricyanide reduction				
78	nNOS	9.5	16	1.7-fold
	iNOS	n/a	65	
76	nNOSrd	7.5	28.5	3.8-fold
	CPR	n/a	72	
79	nNOS	30	85	2.8-fold
80	nNOSrd	25	84	3.4-fold
Flash photolysis				
82, 83	oxyFMN – “output state”	22	262	11.9-fold
84	nNOS	0	36	

Cytochrome *c* reduction is consistently activated by CaM by approximately 10-fold, but the rates of electron transfer vary slightly. Ferricyanide, on the other hand, has a smaller CaM-mediated activation effect, which is probably due to the ability of the smaller electron acceptor to access both the FAD and FMN cofactors. The flash photolysis experiments on the so-called "output state", a construct consisting of only the FMN-binding domain and the oxygenase domain, directly measure the electron transfer between the cofactors. This also exhibited a 10-fold stimulation upon CaM binding but the analogous nNOS rates were much slower. This indicates that the motion of the FMN-binding domain is crucial, having to access the FAD/NADPH-binding domains (the "input state") to perform interflavin electron transfer, as well as the oxygenase domain.

Another reaction of nNOSrd that has been studied in detail is the reduction of the flavin cofactors, i.e. the direct interaction between NADPH and FAD in the absence of an electron acceptor. This reflects not only the hydride transfer step but any subsequent electron transfer between FAD and FMN, and is summarised in Table 1.2. The exact analysis used across different studies varies but the binding of CaM clearly activates the flavin reduction.

Table 1.2 Summary of flavin reduction kinetics in nNOSrd

Study	Enzyme	-CaM / s^{-1}			+CaM / s^{-1}		
76	nNOS	1.5			32		
	nNOSrd	2.5			37		
79	nNOS	9.2		1.6	54		14
80	nNOSrd	42	7.2	2.5	121	16	3.1

1.7 Regulation of catalytic activity

The activation of nNOS by CaM that occurs within the reductase domain could manifest as a result of two major causes; by a structural domain rearrangement and/or by altering the midpoint reduction potentials of the bound flavin cofactors. The reduction potential is a measure of the potential energy when half of the molecules are oxidised and half are reduced, therefore giving an indication of the ease of oxidation or reduction occurring [85]. These thermodynamic measurements have been made in nNOS and nNOSrd and are summarised in Table 1.3.

Table 1.3 Summary of midpoint reduction potentials of nNOSrd cofactors / mV

Ref	Enzyme studied	FMN ox/sq	FMN sq/hq	FAD ox/sq	FAD sq/hq	NADPH
86	nNOSrd – electrochemical	-49	-274	-232	-280	-320
	nNOSrd + CaM	-30	-267	-234	-284	
87	nNOS	-120	-220	-250	-260	
88	nNOSrd + CaM – OTTLE	-98	-300	-296	-320	
	Isolated binding domains	-179	-314	-291	-326	
	FAD/NADPH-domains + $NADP^+$			-304	-290	-356
87	Heme: -320 mV substrate free, -280 mV L-arg bound					

From the values listed, it is clear that the FAD cofactor is poised to accept two electrons from NADPH as a hydride. The FMN cofactor has a higher potential for the oxidised to semiquinone transition so it will cycle between the 1 and 2 electron reduced states, and it is also poised to transfer electrons to the heme in the oxygenase domain. Notably, the binding of CaM has no effect on any of the reduction potentials in either the reductase domain or in the holoenzyme, indicating that it does not regulate electron transfer in this way. The stability of the cofactors is, however, affected by the presence of other domains; the FMN cofactor has a lower reduction potential in the isolated FMN-binding domain and is therefore stabilised in the semiquinone state by the presence of the other binding domains. This stabilisation

has not been observed in related systems (such as CPR) and highlights the importance of the interface region between the domains in nNOSrd.

Discounting any effect of CaM on the thermodynamics of NOS catalysis means that much research into the CaM-mediated activation step has been focussed on structural features. While this would most obviously be solved by obtaining the X-ray crystal structure of a CaM-bound form of nNOSrd or the holoenzyme, great insight has been achieved by mutagenesis at a key number of sites within the reductase domain and the consequent effects on electron transfer.

1.7.1 Calmodulin binding

The binding of CaM is essential for NO synthase activity in all of the NOS isoforms [89]. Heme reduction in nNOS in the absence of CaM is extremely slow and cannot support the production of NO from L-arg. The apparent rate of flavin reduction in nNOS in the absence of CaM is similar to that of heme reduction in the presence of CaM, so it is potentially fast enough to support heme reduction and NO synthesis. It is the case, however, that the electrons are not delivered efficiently to the heme; thus the binding of CaM must play an important role in facilitating electron transfer from the flavin domain to the heme domain. Additionally, CaM stimulates both flavin reduction events; initial FAD reduction by NADPH and the transfer of electrons between the flavins [90].

De-repression by Calmodulin is a common mechanism by which it interacts with other enzymes; for example myosin light chain kinase, calmodulin kinase IV, and calcineurin [91 – 93]. In all of these cases the region of protein architecture denoted as the CaM-binding site, or an adjacent site, serves as a competitive inhibitor that blocks access to the natural substrate until it is displaced by binding CaM. This is not the case for any of the substrates of NOS, or cytochrome *c*, but it was thought that the CaM-binding site could perform a similar function between the reductase domain and the oxygenase domain. This would not explain, however, the fact that the electron-transfer activity of the isolated reductase domain is activated by CaM [89]. Furthermore, structural changes in nNOSrd were found to be induced by CaM-binding, firstly by fluorescence spectroscopy [76], where an increase in flavin and

protein tryptophan fluorescence indicated a greater solvent exposure of the enzyme cofactors in the activated form.

CaM is a 17 kDa dumbbell-shaped protein with N- and C- terminal globular domains connected by an α-helical linker. Figure 1.11(A) shows the sequence and 1.7Å resolution X-ray crystal structure of recombinant bovine CaM, where the central helix is found to be in an elongated conformation [94]. Each of the globular domains, also called lobes, consists of two EF hands; a helix-loop-helix arrangement where each hand binds a Ca^{2+} ion that can also be clearly observed in the structure. Figure 1.11(B) shows the 2.05Å resolution X-ray crystal structure of rat CaM bound to a synthesised eNOS peptide fragment, selected to represent the CaM-binding site of human eNOS (RKKTFKEVANAVKISASLMG) [95]. The overall structure of CaM can now be seen to be different to that of the unbound protein; it surrounds the peptide in a completely globular arrangement. The question still remains, however, as to how this structure relates to the CaM-bound holoenzyme. The presence of the large oxygenase and reductase domains are likely to place constraints on the conformation of CaM, and force it to be bound in a specific conformation that is related to the activation step. Furthermore, the binding to eNOS and nNOS may not be exactly the same due to differences in the binding sites.

Bovine CaM : **ADQLTEEQIA EFKEAFSLFD KDGDGTITTK ELGTVMRSLG** **40**

QNPTEAELQD MINEVDADGN GTIDFPEFLT MMARKMKDTD **80**

SEEEIREAFR VFDKDGNGYI SAAELRHVMT NLGEKLTDEE **120**

VDEMIREADI DGDGQVNYEE FVQMMTAK **148**

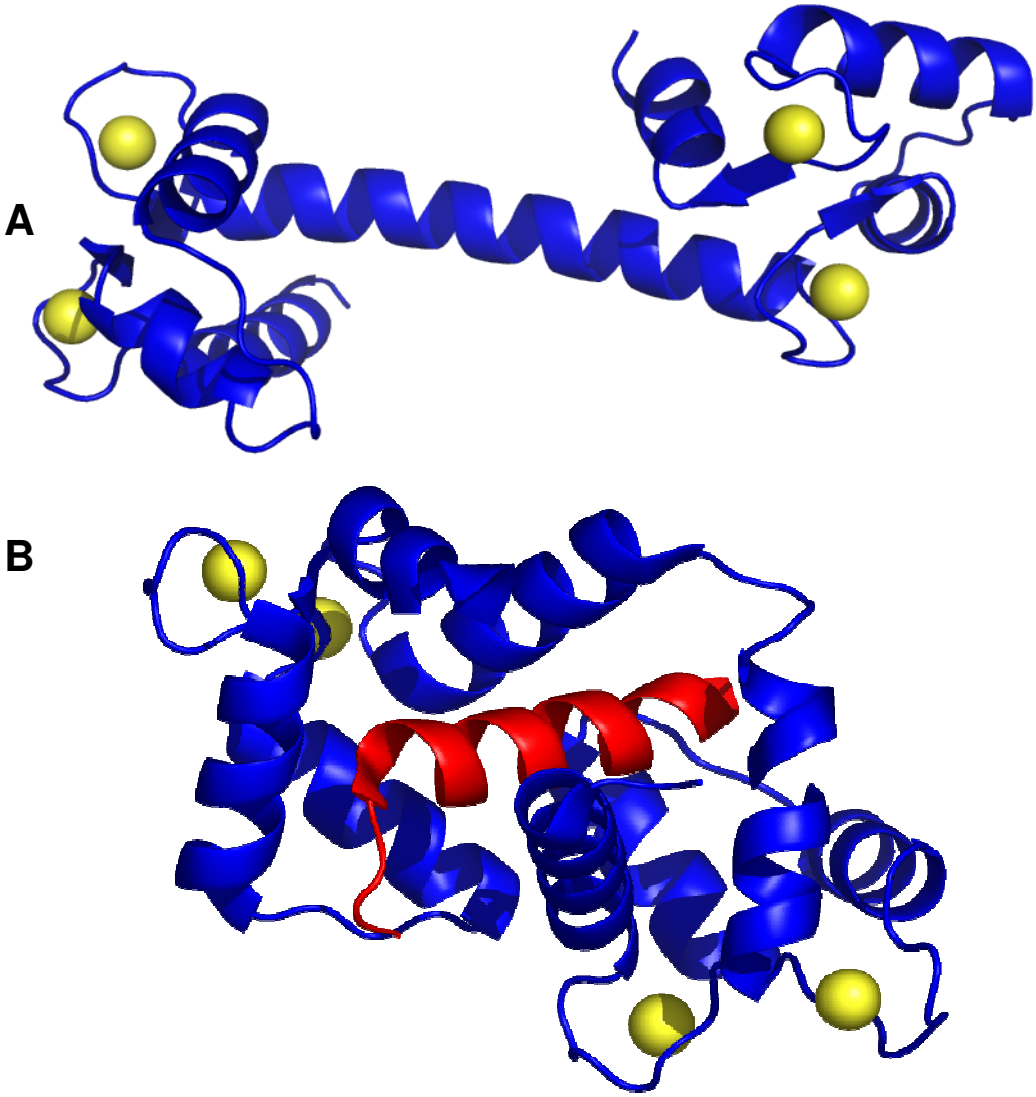

Figure 1.11 Sequence of bovine CaM [143] and X-ray crystal structures of (A) recombinant bovine CaM (PDB code 1CLL) and (B) rat CaM bound to a synthesised eNOS peptide fragment (PDB code 1NIW). Calmodulin residues are coloured blue, calcium ions yellow, and eNOS peptide red.

Certain facts are known about the binding of CaM; it is in an anti-parallel fashion, i.e. the C-terminal lobe of CaM binds to the N-terminal end of the binding site, adjacent to the oxygenase domain, while the N-terminal lobe of CaM binds to the C-terminal end of the recognition sequence, at the reductase domain. Furthermore, these lobes have different affinities for Ca^{2+}, with the C-terminal one displaying 10-fold higher affinity than its N-terminal counterpart [96]. This suggests that the C-terminal lobe

binds first but cannot activate the enzyme until the N-terminal lobe binds and causes activation. It may be the case that the C-terminal lobe is bound even at low Ca^{2+} concentrations (recall that this is near to the oxygenase domain) and then the N-terminal lobe binds at the reductase domain to cause the structural rearrangement that allows electron transfer through the holoenzyme to take place [97].

1.7.2 Autoinhibitory loop

The 'autoinhibitory loop' (AI) is highlighted in Figure 1.12 as the only main difference in sequence comparison between the flavin domains of the cNOSs and iNOS [36]. It is a section of protein architecture 45 amino acids in length that is not found in CPR, its related enzymes, or in any of the flavodoxins or similar FMN-containing proteins.

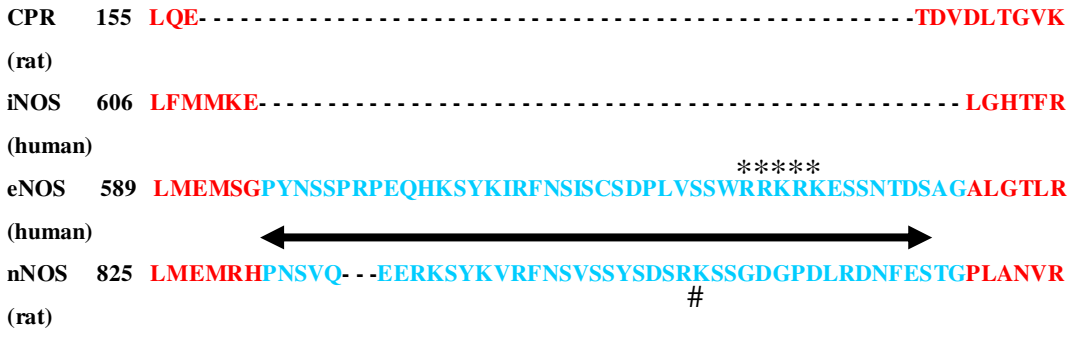

Figure 1.12 Sequence alignment of CPR, iNOS, eNOS and nNOS within the FMN-binding domain. FMN-binding residues are coloured red, Autoinhibitory loop (AI) cyan.

When the loop was first identified, it was speculated to function as a possible autoinhibitory domain, similar to inserts in other CaM-regulated enzymes. However, these inserts are normally acidic and hydrophobic, while the region in the cNOSs does not share those properties. To test if the loop was binding to the CaM-recognition sequence, or an adjacent region, synthesised polypeptides based on the sequence of the AI were used as potential inhibitors of NOS activity. The most effective inhibitors that were made all included the eNOS RRKRK motif, highlighted by asterisks in Figure 1.12, which correlates with the activity of eNOS being the slowest

among the isoforms. These peptides inhibited both the NO synthase activity of nNOS and eNOS and CaM-binding to a similar extent. The inhibition effect was fully reversed by the addition of excess CaM, indicating a competitive mode of inhibition. In addition, the binding of L-arg was unaffected, discounting any interference with the oxygenase domain and its substrate. The polypeptide fragments had no effect on the regulation of other CaM-binding proteins, indicating specificity for the cNOSs, while iNOS activity was unaffected by any of the inhibitors. This was attributed to the lack of an AI loop in iNOS and therefore a lack of any recognition site for it [98].

Further evidence for the competitive binding of the AI to nNOS came from the limited proteolysis of the holoenzyme. In the absence of CaM the preferred cut was made at Arg727 in the centre of the CaM-binding region [99]. With CaM bound, and the protection of its binding site, the cut was made at Lys856 in the centre of the AI loop (marked by # in Figure 1.12). Further analysis of the CaM-free digestion by gel electrophoresis revealed that Lys856 is the preferred cut site following the cleavage at Arg727. It was concluded that this protection and exposure was being caused by CaM displacing the AI of cNOSs.

Deletion of the RRKRK motif in eNOS [100] or substitution of the residues by alanines [101] activated CaM-bound NO synthase activity and CaM-free electron transfer to cytochrome *c*. The removal of the entire loop in nNOS, highlighted by an arrow in Figure 1.12, had a similar effect but the mutant enzyme could also synthesise NO without the binding of CaM [102]. Furthermore, it was capable of electron transfer to the heme in the absence of CaM and tolerated lower levels of Ca^{2+} to maintain CaM-bound maximal activity. This was an indication of the role of the AI in the suppression of CaM-free activity and the sensitivity to Ca^{2+}/CaM binding.

Other deletion studies involved the removal of the loop from chimeras containing eNOS reductase domains and oxygenase domains from the other isoforms [103]. These loopless chimeras had lessened Ca^{2+} dependence which correlated with chimeras that contained the reductase domain of iNOS and therefore no loop. The affinity for calcium in these constructs was up to 20-fold greater than that of wild-type eNOS or nNOS.

Upon publication of the crystal structure of nNOSrd [74], the AI was observed to lie between two strands of β-sheet that interact with the FMN cofactor and was found to contain a central α-helix which makes interactions with other helices from both the

FMN- and NADPH-binding domains (Figure 1.13). There were also a large number of disordered residues (29 out of 45) which is an indication of mobility.

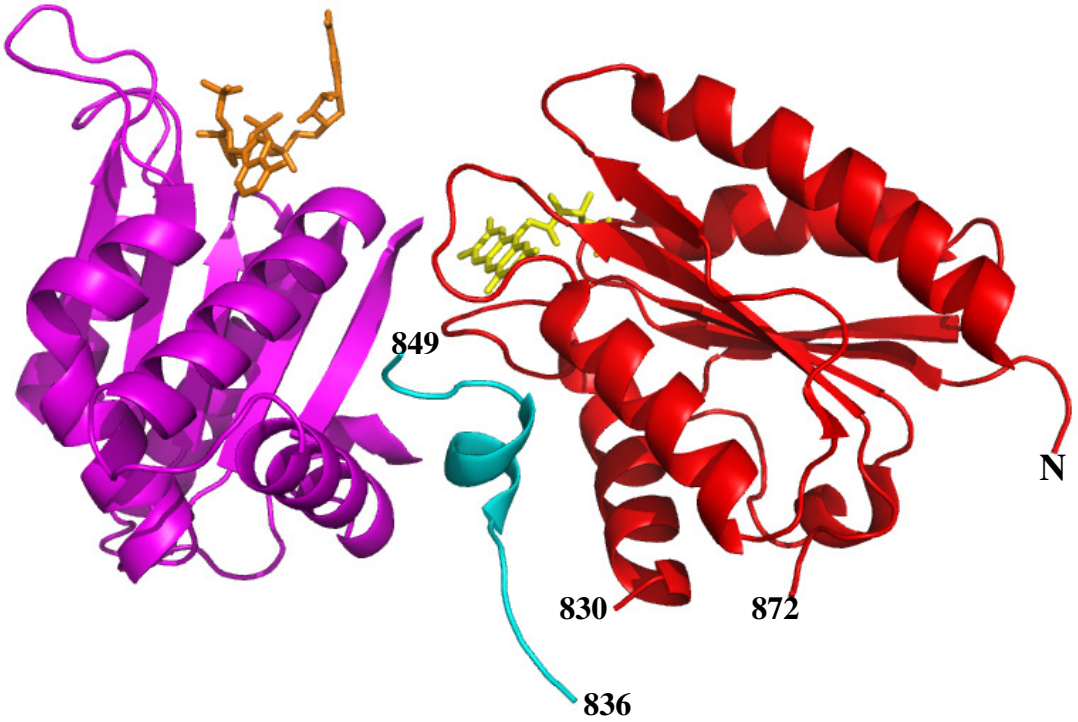

Figure 1.13 Autoinhibitory loop of nNOSrd (PDB code 1TLL). Bound FMN is coloured yellow, NADPH orange, FMN-binding domain red, NADPH-binding domain magenta and AI loop cyan. Other domains have been omitted for clarity.

The structure represented in Figure 1.13 indicates that the AI does not interact with the CaM-binding site in CaM-free nNOS; this region would be on the other side of the FMN-binding domain, marked as the N-terminus. There is the possibility, however, that there is an interaction between bound CaM and the AI; the disordered residues between Ser849 and Gly872, marked on Figure 1.13, could form a long enough linker region to allow the AI to move (to the right in the picture). This movement could thus be part of the activation process that allows large-scale motion of the FMN-binding domain to trigger electron transfer to the heme. The role of the AI would therefore be to suppress CaM-free activity of nNOS in the conformation presented, and to allow the binding of CaM to activate the reductase domain.

1.7.3 C-terminal tail

Sequence alignment between CPR and NOSs at the C-terminal end (Figure 1.14) reveals that all of the NOSs are longer by 21-42 amino acids [36]. This has been designated as the C-terminal extension, or tail (CT), and is shortest in iNOS (21 amino acids) followed by nNOS (33 amino acids) and eNOS (42 amino acids).

CPR 671 RYSLDVWS
(rat)
iNOS 1119 RYHEDIFGAVFSYGVKKGNALEEPKGTRL
(human)
eNOS 1153 RYHEDIFGLTLRTQEVTSRIRTQSFSLQERQLRGAVPWAFDPPGSDTNSP
(human)
nNOS 1389 RYHEDIFGVTLRTYEVTNRLRSESIAFIEESKKDADEVFSS
(rat)

Figure 1.14 Sequence alignment of CPR, iNOS, eNOS and nNOS at the C-terminal end. NADPH-binding domain residues are coloured magenta, C-terminal tail (CT) residues cyan.

Deletion of the tail affects the rate of electron transfer in all three isoforms. In iNOS, the truncated mutant had enhanced activity for all electron transfer reactions measured; cytochrome *c* reduction, NADPH oxidation and NO synthesis. Furthermore, the reduction of FAD by NADPH was faster than for the wild-type enzyme, as was the electron transfer between the flavins [104].

In the cNOSs the effect is slightly different; truncated nNOS was found to catalyse CaM-free cytochrome *c* reduction 21-fold faster than the wild-type enzyme. This was then decreased by the binding of CaM, down to the activated wild-type level. NO synthesis was observed in the absence of CaM, but the rate was decreased relative to the wild-type level in the presence of CaM, presumably due to uncoupled NADPH oxidation as the flavin cofactors reacted more rapidly with oxygen. Ferricyanide reduction activity and flavin reduction by NADPH were both increased in the absence of CaM, and the FMN cofactor no longer formed an air-stable semiquinone species [105]. These results indicated that the CT plays an important role in the regulation of

electron transfer between the flavins and also in the protection of the cofactors from solvent exposure and therefore access to oxygen.

Further investigation involved the addition of the tails from each isoform of NOS to CPR [106]. In all cases the cytochrome *c* reduction activity of the chimeras was lowered relative to CPR, with the iNOS tail having less effect than the nNOS, and the eNOS the most disruption, consistent with their length and the activity of the isoform. The addition of the tails was also found to have an effect in fluorescence spectroscopy studies, indicating a conformational change. A related investigation placed the reductase domain of CPR into a chimera with nNOS and this yielded an enzyme that was more active in electron transfer and NO synthesis than any other [107].

Deletion of the CT was coupled with deletion of the AI and this doubly truncated nNOS had no CaM dependence on reductase activity, which compares with inhibition for CT deletion and slight activation for AI deletion. Removal of both of the features yielded a mutant that reduced cytochrome *c* at the activated wild-type rate [108]. Ferricyanide reduction was investigated in detail and it was reported that previous measurements (i.e. those in Table 1.1) were not carried out at saturating concentrations. The use of 2mM ferricyanide in this study resulted in rates of reduction greater than $500s^{-1}$. Furthermore, the effect of CaM was ascribed to only lowering the binding constant, i.e. increasing the affinity of ferricyanide for nNOS; there was no change in the maximal rate. Wild-type and AI-truncated nNOS exhibited this CaM-mediated effect, while the CT-truncated or double-truncated enzymes were equally accessible to ferricyanide in the absence and presence of CaM.

NO synthesis in the double-truncated mutant still requires CaM for maximal activity, but this could be supported by a mutant of CaM that was a fusion of two C-terminal lobes. This is the part of CaM that has higher Ca^{2+}-affinity and binds near to the oxygenase domain of nNOS. The mutant CaM did not activate wild-type nNOS, which effectively means that any interaction between the N-terminal end of CaM and nNOSrd is not required when the AI and CT are deleted. All of this evidence led to the proposal that the AI and the CT interact with each other in the resting state, and then they interact with CaM, when it binds, to activate the enzyme.

Referring to the crystal structure of nNOSrd [74], the CT contains an α-helix which fits into a negatively-charged groove across the FAD-FMN interface area, shielding the flavins from solvent (Figure 1.15). The ordered CT residues extend from the last

β-strand of the NADPH-binding domain and form a right-angled turn followed by the α-helix. The first four residues are tethered to the FMN- and NADPH- binding domains by hydrogen bonds and to the NADPH molecule through interactions between the 2'-phosphate group and Arg1400, an important residue that is conserved in the constitutive NOSs.

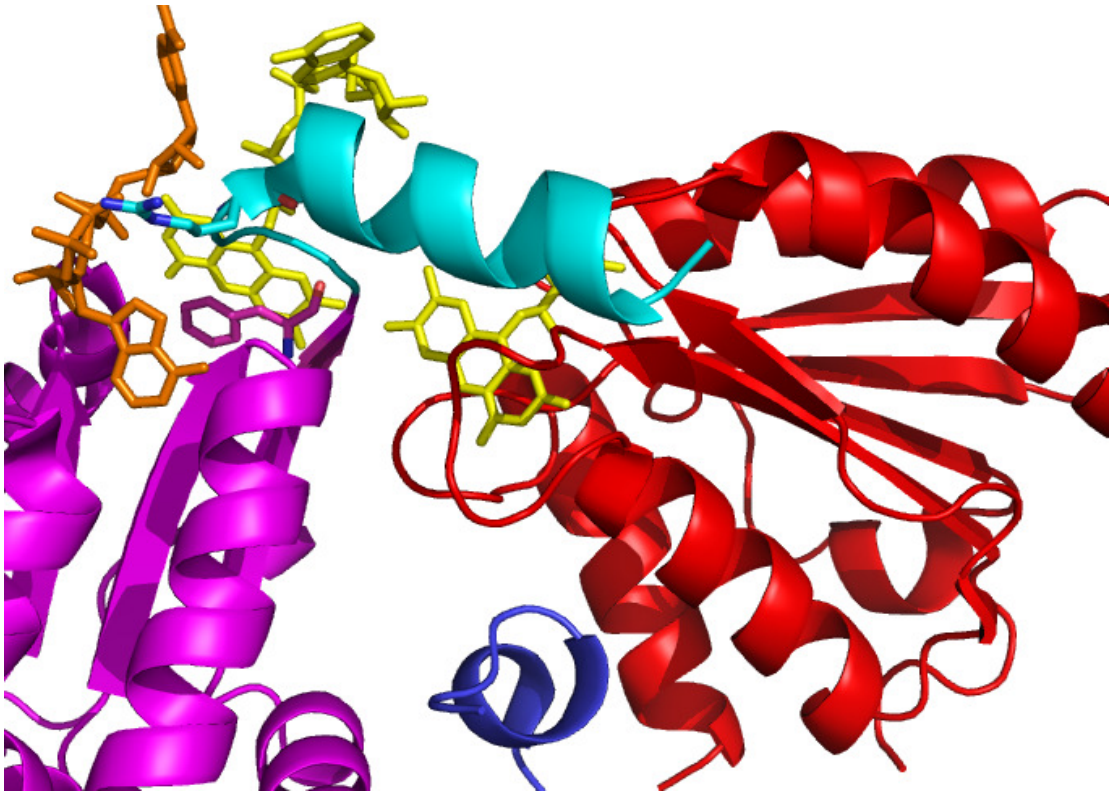

Figure 1.15 C-terminal extension in nNOSrd (PDB code 1TLL). Bound flavin cofactors are coloured yellow, NADPH orange, FMN-binding domain red, NADPH-binding domain magenta, AI loop blue, and CT cyan. Key residues Arg1400 (cyan) and Phe1395 (magenta) are shown in stick conformation. Other domains omitted for clarity.

Following on from the crystallographic studies, the specificity of the effect of the CT has been assessed by varying degrees of truncation in nNOS and nNOSrd [109]. In addition to removing the entire CT (residues 1396 to 1429), only the residues that were disordered in the crystal structure (1413-1429), and the residues that form the α-helix downstream from Arg1400 (1401-1429) were deleted. For cytochrome *c* reduction activity, there were differing trends observed between the independently isolated reductase domain and the holoenzyme, an indication that the CT plays different roles depending on the presence of the oxygenase domain. In general, increasing truncation caused greater rates of CaM-free cytochrome *c* reduction. In

particular, in nNOSrd the fully truncated mutant showed no difference between the CaM-free and CaM-bound states, while the holoenzyme construct was 2-fold faster in the absence of CaM. This was consistent with the previous studies on the deletion mutant. NO synthesis rates were slowed according to the degree of truncation when CaM was bound, due to increased uncoupled NADPH oxidation and therefore slower heme reduction, and only the completely tail-less mutant synthesised NO in the CaM-free state. The reduction of FAD by NADPH was analogous to wild-type nNOSrd in the two shorter truncations, while the complete deletion showed no regulation by CaM [109]. Apparently the latter half of the CT has no role in the suppression of catalysis; it is the α-helix that is the essential structural feature of the CT. This is coupled with the action of the amino acids immediately upstream from it to fully suppress the CaM-free activity of nNOS.

In summary, the CT is crucial to the regulation of electron transfer through nNOSrd. This is confirmed by the rapid activity of the truncated CaM-free mutants, the specificity of the tails from the different isoforms, and the speculated interactions between the CT, the AI and bound CaM.

1.7.4 Phosphorylation and protein-protein interactions

Both of the inherent structural inhibitory features in the reductase domain are targeted by post-translational modifications. Protein kinase-catalysed phosphorylation occurs at Ser847 in the AI loop and Ser1412 in the CT of nNOS [110]. Phosphorylation at the analogous CT site in eNOS caused an increase in NO output, while substitution of the residue with alanine stopped phosphorylation [111]. Substitution of the CT serine by aspartate mimicked the negative charge placed on the residue by the kinase and replicated the effect of activation by phosphorylation, with increased NO synthesis and cytochrome *c* reductase activity [112]. Furthermore the Ca^{2+} affinity of the enzyme was increased, indicating an effect on CaM-binding affinity. It was speculated that the phosphorylation site was a key target for regulation, linked to the action of the CT. This was confirmed by an eNOS mutant that lacked the 27 amino-acids downstream of the serine, which had similar properties to the aspartate mutant;

increased Ca^{2+} affinity, NO synthesis and cytochrome *c* reductase activity [113]. It is probable that the phosphorylation event serves to reposition the CT and therefore increase electron flux through the enzyme.

The corresponding substitution was made in nNOS, S1412D, and this yielded an enzyme with reductase activities, both cytochrome *c* and ferricyanide, that were twice as fast as for the wild-type enzyme [46]. The rate of pre-steady-state flavin reduction was increased in the CaM-free state, while heme reduction was consistently faster than in the wild-type enzyme by 1.5-fold, and the mutant had an increased sensitivity to Ca^{2+}.

Modification of the serine within the AI loop has a more complicated effect than simple activation. It was found to be phosphorylated by a number of CaM-dependent protein kinases, which led to a decrease in NO synthesis and cytochrome *c* reduction rates, an effect attributed to the suppression of CaM binding [114].

A further site was identified in eNOS, a threonine within the CaM-binding region where phosphorylation resulted in the inhibition of NO synthesis [115]. This implicates a balance of positive and negative effects regarding the phosphorylation of eNOS whereby multiple protein kinases and phosphatases may act on the enzyme to stimulate or inhibit NO production by Ca^{2+}/CaM-independent methods.

1.7.5 Hinge region

The strand of protein linking the FMN domain and the connecting domain in the crystal structure of nNOSrd was found to be flexible and denoted as the "hinge" [74]. Also of note in the connecting domain is a "small insertion" (SI) of 7 residues that forms part of a β-hairpin. Both of these features are depicted in Figure 1.16. There is no homology in the SI region between the isoforms, and replacement of the eNOS SI by the iNOS version yielded a mutant that was activated at 5-fold lower Ca^{2+} concentration but did not have any significantly altered catalytic activity [116]. This would indicate that the SI is not as important as either the AI or the CT. Complete deletion of the nNOS SI decreased cytochrome *c* reductase activity, while half deletion of the SI or the substitution of a key glycine gave a slight increase in

reductase activity with no change in CaM-sensitivity [117]. Again, these effects are much slighter than for the other autoinhibitory elements.

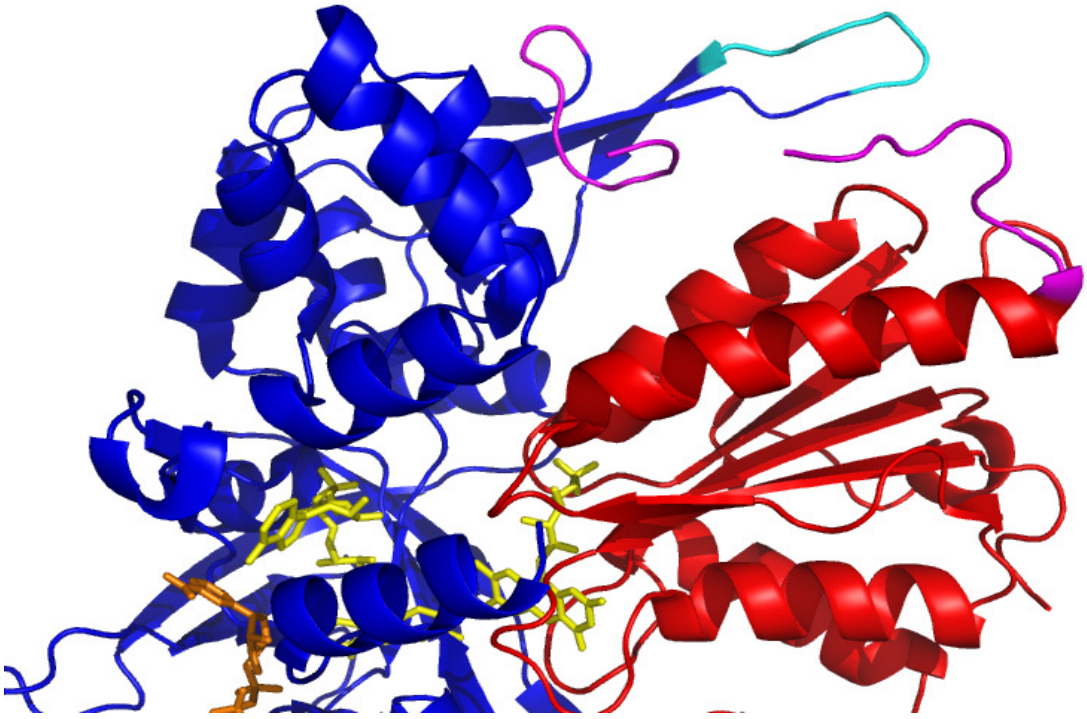

Figure 1.16 Hinge region of nNOSrd (PDB code 1TLL). Bound flavin cofactors are coloured yellow, NADPH orange, FMN-binding domain red, connecting/NADPH/FAD-binding domains blue, hinge region magenta and small insertion (SI) cyan.

The importance of the hinge region was investigated by creating an eNOS chimera containing the nNOS hinge. This results in a 4-fold increase in NO synthase activity, up to two-thirds of the nNOS level [118]. Also studied was a proline residue in eNOS that was substituted by isoleucine, while the corresponding isoleucine in nNOS was changed to proline. The eNOS single mutant was more active than wild-type eNOS and the nNOS single mutant was less active than wild-type nNOS, consistent with the role of the proline in restricting flexibility. NADPH oxidation and heme reduction correlated with NO synthesis and the coupling in the eNOS chimera was actually better than in wild-type eNOS.

Flavin reduction rates in the hinge mutants were unaffected, while cytochrome *c* reduction activities were altered according to the same trend as NO synthesis but to a lesser extent, with the eNOS chimera more akin to eNOS than nNOS. In contrast, its NO synthesis rate resembled that of an eNOS chimera with the entire nNOS reductase domain [37]. The other regulatory features in the reductase domain have a greater

impact on specific reductase activities rather than NO synthesis. The opposite case with the hinge region implies that its role is specifically centred on the interaction between the FMN-binding and oxygenase domains.

1.7.6 FMN accessibility

Activation of the holoenzyme by CaM is achieved by the triggering of flavin to heme electron transfer [30]. This has been further assigned to a specific motion of the FMN-binding domain relative to the other constituent parts of the reductase domain, allowing the electron acceptor access to the bound FMN cofactor [76]. This accessibility was investigated in the isolated reductase domain by the pre-steady-state reduction of cytochrome *c* by fully reduced (i.e. chemically 4-electron-reduced) wild-type nNOSrd [119]. This first order reaction provides insight into the ease of interaction between the bound FMN cofactor and the exogenous cytochrome *c* molecule. It was found that the binding of CaM caused a 2.5-fold increase in the second order rate constant associated with the reduction of sub-stoichiometric amounts of cytochrome *c*, which suggested that there was an increase in the accessibility of FMN to the electron acceptor upon CaM-binding. The more interesting results, however, came in experiments with NADPH added; when NADPH was bound to the CaM-free enzyme, the rate constant was 14-fold lower than in the corresponding NADPH-free experiment. The CaM-bound enzyme was unaffected by the binding of NADPH, which indicated that the FMN is much less accessible to the electron acceptor when NADPH is bound, and that this "locked" conformation is relieved by the binding of CaM. This was confirmed by performing the same accessibility experiment with the isolated FMN-binding domain. The rate of electron transfer was the same in the smaller construct and in CaM-bound nNOSrd [120]. According to the relative cytochrome *c* reduction rates the FMN is fully accessible when CaM is bound, 45% accessible in the absence of CaM, and only 3% accessible when NADPH is bound and CaM is not.

The specificity of the inhibitory effect of β-NADPH was examined by comparing the binding effect of analogues [120]. α-NADPH and 2'5'-ADP only induced a 50%

drop in rate in comparison to the natural substrate, while 2'5'-ATP-ribose only lacks the nicotinamide substituent so had a greater effect, 75%. β-NMN (nicotinamide mononucleotide) caused a 60% inhibition which was surprising given that it has no adenosine group. Furthermore, the binding of CaM did not fully relieve this effect. β-NAADP$^+$ contains nicotinic acid instead of the amide group, and failed to inhibit at all. This means that the simple change of the nicotinamide to carboxylic acid abolishes the locking effect. The full lock could not be replicated by any combination of analogues, even 2'5'-ATP-ribose with nicotinamide, or 2'5'-ADP plus β-NMN. Clearly in β-NADPH the weakly-bound nicotinamide substituent has an important role to play. Further evidence of the specificity was found in a study with full-length nNOS and eNOS [121], where analogues with only the adenine moiety of NADPH competitively inhibited the binding of β-NADPH and activated NO synthesis activity. The binding of NADPH to the protein backbone of nNOSrd is clearly visible in the crystal structure [74], with contacts made between the adenosine group and the residues Ser1313, Arg1314, Tyr1322, and Arg1400, as presented in Figure 1.17. The first three of these residues are a conserved triad that determine NADPH binding affinity and selectivity in related flavoproteins [122, 123]. The nicotinamide group of NADPH is solvent-exposed and is bound away from the FAD cofactor where it must stack to facilitate hydride transfer, meaning it is flexible and must rotate to deliver a hydride efficiently.

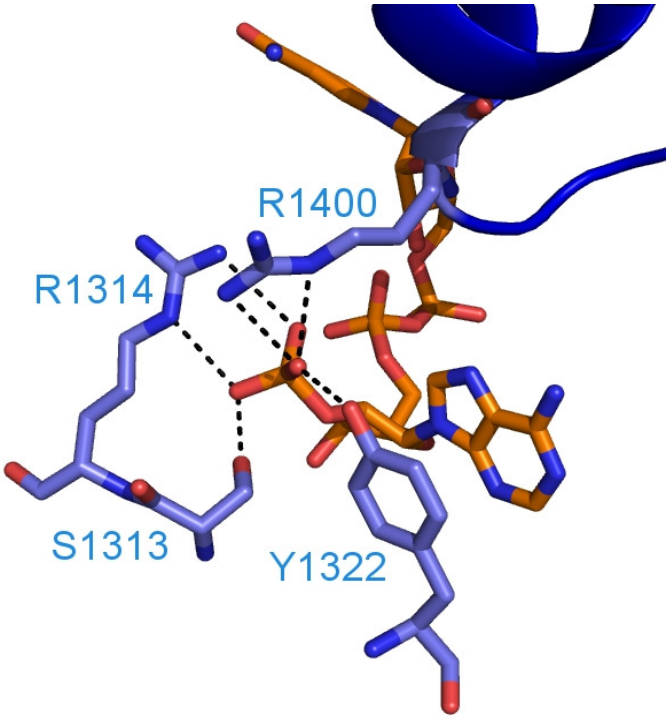

Figure 1.17 NADPH binding in nNOSrd (PDB code 1TLL). NADPH and backbone residues are shown in stick conformation and coloured orange and blue respectively. The CT is shown in blue ribbon format.

Arg1400 is unique to the cNOSs (it is a serine in iNOS), and the effects of substitution by serine and glutamate were studied in both the holoenzyme and nNOSrd [124]. NO synthesis was slower in the Arg1400-substituted mutants of nNOS but the corresponding NADPH oxidation rates were higher. Heme reduction was faster in the mutants, with the slowest NO synthesis rate correlating with the fastest rate of heme reduction (R1400E). The build-up of ferrous heme-NO complex was faster than for wild-type nNOS, but this could be attenuated by the use of different forms of CaM which supported differing rates of heme reduction, in accordance with the global catalytic model predicted for the S1412D mutant (see section 1.2.3).

Cytochrome *c* reduction was less repressed in the reductase domain mutants (4-fold and 2-fold activation by CaM), which could sustain a higher rate of turnover with NADH than with NADPH, with K_m values for both nucleotides being higher. Flavin reduction rates also reflected less repression in the CaM-free state for the R1400S mutant and no repression for R1400E. NADPH binding caused an increase in the rate of pre-steady-state cytochrome *c* reduction for both mutants, rather than a decrease such as that observed for the wild-type enzyme [124].

The interaction between the phosphate group of NADPH and Arg1400 causes specificity for the nucleotide over NADH, and also forms part of a longer-range effect on the suppression of electron transfer that starts at the hydride source, is mediated through the CT which includes Arg1400, and ultimately affects the movement of the FMN-binding domain and its accessibility to heme electron acceptors.

1.7.7 Hydride transfer

The first step in the catalytic action of nNOSrd is the transfer of hydride from the nicotinamide group of NADPH to the N5 position of the bound FAD cofactor. This event is activated by CaM-binding (see Table 1.1) and also by the removal of the CT or charge reversal at Arg1400 in the CaM-free state. In order to achieve the hydride transfer, the NADPH must re-orientate from the non-productive conformation observed in the crystal structure of nNOSrd [74], and π-stack to the re-face of FAD. The motion of the nicotinamide group must also occur in CPR and FNR, where the presence of a conserved aromatic residue was found to be important [125]. Figure 1.18 presents the interaction between bound NADPH and FAD in CPR, with the highlighted residue Trp677 π-stacking with the re-face of FAD. Deletion of the tryptophan, on the right hand side of the picture, allowed the nicotinamide to stack productively, where key residues Cys630 and Ser457 are within hydrogen bonding distance of the NADPH and FAD respectively. The W677X mutant's catalytic activity was unaffected in terms of electron transfer, but the NADPH affinity was altered [126].

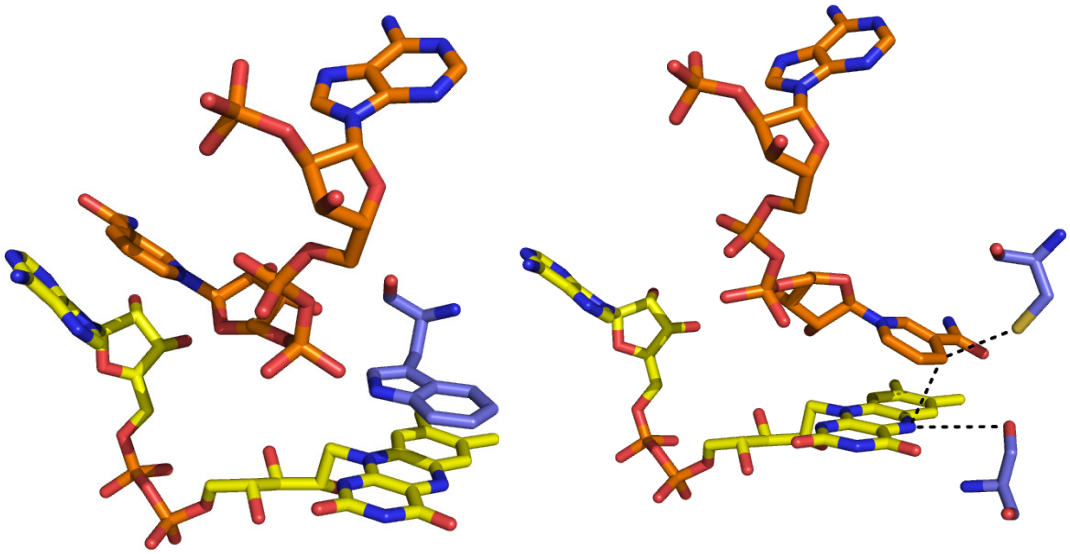

Figure 1.18 FAD-active sites of CPR mutants S457A/C630A/D675N (PDB code 1JA1, left) and W677X (1JA0, right). FAD is coloured yellow, NADPH orange, backbone residues blue. Key interactions are marked with black dashed lines

In nNOS the aromatic residue, equivalent to Trp677, is Phe1395 which is the last residue in the NADPH-binding domain before the CT, and was observed to perform the same shielding role at the re-face of FAD in the first crystal structure of nNOSrd (the FAD/NADPH binding domains only [73]). Mutational studies were made in the nNOS holoenzyme; F1395Y which only slightly altered the aromatic character of the side chain, and F1395S which completely abolished the π-stacking interaction [127]. The properties and activity of the F1395Y mutant were very similar to wild-type nNOS, as expected. The F1395S mutant caused an increase in CaM-free cytochrome *c* reduction activity, by a factor of 4 relative to the wild-type enzyme, and also had slow but detectable NO synthesis. The binding of CaM to F1395S nNOS did not cause an increase in reductase activity, and only enhanced NO synthesis to 10% of the wild-type value. NADPH oxidation was extremely rapid and uncoupled, while the rate of flavin reduction lacked any repression in the CaM-free state. In contrast, heme reduction in the mutant was 800-fold slower than wild-type, indicating that the flavins are reacting with oxygen more rapidly [127].

Further studies of the F1395S mutation were made in the isolated nNOSrd, where the mutant's cytochrome *c* reductase activity was similar to that observed in the holoenzyme; 50% of the wild-type rate and showing no CaM-dependent enhancement [128]. Flavin reduction was also similar to that in the holoenzyme, with no repression of the rate in the absence of CaM. Pre-steady-state reduction experiments were

carried out using F1395S nNOSrd and it was found that the addition of NADPH did not fully repress electron transfer from the FMN hydroquinone species, which was a similar observation to that made in R1400E.

The $NADP^+$-affinity was measured and found to be increased relative to the wild-type enzyme, with a larger proportion stacked to the bound FAD cofactor. Furthermore, the $NADP^+$-dissociation rate was 8-fold slower in F1395S nNOSrd than in the wild-type, where CaM has no effect on the rate. This slow dissociation of $NADP^+$ is responsible for limiting the electron transfer activity of the mutant. The aromatic side chain of Phe1395 is an essential feature which represses the CaM-free activity of nNOS and also relieves the repression upon CaM-binding. This is another interaction that can be assumed to be mediated through the adjacent CT extension [128].

The π-stacking of Phe1395 to FAD in the crystal structure of nNOSrd [74] is represented in Figure 1.19, along with the cysteine and serine that are present in the same relative orientation as in CPR. Following hydride transfer between NADPH and FAD, electron transfer occurs between the two flavin cofactors rapidly and easily, as they are only approximately 5 Å apart, which leaves a proton to be removed from N5 of FAD before another catalytic cycle can occur. Ser1176 is within hydrogen bonding distance of N5 and of another conserved residue, Asp1393, which in turns forms interactions with His1032 and Arg1229, the surface-exposed residue that forms salt-bridging interactions at the FAD/FMN interface. This network of residues therefore serves as a putative proton transfer pathway between FAD and solvent.

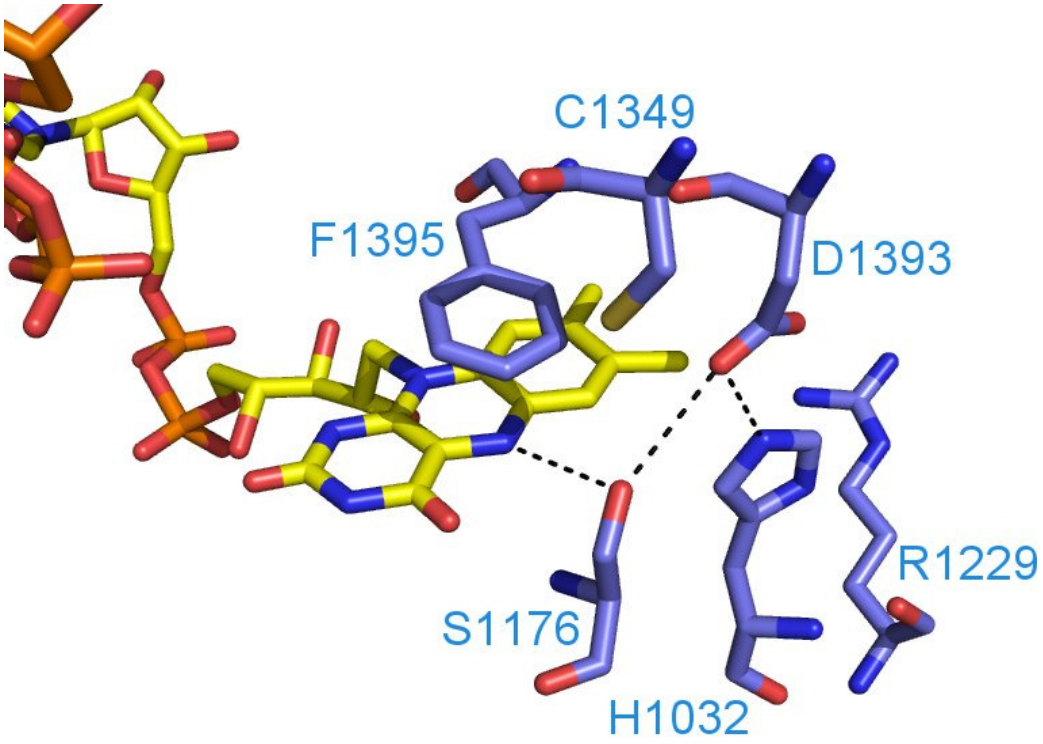

Figure 1.19 Interaction between bound FAD and backbone residues in nNOSrd (PDB code 1TLL). FAD is coloured yellow, NADPH-binding domain residues blue. Key interactions are marked with black dashed lines.

The conserved residue Ser1176 was substituted in nNOS by threonine, which retained the H-bonding properties, and alanine which abolished any interactions [129]. As expected, the effect of the S1176A mutation was greater, with lower cytochrome *c* reductase activity that was still CaM-sensitive, 20-fold slower ferricyanide reduction and 3-fold slower NO synthesis. S1176T, on the other hand, had similar NO synthesis rates to wild-type nNOS but 5-fold slower reductase activity. Rate constants for flavin reduction in the mutants were severely decreased compared to wild-type, but again were activated by CaM-binding. The midpoint reduction potentials of the flavin cofactors were measured by titration and there was little change for the threonine mutant, while S1176A nNOS destabilised the FAD semiquinone state. Clearly the hydrogen-bonding properties of the serine, with possible interactions to the FAD cofactor or to Asp1393, are crucial for stabilising hydride transfer to FAD during catalysis.

Asp1393 has been studied in both the holoenzyme and in nNOSrd. In the full-length study, substitutions were made with valine, asparagine and glutamate [130]. The D1393V substitution was particularly severe, with practically no reductase activity or NO synthesis observed, along with 1000-fold lower flavin reduction than wild-type

nNOS. Clearly, the hydride transfer step is compromised by the lack of hydrogen-bonding ability in the D1393V mutant. The D1393E and D1393N mutants had low cytochrome *c* reductase activity which was enhanced by the binding of CaM. Their rates of NO synthesis were 3-fold lower than the wild-type enzyme, while they had good coupling of NADPH oxidation, and flavin and heme reduction rates showed a decrease in line with reductase activity.

The asparagine and valine mutants were further characterised in nNOSrd. In general, their activities were lower than in the wild-type enzyme, retained CaM-sensitivity, and were most affected in the D1393V mutant [80]. The D1393N mutant exhibited faster NADPH oxidation rates than wild-type nNOSrd in both the CaM-free and CaM-bound states, while its flavin reduction was affected in both the hydride transfer to FAD and the inter-flavin electron transfer step. Pre-steady-state cytochrome *c* reduction rates revealed that the binding of NADPH failed to produce the locked conformation seen in wild-type nNOSrd. The isolated FAD/NADPH-binding domains were used to characterise the thermodynamics of the bound FAD cofactor, and the D1393 mutants had a destabilised semiquinone state meaning that interflavin electron transfer would be less favourable than in the wild-type. These effects of Asp1393 could be related to the hydrogen-bonding interactions around the bound FAD cofactor, or its proximity to Phe1395 that also affects the repression of activity.

1.7.8 FAD/FMN interface

The two bound flavin cofactors in nNOSrd, FAD and FMN, are held in close contact so that they are only 4.8 Å apart in the crystal structure of nNOSrd [74] and can transfer electrons directly between each other. This means that the protein architecture that surrounds them must also come into close contact, and this interaction is stabilised by the presence of an electronegative patch of residues on the FMN-binding domain and a corresponding electropositive patch on the FAD domain. The electronegative region is analogous to the surface of the FMN-binding domain of CPR, where investigations into the interactions with oxygenase partners revealed the presence of two acidic clusters in the FMN-binding domain which were important for catalysis [131]. Cluster 1 was designated as three aspartates in succession and cluster

2 was a sequence of two glutamates and an aspartate. Sequence alignment with the NOSs revealed the conservation of two of the cluster 1 residues, along with an upstream phenylalanine. All three were found to be on the surface of the FMN-binding domain in the crystal structure of CPR, and it was thought that they would have the same function of controlling electron transfer to the heme domain in nNOS. However, substitution of any of the residues (Phe892, Asp918, and Glu919) by alanine in nNOS destabilised the binding of FMN to the enzyme [79]. These mutants had clearly compromised catalytic activities, however some interesting properties were noticed; CaM-free ferricyanide reduction and CaM-free flavin reduction by NADPH were activated compared to wild-type nNOS. This meant that the removal of the FMN cofactor at the interface affected hydride transfer to the FAD cofactor.

The electronegative patch in nNOS was identified from the crystal structure [74] and consists of six residues; Glu762, Glu789, Glu790, Asp813, Glu816 and Glu819, all of which were substituted to either reverse their charge (substitution by arginine), neutralise it (asparagine) or to remove the functionality (alanine). The cytochrome *c* reductase activities of the resulting nNOS mutants were all greater than wild-type in the CaM-free state and they were all sensitive to the binding of CaM [81]. There was a range of CaM-bound reductase activities relative to wild-type, from 65% up to 180%, and they all oxidised NADPH at a faster rate than wild-type in the absence of CaM, but had no detectable CaM-free NO synthesis. Only one mutant had greater CaM-bound NO synthesis activity than the wild-type enzyme, this being the E762N charge neutralisation mutant form. Notably, all of the mutants had slower heme reduction rates than wild-type nNOS and some of them had extremely large uncoupling of NADPH oxidation.

Overall, it was reported that the greatest effects were seen in the Glu762 mutants, followed by Glu816 and Glu819. Referring back to the crystal structure [74], Figure 1.20, it can be seen that these three residues are the ones in closest contact with Arg1229 from the FAD domain. While Glu816 is closest to the arginine in the published version, a small motion of the FMN-binding domain would allow either of the other two residues to form salt-bridging interactions.

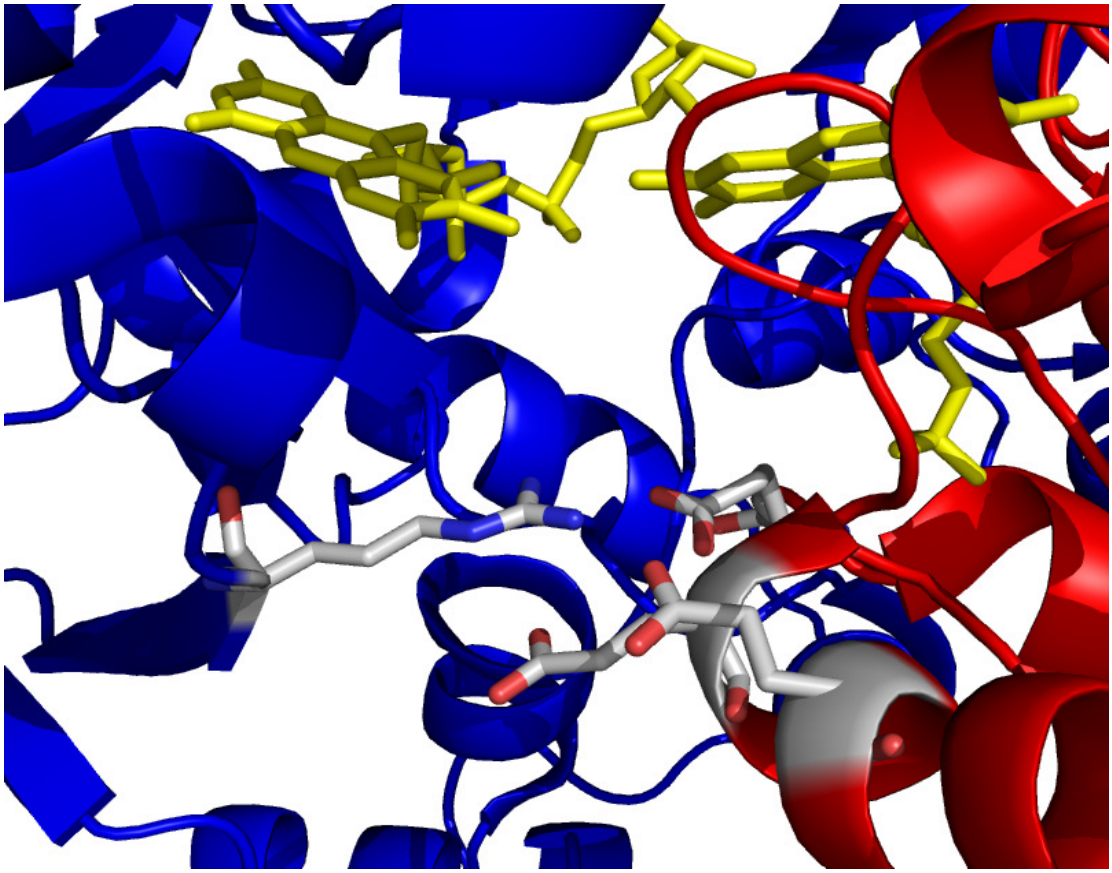

Figure 1.20 Interface region between FAD- and FMN- binding domains in nNOSrd (PDB code 1TLL). Bound flavin cofactors are coloured yellow, FMN-binding domain red, connecting/NADPH/FAD-binding domains blue. Key residues Arg1229, Glu762, Glu816, Glu819 are present in stick conformation.

In addition to direct interactions that can be observed in the crystal structure, the interface region between the FMN- and FAD- binding domains in nNOSrd includes the unique regulatory features; the SI, AI and CT, as well as the bound flavin cofactors themselves. This infers that any motion at the interface can be linked to the regulation of hydride transfer by NADPH, through the CT, Arg1400, Phe1395 and phosphorylation events. Additionally the H-bonding network from FAD to the surface at Arg1229 will be involved in this interface.

Interactions between the AI and CT have been predicted to occur in the absence of CaM [108], while the binding of CaM to its recognition site may form new interactions, remove the regulatory features from the interface and cause motion which ultimately results in the "unlocking" of nNOSrd and the movement of the FMN-binding domain, a crucial step in the catalysis of NO from nNOS.

1.8 Aims of the thesis

The regulation of NO synthesis by the constitutive NOSs is fundamentally important, as the over- or under- production of NO in the central nervous system or the cardiovascular system could be fatal. Due to the biological implications of the production of NO, the regulation of nNOS is an extremely complex sequence of events, where a key number of questions remain to be answered:

1. **How does CaM activate nNOS?**

   It is known that the binding of CaM initiates the flow of electrons through nNOS as a consequence of a structural rearrangement in the di-flavin reductase domain. However, the exact nature of this step remains unknown. Studies focussing on the effect of CaM on the reductase domain catalytic events will be used to address this.

2. **Which individual steps are affected?**

   Within the reductase domain, CaM has been reported to be able to activate the hydride-transfer step, the interflavin electron transfer step, and the flavin to heme electron transfer step. Each of these has been speculated as being the rate-limiting step, but it could feasibly be another event such as productive stacking between nucleotide and flavin, which has also been investigated previously. Detailed stopped-flow analyses and kinetic isotope effects in this study reflect on all of these events.

3. **How important is the FAD/FMN interface?**

   The interface region has been shown to contain the two flavin cofactors in close proximity, along with nNOS's unique regulatory features. These mobile pieces of protein architecture may interact with CaM and influence its activation of the reductase domain. The interface must also be affected by the redox state of the FMN cofactor, as it makes interactions with the protein backbone. Furthermore, the breaking of the salt bridge at Arg1229 affects the structure of the interface region, with knock-on effects on catalysis.

4. **Proton transfer pathway?**

The mechanism of hydride transfer is well understood, with NADPH moving from a non-productive to a productive conformation and the displacement of F1395. Following on from electron transfer events, the proton attached to FAD must be removed. The conserved residues S1176, D1393 and H1032 have a role to play in this step, as they are all closely interacting near to the bound FAD cofactor. Substitution of these residues to alter the H-bonding properties will alter the structure around the flavin cofactor, and affect the catalytic cycle of nNOSrd.

Chapter 2
Experimental procedures

2.1 Protein Expression

2.1.1 Plasmid DNA

The template used for the expression of mutants of recombinant rat nNOSrd was pCRNNR [77], which co-expresses residues 695-1429 of rat nNOS and bovine brain CaM, with carbenicillin resistance. Full-length nNOS, wild-type and R1229E, was made using the pCWori expression vector [75] which has carbenicillin and chloramphenicol resistance. Site-directed mutagenesis was carried out using the Stratagene QuikChange® XL site-directed mutagenesis kit. The primers used are listed in Table 2.1, where mismatches are underlined. pGroESL [132], which expresses chaperone proteins, was co-transformed into the *E. coli* strain with the nNOS expression vector.

Table 2.1 Primers and plasmids

mutant	primers	plasmid
R1229E	GTCCCCTGCTTCGTGGAAGGTGCCCCTAGCTTC GAAGCTAGGGGCACCTTCCACGAAGCAGGGGAC	pCM199 (rd) pCM226 (fl)
S1176A	CAGCCTCGCTACTACGCCATCAGCTCCTCTCC GGAGAGGAGCTGATGGCGTAGTAGCGAGGCTG	pCM198 (rd)
D1393E	CGGTACCACGAGGAGATCTTTGGAGTCACC GGTGACTCCAAAGATCTCCTCGTGGTACCG	pCM200 (rd)
H1032A	CCAGCCAGGGGACGCCCTGGGTGTCTTC GAAGACACCCAGGGCGTCCCCTGGCTGG	pCM194 (rd)
H1032E	CCAGCCAGGGGACGAGCTGGGTGTCTTCC GGAAGACACCCAGCTCGTCCCCTGGCTGG	pCM195 (rd)
H1032Q	CAGCCAGGGGACCAGCTGGGTGTCTTCC GGAAGACACCCAGCTGGTCCCCTGGCTG	pCM196 (rd)
H1032S	CCAGCCAGGGGACTCCCTGGGTGTCTTC GAAGACACCCAGGGAGTCCCCTGGCTGG	pCM197 (rd)

2.1.2 Cell transformation

Table 2.2 Media and agar	
LB-Agar	10 g/l bacto-tryptone 5 g/l yeast extract 5 g/l NaCl 15 g/l agar
Super Optimal Catabolite (SOC)	5 g/l bacto-tryptone 5 g/l yeast extract 10 mM NaCl 2.5 mM KCl 10 mM $MgSO_4$ 10 mM $MgCl_2$ 20 mM glucose
Terrific Broth (TB)	20 g/l bacto-tryptone 10 g/l yeast extract 4 ml/l glycerol 2.65 g/l KH_2PO_4 5.3 g/l K_2HPO_4
Preparation	Millipore Q Ultrapure water Autoclave sterilised at 121^{o}C, 20 mins (Kestrel LTE Scientific)

30 µl of competent *E. coli* BL21 (DE3) cells were thawed on ice and mixed with 5 to 10 ng of plasmid DNA in a volume of 1 to 5 µl. The mix was incubated for 30 minutes on ice before heat-shocking for 5 minutes in a 42 ^{o}C water bath and placing back on ice. 250 µl of warm SOC medium (Table 2.2) was added and this mixture was incubated at 37 ^{o}C for one hour at 225 rpm. Two LB-agar plates were prepared with 25 µg/ml carbenicillin and to these 10 µl or 100 µl of the transformation mixture was added, before incubation overnight at 37 ^{o}C.

2.1.3 Cell growth

Starter cultures were prepared with 35 ml of TB media, 50 μg/ml carbenicillin, and inoculated with single bacterial colonies using a sterile loop. These were grown overnight at 37°C, 200 rpm, and the resultant culture was used to prepare DMSO freezer stocks (77 μl DMSO per 1 ml culture).

Large scale growth was carried out in 1 litre baffled flasks, filled with 350 ml of TB, 50 μg/ml carbenicillin. These were inoculated with 1 ml of starter culture and grown at 37°C, 120 rpm. Optimal growth conditions varied for nNOSrd and nNOS preparations, with the nNOSrd expression strain requiring no induction of expression. In this case the bacteria were grown for 24 hours before harvesting.

In the preparation of nNOS, the antibiotics present were carbenicillin (25 μg/ml) and chloramphenicol (35 μg/ml), and the bacteria were grown until the optical density at 600 nm was approximately equal to 1. ATP and IPTG were then added to final concentrations of 1 mM and the temperature was decreased to 30 °C. The cells were harvested after 40 hours of growth post-induction, by centrifugation at 8000 rpm (Sorvall RC-5B centrifuge fitted with an SLA-3000 rotor, at 4°C) for 10 minutes, and frozen at -20°C.

2.2 Protein extraction and purification

2.2.1 Cell lysis

Table 2.3 Purification buffers	
Buffer A	50 mM Tris-HCl pH 7.5 100 mM KCl 5% glycerol 10 mM DTT 1 mM PMSF
Buffer B	50 mM Tris-HCl pH 7.5 100 mM KCl 2 mM DTT
Buffer C	50 mM Tris-HCl pH 7.5 100 mM KCl 10 % glycerol 1 mM DTT
Buffer D	50 mM Tris-HCl pH 7.5 1 mM $CaCl_2$
Buffer E	50 mM Tris-HCl pH 7.5 1 mM $CaCl_2$ 500 mM NaCl
Buffer F	50 mM Tris-HCl pH 7.5 1 mM EGTA

Frozen cell pellets containing nNOSrd, typically 25 g (wet weight), were defrosted and resuspended in 100 ml of buffer A (Table 2.3) containing 10 ml of protease inhibitor cocktail for non-His tagged proteins (Sigma-Aldrich) and 15 mM $CaCl_2$. Cells were disrupted by sonication on ice (MSE soniprep 150, 12-15 microns) for 8 × 10 seconds with 20 seconds rest between each burst. Soluble protein was separated from cell debris by centrifugation at 20000 rpm (Sorvall RC-26 fitted with an SS-34

rotor) for 1 hour at 4°C. The resulting supernatant had a further 2 ml of protease inhibitor cocktail added to it, along with 10 mM DTT, before further purification.
The same sonication protocol was carried out for the preparation of nNOS, however the lysis buffer in this case was buffer C augmented with 1 mM PMSF, 4 mM H_4B (Sigma-Aldrich) and 3 EDTA-free protease inhibitor tablets (Sigma-Aldrich).

2.2.2 Purification of nNOSrd

The purification of nNOSrd was carried out at 4°C, with the use of degassed buffer solutions and sealed columns such that they were always under a nitrogen atmosphere. Additionally, the preparation was carried out from start (the cell lysis stage) to finish (purified protein) in as short a time as possible, typically 8-10 hours.
Cell extracts were loaded onto a 15 ml 2'5'-ADP-agarose (Sigma-Aldrich) affinity column, pre-equilibrated with buffer A, 15 mM $CaCl_2$. Protein bound to the column in a dark green band was then washed with 50 ml buffer A plus 2 mM $CaCl_2$ and 100 ml buffer A with 1 mM EGTA to remove calmodulin bound to the reductase domain. This was followed by a further wash with 50 ml buffer A and 2 mM $CaCl_2$ before elution using 20 ml buffer A containing 2 mM $CaCl_2$, 20 mM $NADP^+$ (Sigma-Aldrich) and KCl made up to 500 mM.
The eluted protein was loaded directly on to a 10 ml calmodulin-agarose (Sigma-Aldrich) affinity column, pre-equilibrated with buffer A and 2 mM $CaCl_2$. Two washes were carried out; 100 ml buffer A plus 2 mM $CaCl_2$, and 50 ml buffer B. Elution was performed by using 20 ml buffer B supplemented with 0.5 mM EGTA and 400 mM KCl. nNOSrd was concentrated to approximately 40 μM using a Vivaspin 20 concentrator (Vivascience, cut off 30 kDa), flash-frozen in liquid nitrogen and stored at -80°C.

2.2.3 Purification of nNOS

This procedure was carried out at 4°C. The cell lysate was passed through a 10 ml diethylaminoethyl (DEAE) sepharose (GE Healthcare Biosciences) column, pre-equilibrated with buffer C. $CaCl_2$ was added to 5 mM prior to loading onto a 10 ml CaM-agarose column (as before). The bound protein was washed with 100 ml of buffer C and 1 mM $CaCl_2$, eluted with 50 ml buffer C plus 0.5 mM EGTA, concentrated and stored as for nNOSrd.

2.2.4 Purification of calmodulin

All of the washings collected from the 2'5'-ADP-column during the purification of nNOSrd were stored at -20°C and used in batches to extract the calmodulin that they contained.

After thawing, all fractions were treated with $CaCl_2$ to an approximate concentration of 10 mM prior to loading onto a 200 ml phenyl-sepharose column (Sigma-Aldrich), pre-equilibrated with buffer D (Table 2.3). Washings were then carried out with 1 litre of buffer D, 1 litre of buffer E and 1 further litre of buffer D. Calmodulin was eluted using buffer F, with 2 ml fractions collected. Fractions containing CaM were identified with SDS-PAGE (see section 2.3.1), pooled and dialysed against buffer D before freeze-drying (Edward Super Modulyo) and storage at -20°C.

2.3 Protein characterisation

2.3.1 Gel electrophoresis

Table 2.4 SDS-PAGE components	
Gel	Pre-poured NuPAGE® 4-12% Bis-Tris
Running buffer NuPAGE® MES SDS	25 mM Tris-HCl pH 8.3 192 mM Glycine 0.1% Sodium dodecyl sulphate
Sample buffer NuPAGE® LDS	50 mM Tris-HCl pH 6.8 100 mM DTT 2% sodium dodecyl sulphate 0.1% bromophenol blue 10% glycerol
Stain	0.25% (w/v) Coomassie Brilliant Blue 40% (v/v) methanol 10% (v/v) glacial acetic acid 50% (v/v) dH_2O
Destain	40% (v/v) methanol 10% (v/v) glacial acetic acid 50% (v/v) dH_2O

The purity of prepared protein samples was assessed by SDS-PAGE (sodium dodecyl sulphate polyacrylamide gel electrophoresis) in pre-cast gels (Invitrogen), as per table 2.4. Sample buffer (5 µl) was added to a 20 µl solution of protein before boiling for 5 minutes. Protein samples of 5 – 10 µl were loaded into the gel, with at least one well containing SeeBlue Plus 2® molecular weight markers (5 µl). The gel was resolved for 1 hour at 150V and stained using Coomassie Brilliant Blue.

2.3.2 UV-visible spectrometry

For calculations of co-factor concentrations, full range UV-visible spectra were recorded (250 – 800 nm) using either a Shimadzu 1601 or Cary Scan 50 spectrophotometer.

Prepared aliquots of nNOSrd were fully oxidised by the titration of sub-stoichiometric additions of potassium ferricyanide (Fisher scientific) and the concentration was calculated using the molar extinction coefficient (ε_{456}) of 20940 $M^{-1}cm^{-1}$ [120].

Analysis of the heme bound to full-length nNOS was carried out using the CO-bound spectrum. Enzyme samples were firstly fully reduced by addition of excess sodium dithionite (Fisher scientific) and the solution was then bubbled with CO gas (Sigma-Aldrich). The difference spectrum was calculated by subtraction of the reduced spectrum from the CO-bound, and the difference in absorbance between 444 nm and 467 nm was used to calculate concentration, with the molar extinction coefficient ($\varepsilon_{444-467}$) equal to 55000 $M^{-1}cm^{-1}$ [102].

2.4 Synthesis of NADPD

Samples were prepared in Tris-HCl buffer, pH 9, typically containing 2 mM $NADP^+$ (Sigma-Aldrich), 1 M d_6-ethanol (Sigma-Aldrich) and 20 units of alcohol dehydrogenase from *Thermoanaerobium brockii* (Sigma-Aldrich) in a 5 ml sample. Incubation took place at 42°C for 45 minutes and the UV-visible spectra were recorded to assess the increase of deuterated substrate by the appearance of an absorption maximum at 340nm. The enzyme in solution was removed by centrifugation at 3300 rpm (Falcon 6-300 centrifuge) with a Vivaspin 20 (Vivascience) concentrator, 10kDa cut off. The resulting mixture of $NADP^+$ and NADPD was then purified using a 1 ml Q-sepharose Resource-Q column on an FPLC (Fast protein liquid chromatography) system (AKTA P-900). The running buffer was 10 mM NH_4HCO_3 and after binding the nucleotides were eluted using a 50 column volume gradient of 500 mM NH_4HCO_3, collecting fractions of 1ml volume. The fractions were assessed for the presence of NADPD by recording their UV-visible

spectra and comparing the absorption at 260 nm (non-deuterated) and 340 nm (deuterated). The extinction coefficients are (ε_{260}) 18,000 $M^{-1}cm^{-1}$ and (ε_{340}) 6200 $M^{-1}cm^{-1}$ respectively [133], so all samples with a ratio of 260:340 less than 3 were pooled together for lyophilisation (Edward Super Modulyo) and storage at -20°C.

2.5 Steady-state kinetics

All steady-state kinetic experiments were performed at 25°C in 50 mM Tris-HCl buffer, pH 7.5, with the addition of 100 mM NaCl unless otherwise varied. Data were plotted and analysed using Origin 7.5 (Microcal).

2.5.1 Cytochrome *c* reduction

Solid cytochrome *c* from horse-heart (Sigma-Alrdrich) was prepared in the assay buffer at a range of concentrations (typically 1-100 μM) and incubated in a water-bath at 25°C. 1 ml aliquots were then treated with NADPH (final concentration 1 mM) and if appropriate, Ca^{2+} / CaM (100 μM / 10 μM). The reaction was initiated by addition of nNOSrd, typically at concentrations of 3 - 20 nM, but varying depending on the enzyme used. Monitoring was carried out on a UV-visible photospectrometer (as before) at 550 nm where the appearance of an absorption maximum is characteristic of the heme being reduced from ferric to ferrous form. The molar extinction coefficient for the absorbance change (ε_{550}) is 22640 $M^{-1}cm^{-1}$ [135], and the initial rate of turnover was used in each case to determine the observed rate constant at different concentrations of cytochrome *c*.

Turnover experiments with NADPD were carried out using a stopped-flow mixing method (see section 2.6 below) [136]. Syringe A contained NADPH or NADPD (2-10 μM) mixed with nNOSrd (0.1 μM) and syringe B contained ferric cytochrome *c* (100 μM). The reaction was monitored using the single wavelength apparatus over approximately 1 minute at 550 nm. The resultant traces of absorbance vs. time were

used to calculate the amount of substrate consumed in the reaction and this was converted to the rate of turnover by differentiating the graph using Origin 7.5 (Microcal). These traces could then be fitted to Equation 2.6 to give values for k_{cat} and K_m.

2.5.2 Ferricyanide reduction

Potassium ferricyanide (Fisher Scientific) was prepared in a similar manner to cytochrome *c* but a higher range of concentrations (typically 0.2 - 2 mM), while the amount of nNOSrd added to it in the assays was also higher (15 - 150 nM). The reaction was monitored at 420 nm, where the disappearance of the absorption band occurs as the electron acceptor is reduced. Initial rates were calculated with the molar extinction coefficient (ε_{420}) equal to 1010 $M^{-1}cm^{-1}$ [108].

2.5.3 NO synthesis

The rate of NO synthesis was determined by the NO-mediated conversion of oxyhemoglobin to methemoglobin. The assay consisted of 10 µM oxyhemoglobin, 100 µM NADPH, 10 units/ml superoxide dismutase and catalase (Sigma-Aldrich), 10 µM H_4B, 0.1 mM DTT, 1 mM L-arginine, 50 µg/ml CaM, 1 mM $CaCl_2$, in 50 mM Tris-HCl buffer, pH 7.5, and initiated with the addition of nNOS (20 nM). Monitoring of the reaction took place at 401 nm as an absorbance increase using a methemoglobin minus oxyhemoglobin molar extinction coefficient ($\Delta\varepsilon_{401nm}$) of 49000 $M^{-1}cm^{-1}$ [102].

2.6 Pre-steady-state kinetics

Stopped-flow analysis allows the rapid mixing of two solutions and the immediate monitoring of any spectral changes over the initial reaction period, illustrated in Figure 2.1. This method allows the measurement of reactions that occur on the millisecond timescale.

All pre-steady-state kinetic experiments were carried out at 25°C in an anaerobic glove box (Belle Technology, oxygen level < 5 ppm) using an SX.18MV stopped-flow spectrophotometer (Applied Photophysics) fitted with either a diode-array or single-wavelength detector. The assay buffer was 50 mM Tris-HCl, pH 7.5, 100 mM NaCl, degassed for two hours on the bench by bubbling with nitrogen gas and left to equilibrate in the glove box overnight. All reagents were put into the box in solid form and prepared in deoxygenated buffer, with the exception of nNOSrd which was in solution, then prepared as detailed for each experiment.

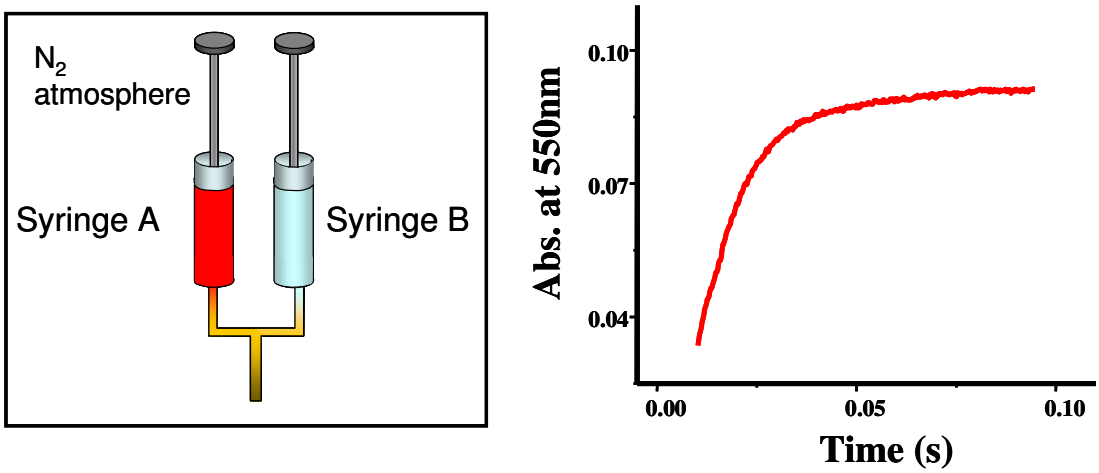

Figure 2.1 Representation of the stopped-flow apparatus for pre-steady-state experiments

2.6.1 Cytochrome *c* reduction

Syringe A contained ferric cytochrome *c* (from horse heart, as before), at a concentration of approximately 8 μM. Syringe B contained nNOSrd that had been fully reduced to the 4-electron-reduced form by addition of excess sodium dithionite and passed down a 10 ml G25-Sephadex (GE Healthcare Biosciences) column to remove excess reductant, with the resulting nNOSrd concentration approximately 20 μM. After mixing, cytochrome *c* accepts one electron from the bound FMN of nNOSrd which manifests as an increase in absorption at 550 nm. The single-wavelength detector was used to monitor this increase and produce an exponential curve from which the rate of electron transfer was calculated.

The enzyme was either reacted alone, or with the addition of NADPH (100 μM), Ca^{2+} / CaM (600 μM / 60 μM) or both NADPH and CaM. For the inhibition studies, ferrous cytochrome *c* was prepared using excess sodium dithionite and G25-Sephadex as for nNOSrd and added to syringe B prior to mixing.

2.6.2 Flavin reduction

Syringe A contained nNOSrd that was prepared in one of two ways. For the fully oxidised form, stock enzyme was treated with excess potassium ferricyanide (as before) before being passed down a 10 ml G25-Sephadex column. In the case of the one-electron reduced nNOSrd (FMN semiquinone form), the stock enzyme was initially passed down the G25-Sephadex column before stoichiometric titration with sodium dithionite until the absorbance at 592 nm was maximal (ratio of A_{456}:A_{592} approximately 4:1 in the case of the wild-type), using a Cary Scan 50 spectrophotometer inside the glove box. Typical enzyme concentrations were 20 μM prior to mixing and Ca^{2+} / CaM (600 μM / 60 μM) were added when required. This was then mixed with syringe B that contained NADPH at a concentration of 200 μM.

The reaction between NADPH and nNOSrd causes the reduction of the bound flavin co-factors that can be observed at both 457 nm and 592 nm using the diode-array

software. For more accurate measurement of the rate of reduction at 457 nm the single-wavelength apparatus was used. Inhibition studies again required the addition of ferrous cytochrome *c*, to the syringe containing nNOSrd.

2.7 Spectroelectrochemistry

The OTTLE (Optically Transparent Thin Layer Electrode) method allows the coupling of spectral changes to the application of a known potential to calculate the midpoint reduction potential of the cofactors in solution. The OTTLE cell is illustrated in Figure 2.2 and was constructed from a modified quartz EPR cell with a 0.3 mm path length containing a Pt/Rh (95/5) gauze working electrode (wire diameter 0.06 mm, mesh size 1024 cm^{-1}, Engelhardt), a platinum wire counter electrode (Sigma-Aldrich) and an Ag/AgCl reference electrode (model MF2052, Bioanalytical Systems). The reference electrode was calibrated against indigotrisulfonic acid (E_m = -99 mV vs SHE) and FMN (E_m = -200 mV vs SHE) and all resultant potentials were adjusted accordingly.

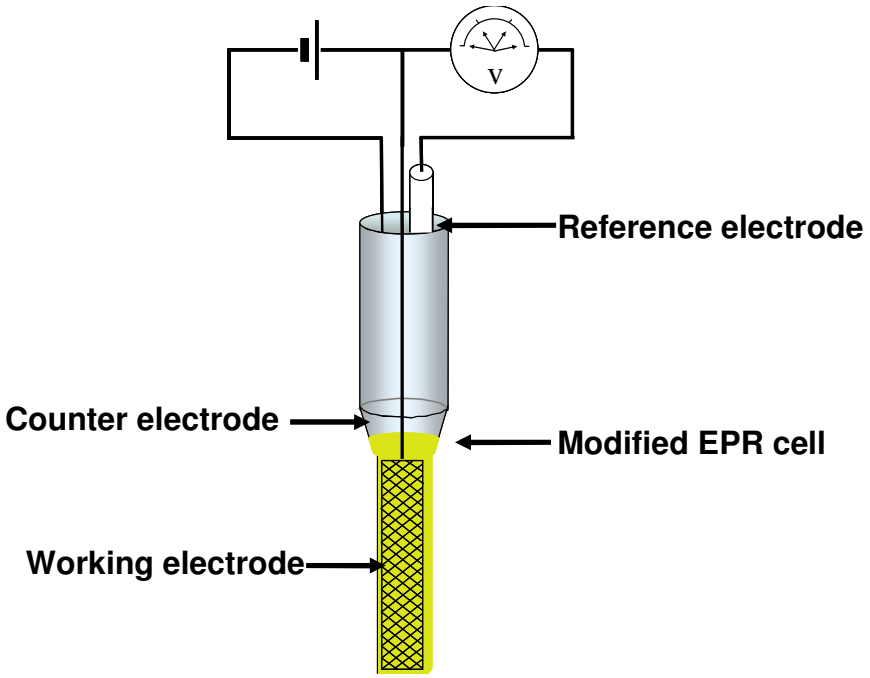

Figure 2.2 Representation of the OTTLE cell used for spectroelectrochemical experiments

Preparation of the OTTLE cell was carried out in an anaerobic glovebox (as before). Concentrated enzyme samples (1 ml × 300 μM) were passed down a G25-Sephadex column pre-equilibrated with sample buffer (100 mM Tris-HCl pH 7.5, 500 mM KCl, 10% glycerol) and had mediators added, as detailed in table 2.5. The working electrode was added to the protein solution in the cell, before layering with buffer (100 mM Tris-HCl pH 7.5, 500 mM KCl) and addition of the counter and reference electrodes. The OTTLE cell was then sealed and removed from the anaerobic environment before spectroelectrochemical titrations were performed using an Autolab PGSTAT10 potentiostat and a Cary Scan 50 spectrophotometer.

Table 2.5 Mediators used in OTTLE potentiometry

	Midpoint reduction potential vs SHE (mV)	Mass (Da)	Concentration used in ottle
5-hydroxy-1,4-naphthoquinone	-3	174	23μM
Pyocyanine	-34	210	19μM
2-hydroxy-1,4-naphthoquinone	-145	174	23μM
Flavin mononucleotide (FMN)	-200	478	8μM
Benzyl viologen	-311	409	10μM
Methyl viologen	-430	257	15μM

The potential of the working electrode was decreased in 30 mV steps until the enzyme was fully reduced and increased stepwise until re-oxidation was complete. During each equilibration the current and UV/Vis absorption spectrum were monitored until no further change occurred, a process that typically took 90-120 minutes. Absorbance changes associated with the oxidised flavins (456 nm) and the FMN semiquinone (592 nm) were plotted against the applied potential and fitted simultaneously to the modified Nernst equation (Equation 2.1) using Origin 7.5 (Microcal).

$$\frac{a\log_{10}^{-1}\left[\frac{E-E_1}{59}\right]+b+c\log_{10}^{-1}\left[\frac{E_2-E}{59}\right]}{1+\log_{10}^{-1}\left[\frac{E-E_1}{59}\right]+\log_{10}^{-1}\left[\frac{E_2-E}{59}\right]}+\frac{a\log_{10}^{-1}\left[\frac{E-E_3}{59}\right]+b+c\log_{10}^{-1}\left[\frac{E_4-E}{59}\right]}{1+\log_{10}^{-1}\left[\frac{E-E_3}{59}\right]+\log_{10}^{-1}\left[\frac{E_4-E}{59}\right]}$$

Equation 2.1 a,b,c = absorbance of oxidised, semiquinone and hydroquinone flavin. E = Potential of working electrode. E1, E2 = FMN transitions. E3, E4 = FAD transitions.

Chapter 3
Preparation and characterisation

3.1 nNOSrd

Wild-type and mutant forms of nNOSrd were purified as described in section 2.2.2, using ADP-agarose and CaM-agarose as reported previously [88, 119], with the additional use of de-oxygenated buffer solutions in order to maintain the bound FMN in the semiquinone form. This was found to be essential to attaining the maximal activity of nNOSrd, as the unintentional oxidation of the FMN cofactor during purification produced an enzyme with only 60% of the cytochrome *c* reduction rate of a 1-electron reduced form. During purification, the protein solution was green in colour, rather than the yellow of the fully-oxidised form, which allowed it to be easily monitored while bound to the affinity columns. Figure 3.1 depicts the SDS-PAGE analysis of a typical preparation, where from the cell free extract (lane 2) and the flow-through from the ADP-agarose column (lane 3) it can be seen that the majority of proteins in the *E. coli* cells did not bind and were collected and discarded after the first step in purification. The ADP-agarose wash with EGTA-augmented buffer removed CaM that was bound to nNOSrd and this was collected for subsequent purification (lane 4). Elution of nNOSrd from the ADP-agarose column was followed by direct loading onto the CaM-agarose column, and the flow-through from this column contained no other proteins (lane 5). The elution of nNOSrd from the CaM-agarose column was achieved with EGTA-augmented buffer (lane 6), after which the purified protein solution was concentrated if necessary and stored at -80^{o}C.

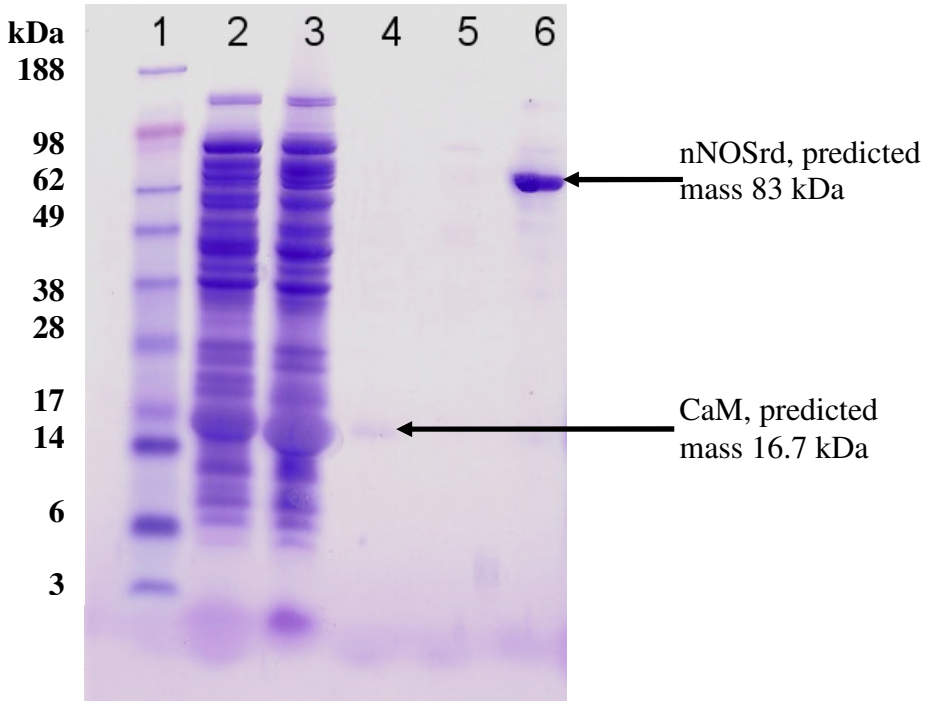

Figure 3.1 SDS-PAGE analysis of nNOSrd. Lane 1 = MW marker. Lane 2 = Cell free extract. Lane 3 = ADP-agarose flow through. Lane 4 = ADP-agarose wash with EGTA. Lane 5 = CaM-agarose flow through. Lane 6 = CaM-agarose elution

Each of the nNOSrd mutants R1229E, S1176A, D1393E, H1032S and H1032Q were purified in the same manner as the wild-type enzyme and they all formed single bands on a gel, as presented in Figure 3.2. The yields of protein prepared varied between wild-type and the mutant enzymes and are listed in Table 3.1. The H1032E and H1032A nNOSrd mutants were not expressed well in the BL21(DE3) *E. coli* cells and were not further investigated in this study.

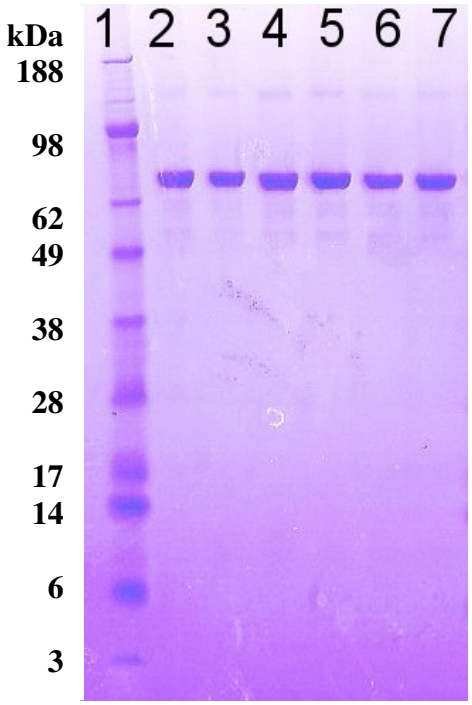

Figure 3.2 SDS-PAGE analysis of nNOSrd mutants. Lane 1 = MW marker. Lane 2 = wild-type. Lane 3 = R1229E. Lane 4 = S1176A. Lane 5 = D1393E. Lane 6 = H1032S. Lane 7 = H1032Q.

Table 3.1 Yield of wild-type and mutant forms of nNOSrd

Enzyme	wild-type	R1229E	S1176A	D1393E	H1032Q	H1032S
yield / mgl^{-1} of culture	9.1	7.5	6.0	4.5	3.2	3.0

The UV-visible absorption spectrum of the bound flavin co-factors was used to determine the concentration of wild-type and mutant forms of nNOSrd. The collected spectra are presented in Figure 3.3(A), where all of the mutants can be seen to have similar spectra compared to the wild-type enzyme. Titration with sodium dithionite solution was used to prepare the one-electron reduced FMN semiquinone form, as highlighted in Figure 3.3(B). Each addition of dithionite solution caused a decrease in absorption at 456 nm and an increase at 592 nm, to a maximum level where the ratio of the two peaks was approximately 4:1. All of the nNOSrd mutants were prepared in the one-electron reduced forms in the same manner.

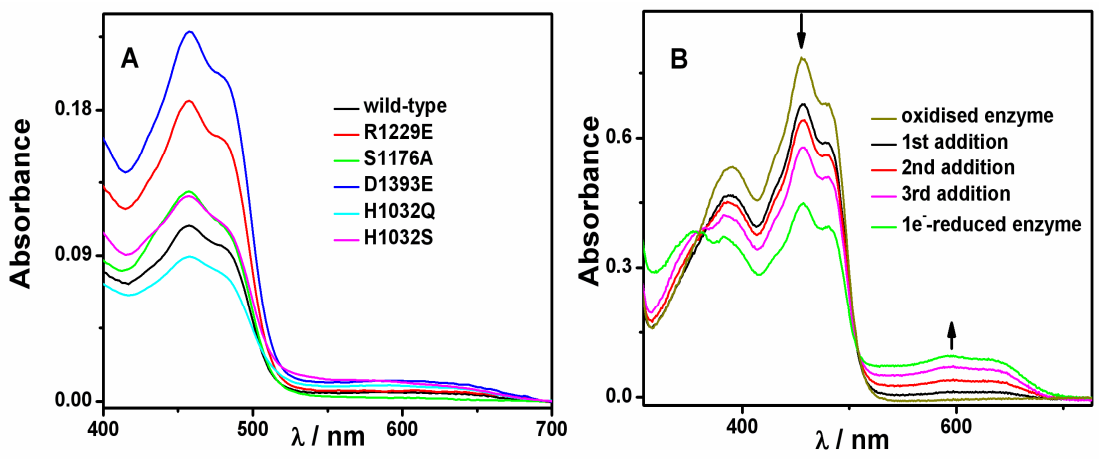

Figure 3.3 UV-visible absorption spectra of (A) wild-type and mutant forms of nNOSrd and (B) preparation of a one-electron reduced form of nNOSrd with the addition of 2 µl aliquots of 10 mM sodium dithionite.

3.2 nNOS

The wild-type and R1229E mutant forms of full-length nNOS were purified using DEAE-sepharose and CaM-agarose as described in section 2.2.3. The resulting enzyme samples were analysed using SDS-PAGE (Figure 3.4) and CO-binding UV-visible absorption spectrometry (Figure 3.5). The polyacrylamide gel shows the specificity of the CaM-agarose column; following the removal of a small number of proteins between the cell free extract (lane 2) and the DEAE-sepharose column (lane 3), the majority of proteins do not bind to the CaM-agarose and were present in the flow-through (lane 4). Elution of R1229E nNOS (lane 5), yielded a heterogeneous sample containing a large band at approximately 160 kDa, and two smaller bands at approximately 80 kDa and 60 kDa, representing the two domains proteolysed during purification. This was similar to a wild-type nNOS preparation (lane 6).

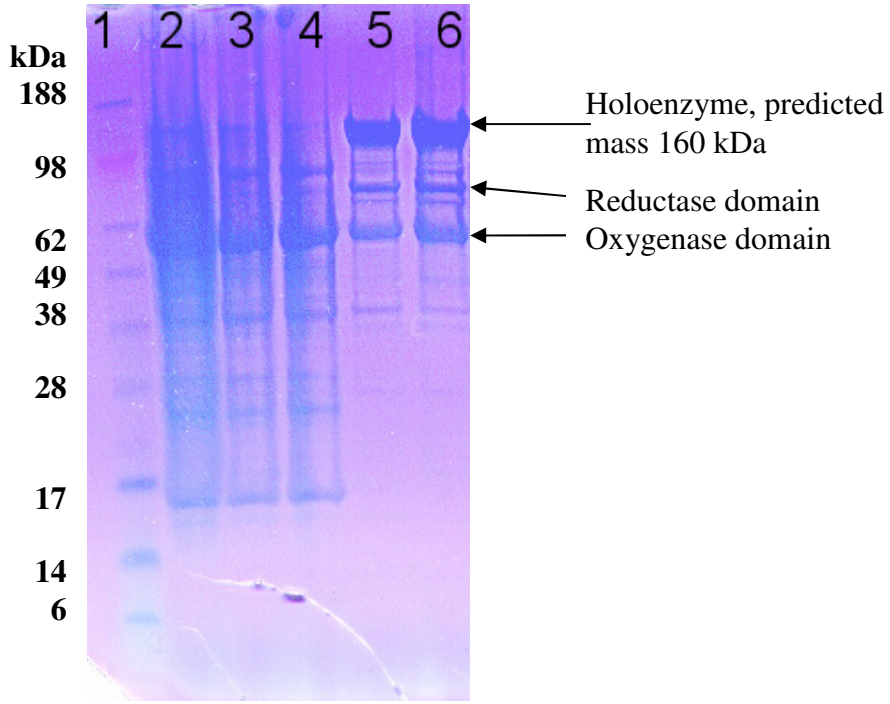

Figure 3.4 SDS-PAGE analysis of nNOS. Lane 1 = MW marker. Lane 2 = cell free extract. Lane 3 = DEAE-sepharose flow-through. Lane 4 = CaM-agarose flow-through Lane 5 = eluted R1229E nNOS. Lane 6 = wild-type nNOS.

Figure 3.5 is a plot the characteristic UV-visible absorption spectra of the ferrous form of nNOS before and after bubbling of CO gas to form the CO-bound spectrum. The difference spectrum, between the ferrous and ferrous-CO, was used to calculate the concentration of heme bound to nNOS.

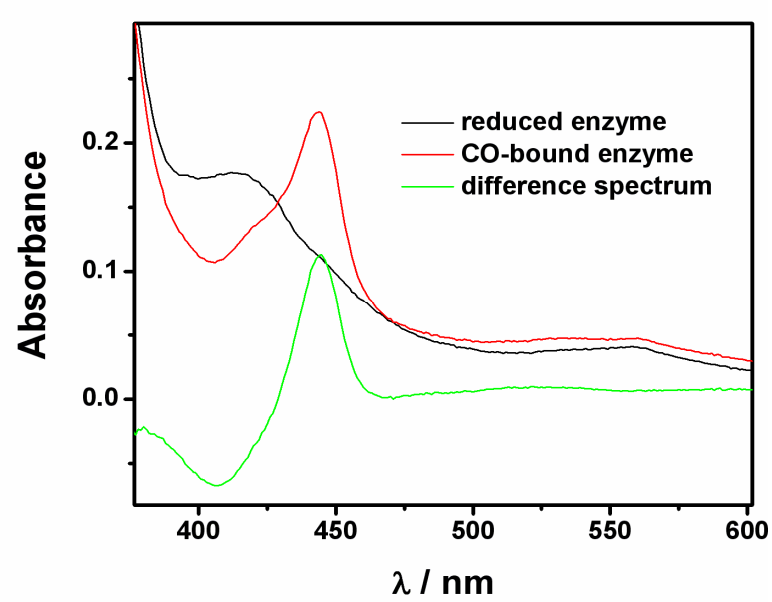

Figure 3.5 UV-visible absorption spectra of nNOS before and after the addition of CO gas

3.3 Calmodulin

Bovine brain CaM is co-expressed with nNOSrd in the plasmid pCRNNR [77] and was purified from washings of the ADP-agarose column during purification as described in section 2.2.4. Typically, 2 litres of solution were used to extract CaM in each purification. The fractions eluted from the phenyl-sepharose column were analysed using SDS-PAGE and the lyophilised CaM was assessed for activity in the steady-state turnover of cytochrome *c* by nNOSrd. Figure 3.6 shows the developed gel from a preparation, where the extracts from the nNOSrd preparation (lanes 1 and 2) were passed down the phenyl-sepharose with the majority of proteins not binding to the column. Following washes with high salt buffers to remove any other proteins bound (lanes 3, 4 and 5), buffer augmented with EGTA was applied to elute the purified CaM (lanes 6-11). Dialysis with a calcium-rich buffer was then used before lyophilisation and storage at -20^{o}C.

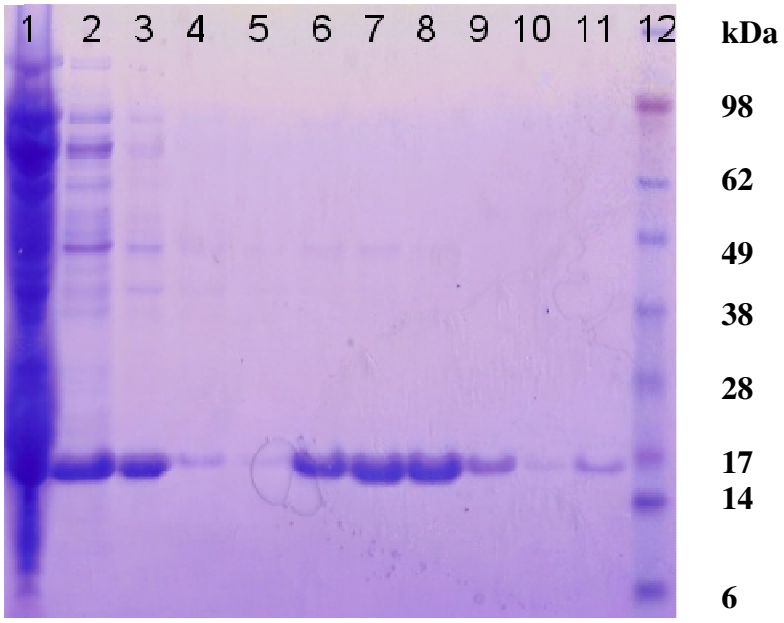

Figure 3.6 SDS-PAGE analysis of calmodulin. Lanes 1,2 = crude extracts. Lanes 3-5 = phenyl-sepharose washes 1-3. Lanes 6-11 = eluted fractions from phenyl sepharose containing purified CaM. Lane 12 = MW marker.

3.4 NADPD

The preparation of NADPD was carried out as described in section 2.4. Previous preparations [133, 137] using enzymatic methods have utilised a mixture of alcohol dehydrogenase and aldehyde dehydrogenase. Repetition of these conditions produced a mixture of product and starting material that could not be separated by liquid chromatography at varying pH. Thermophilic alcohol dehydrogenase (from *Thermoanaerobium brockii*) was used alone because the reaction that takes place produces only aldehyde product, rather than aldehyde and acid together. By not using the aldehyde dehydrogenase the yield of NADPD was lowered, so the equilibrium position was altered by increasing an excess of d_6-ethanol in the reaction. Figure 3.7 plots the UV-visible spectra obtained during a typical purification. The crude reaction mixture contains absorption maxima at 260 nm and 340 nm, while purified fractions of NADPD contain the same peaks in the correct ratio.

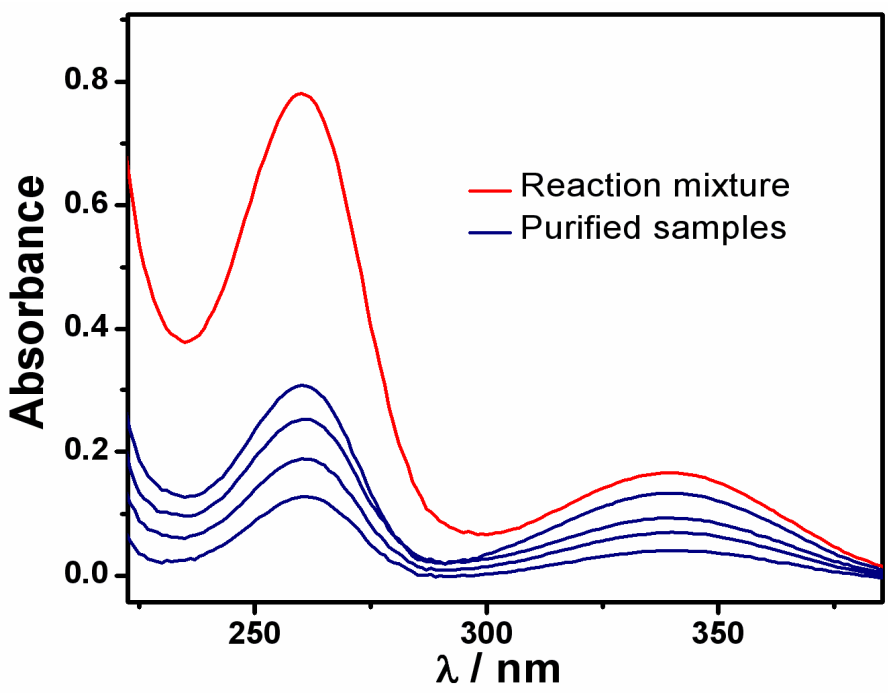

Figure 3.7 UV-visible absorption spectra from the preparation of NADPD.

Chapter 4
Calmodulin-mediated activation of nNOSrd

4.1 Introduction

The rate of NO production in nNOS correlates with the rate at which electrons are transferred from the reductase domain to the oxygenase domain [30], while the binding of CaM activates the transfer of electrons through the reductase domain in the holoenzyme and activates the isolated nNOSrd to the same extent [76]. This is represented in Appendix I.

The turnover of electrons through nNOSrd can essentially be divided into three steps, as illustrated in Figure 4.1. Firstly hydride transfer from NADPH to FAD (species 1 to 2), then internal electron transfer from FAD to FMN (2 to 3 and 4 to 5), and finally the transfer of an electron from hydroquinone FMN to an external electron acceptor or to the oxygenase domain of holo-nNOS (3 to 4 and 5 to 1). Each of these has been speculated to be the rate-limiting step in nNOSrd catalysis and the event activated by CaM [76, 90, 119], however the deprotonation of the FAD cofactor (species 4 to 5) may be important in the catalytic cycle. The aim of this chapter is to provide mechanistic detail into the activation of nNOSrd by CaM.

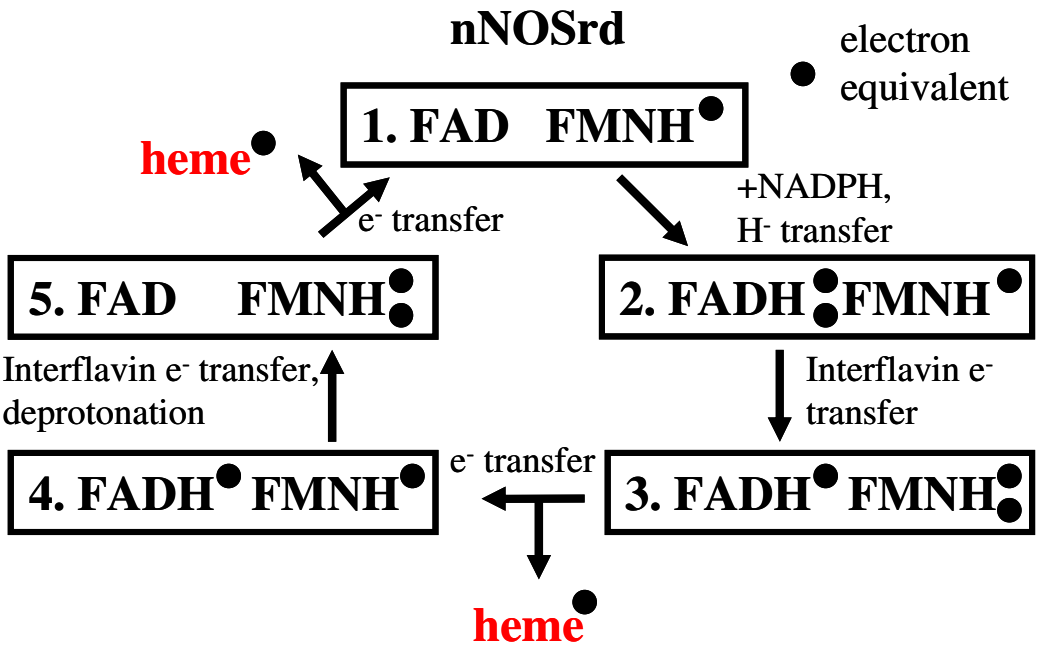

Figure 4.1 Schematic representation of electron transfer through nNOSrd during turnover reactions

4.2 Steady-state turnover

During the steady-state turnover of nNOSrd, cytochrome *c* reacts in the same manner as the oxygenase domain of nNOS, accepting a single electron from the bound FMN hydroquinone [75]. Ferricyanide, due to its smaller size, can accept electrons from both bound FAD and FMN [79], i.e. species 2 and 4, as well as 3 and 5 in Figure 4.1. Additionally, due to its high reduction potential (+430 mV vs. +250 mV for cytochrome *c* [138]), it can oxidise the stable FMN semiquinone and therefore probably react with all of the species present in Figure 4.1. This may lead to the faster rate of reduction of ferricyanide observed, and a lesser CaM-mediated activation effect, as summarised in Table 1.1.

4.2.1 Cytochrome *c* reduction

Previous studies of the steady-state reduction of cytochrome *c* by nNOSrd have shown a 10-fold enhancement on binding of CaM (see Table 1.1). This effect was consistent in the anaerobic preparation of nNOSrd from BL21 (DE3) *E. coli* in this study. Figure 4.2 plots the measured rate constants of cytochrome *c* reduction against cytochrome *c* concentration in the CaM-free and CaM-bound states. The data were fitted to the Michaelis Menten equation (Equation 6, Appendix I) and the derived kinetic parameters are listed in Table 4.1. The enzyme here retained the 10-fold enhancement effect by CaM while performing electron transfer at a faster rate than reported previously for nNOSrd [80], but analogous to a recent study of nNOS [81].

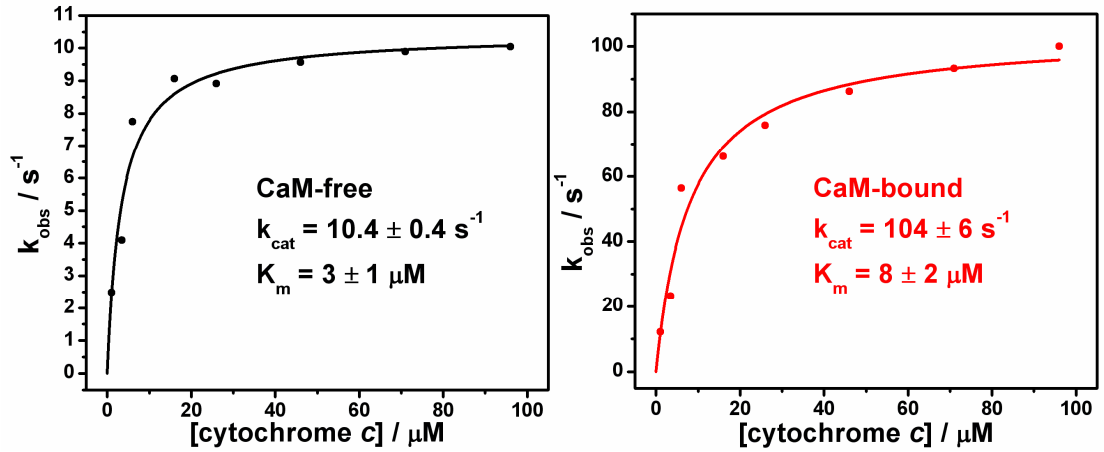

Figure 4.2 Steady-state cytochrome *c* reduction by nNOSrd. Assays were performed at 25°C in 50mM Tris buffer, pH 7.5 + 100mM NaCl. Data points were fitted to the Michaelis-Menten equation.

The effect of increasing salt concentration in the assay was studied, the results of which are plotted in Figure 4.3. Again the rate constants were fitted to equation 6 and the parameters are listed in Table 4.1. In all cases the affinity for cytochrome *c* decreased as the ionic strength increased, similar to the effect in holo-nNOS [139]. Increasing salt concentration in the assay buffer had little effect on the maximal rate of turnover when CaM was bound but an increase was seen in the CaM-free enzyme, which was 2-fold faster in the presence of 250mM NaCl. Thus there is a large decrease in CaM-dependent enzyme activation at higher ionic strength, indicating that the rate-determining step for steady-state cytochrome *c* reduction in the absence of CaM is ionic strength dependent.

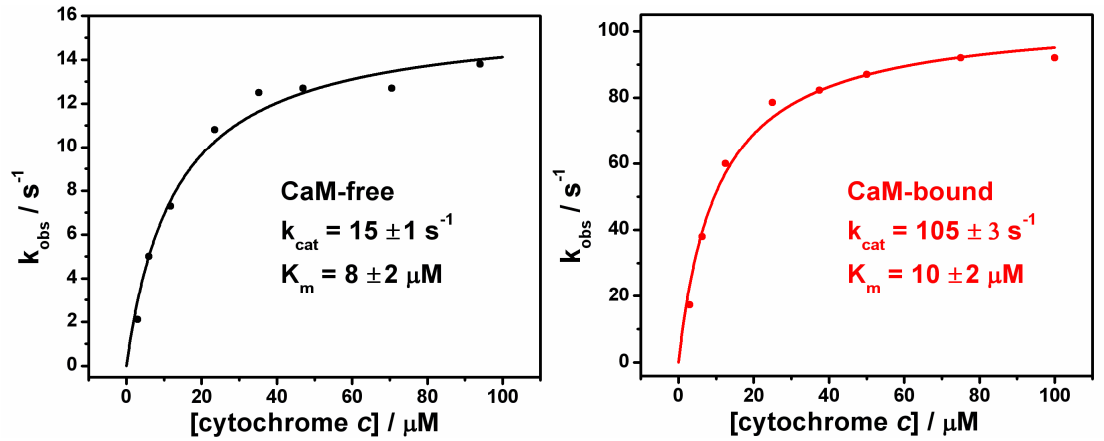

Figure 4.3 Steady-state cytochrome *c* reduction by nNOSrd with 150mM NaCl buffer. Assays were performed at 25°C in 50mM Tris buffer, pH 7.5 + 150mM NaCl. Data points were fitted to the Michaelis-Menten equation.

Table 4.1 Steady-state cytochrome *c* reduction by nNOSrd

Buffer – 50mM Tris pH 7.5 +	Ca^{2+} / CaM	k_{cat} / s^{-1}	K_m^{cytc} / μM
100 mM NaCl	-	10.4 ± 0.4	3 ± 1
	+	104 ± 6	8 ± 2
150 mM NaCl	-	15 ± 1	8 ± 2
	+	105 ± 3	10 ± 2
250 mM NaCl	-	23 ± 1	12 ± 2
	+	95 ± 6	12 ± 3

4.2.2 Ferricyanide reduction

Rate constants for the steady-state reduction of ferricyanide by nNOSrd are plotted in Figure 4.4. In both the CaM-free and CaM-bound states the rate of turnover increased linearly with the concentration of ferricyanide. The gradient of the straight-line fit represents catalytic efficiency (k_{cat}/K_m), which was enhanced by CaM by approximately 1.5-fold (Table 4.2). This is consistent with a previous report where rates in excess of 500 s^{-1} were reported and the binding of CaM altered the K_m by a factor of 2.4 [108]. Both of the lines have a positive non-zero y-intercept, which is likely to be caused by the preferential reaction of ferricyanide at the FMN site. It therefore gives an indication of the rate of transfer of electrons from FAD to FMN, whereas the electron transfer from FAD to ferricyanide causes the linear increase [79]. The intercept values, with and without bound CaM, correspond approximately to the rates of cytochrome *c* reduction and the binding of CaM is seen to cause an increase in electron-flux through the enzyme. The rate of hydride transfer from NADPH to FAD is apparently fast enough to support ferricyanide reduction at rates in excess of 100 s^{-1} regardless of whether or not CaM is bound. This suggests that electron transfer from FAD to FMN is slow and limits the turnover of nNOS with cytochrome *c*. If this were the case, this step would then be the event activated by CaM.

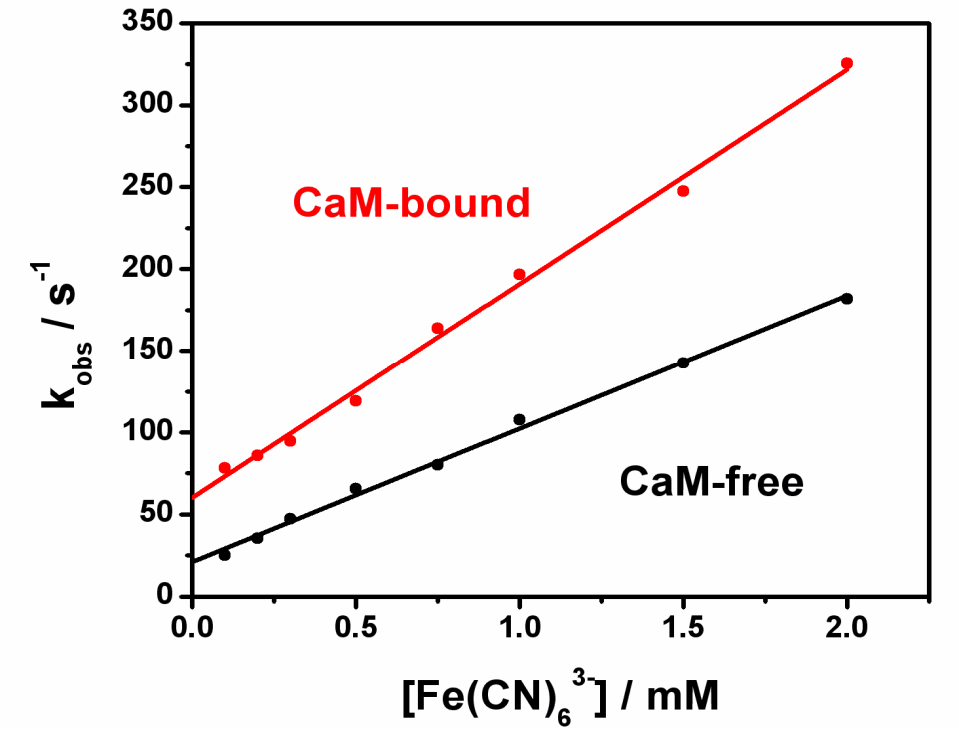

Figure 4.4 Steady-state ferricyanide reduction by nNOSrd. Assays were performed at 25°C in 50mM Tris buffer, pH 7.5 + 100mM NaCl. Data points were fitted to a straight-line equation.

Table 4.2 Steady-state ferricyanide reduction by nNOSrd

Enzyme	Ca^{2+} / CaM	gradient / $mM^{-1}s^{-1}$	y-intercept / s^{-1}
wild-type	-	81 ± 2	21 + 2
	+	131 ± 4	60 ± 4

4.2.3 Kinetic isotope effects

Steady-state experiments using NADPD as substrate were performed using a stopped-flow mixing method, where a catalytic amount of nNOSrd was pre-incubated with NADPH or NADPD and reacted with an excess of ferric cytochrome *c*. The reaction was monitored by the formation of ferrous cytochrome *c* at 550 nm. Figure 4.5, Panel A, plots the traces obtained for deuterated substrate and NADPH in the absence and presence of CaM, which are corrected for the concentration of substrate consumed in

the reaction. The derivatives of each trace, Panel B, give values for steady-state rate constants during the reaction. These are plotted against the concentration of substrate and, although they do not reach saturation, they can still be used to give isotope effect ratios. Each derivative plot (Panel B) was fitted to the Michaelis-Menten equation to obtain values for k_{cat}, K_m^{NAPDH}, and catalytic efficiency. These were then compared to yield values of D_V – the isotope effect on the maximal rate, and $D_{V/K}$ – the isotope effect on the catalytic efficiency, as listed in Table 4.3. Both isotope effects are relatively low, between 1 and 2, and the binding of CaM has little impact on the kinetic isotope effect, consistent with a previous report [140].

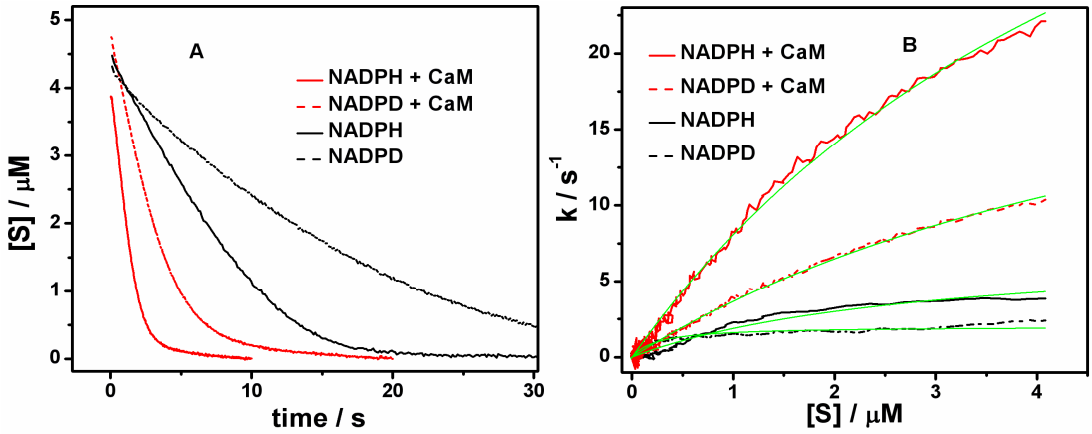

Figure 4.5 Steady state cytochrome *c* reduction using NADPD and NADPH as substrate.
(A) Traces collected at 550 nm corrected for concentration of substrate.
(B) Corresponding derivative plots fitted to the Michaelis-Menten equation (green lines). Assays were performed at 25°C in 50mM Tris buffer, pH 7.5 + 100mM NaCl.

Table 4.3 Steady-state kinetic isotope effects

Enzyme	Ca^{2+} / CaM	D_V	$D_{V/K}$
wild-type	-	1.9 ± 0.2	2.1 ± 0.3
	+	1.4 ± 0.2	1.4 ± 0.1

Primary kinetic isotope effects, i.e. those that have a value of greater than unity, indicate that the bond to the isotopic atom is broken [141]. This is clearly the case here, with deuteride being transferred from the nicotinamide moiety to the FAD cofactor of nNOSrd. This transfer is not entirely rate-limiting however, as the value for a primary kinetic isotope effect can be up to eight or above. Also, the similar

effects on maximal rate and catalytic efficiency indicate that there is no change in affinity for the substrate when it is deuterated.

4.3 Pre-steady-state kinetics

The first step in nNOSrd catalysis is hydride transfer from NADPH to FAD, which can be monitored *in vitro* by UV-visible spectrometry as the reduction of the flavin cofactor. This reaction has been carried out in many investigations, but with conflicting evidence and arguments. From Table 1.2, the binding of CaM appears to activate flavin reduction, however the rate constants obtained vary due to differing exponential fit-functions. Another study [137] used a global analytical technique and reported no CaM-mediated activation, while the temperature also varies across different studies. Furthermore, the enzyme preparations used were almost entirely fully oxidised, which is a non-physiologically relevant form, but may be formed in the steady-state reaction with ferricyanide. The one-electron reduced form is a natural component of both the NO synthesis and cytochrome *c* reduction catalytic cycles; the FMN semiquinone cannot be oxidised by either of the ferric heme species involved in these reactions. Wild-type nNOSrd has been analysed here in the oxidised and one-electron reduced forms, to assess the importance of the redox state of the bound FMN in the hydride transfer reaction.

4.3.1 Flavin reduction by NADPH

The stopped-flow mixing of nNOSrd with a 10-fold excess of NADPH allows investigation of the initial hydride transfer step in the catalytic cycle of nNOSrd, as represented in Appendix I. Upon binding of NADPH, the nicotinamide moiety will π-stack with the bound FAD and transfer a hydride to the N5 position of the flavin (see section 1.7.7). In these pre-steady-state experiments, the enzyme will react further depending on the oxidation state of the FMN, as illustrated in Figure 4.6. If the enzyme is fully oxidised, the initial hydride transfer from NADPH to FAD will be followed by two consecutive electron transfers to the FMN. The first of these electron transfers will be essentially irreversible, forming the stable FMN

semiquinone, whereas the second should reach an equilibrium indicated by formation and decay of a di-semiquinone species. Reaction with a second equivalent of NADPH should complete the reduction process. Inter-enzyme electron transfer reactions (FMN to FMN) are likely to complicate the latter stages of reduction leading to extended slow phases.

When bound FMN is present as the air-stable one-electron reduced semiquinone, the reaction proceeds differently, and should primarily be with a single equivalent of NADPH before slower inter-molecular electron transfers occur.

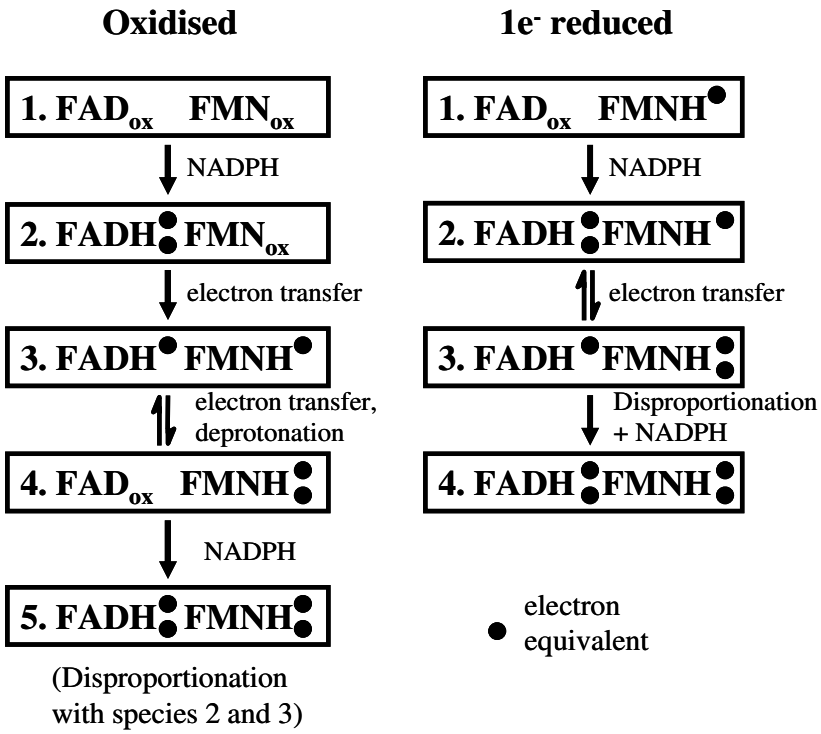

Figure 4.6 Scheme of electron transfer through oxidised and one-electron reduced nNOSrd during pre-steady-state reduction by excess NADPH.

The data for the reduction of the oxidised enzyme are shown in Figure 4.7, where panels A and B represent the CaM-free and CaM-bound states respectively. The reduction of the flavins is observed as a decrease in absorbance at 457 nm and is plotted as a time-course in panel C. Formation of flavin semiquinone is shown by an increase at 592 nm. At 457 nm a large rapid decrease in absorbance is observed indicating that reaction with two equivalents of NADPH has occurred within 0.2s. These data fit well to double-exponential fitting functions over 1 second, and the corresponding parameters are listed in Table 4.4. For the CaM-free enzyme, the two

hydride transfer steps occur in separate kinetic phases, the first being 10-fold faster than the second. When CaM is bound most of the absorbance change occurs in the fast phase, indicating that the two steps cannot be separated easily and are occurring in rapid succession.

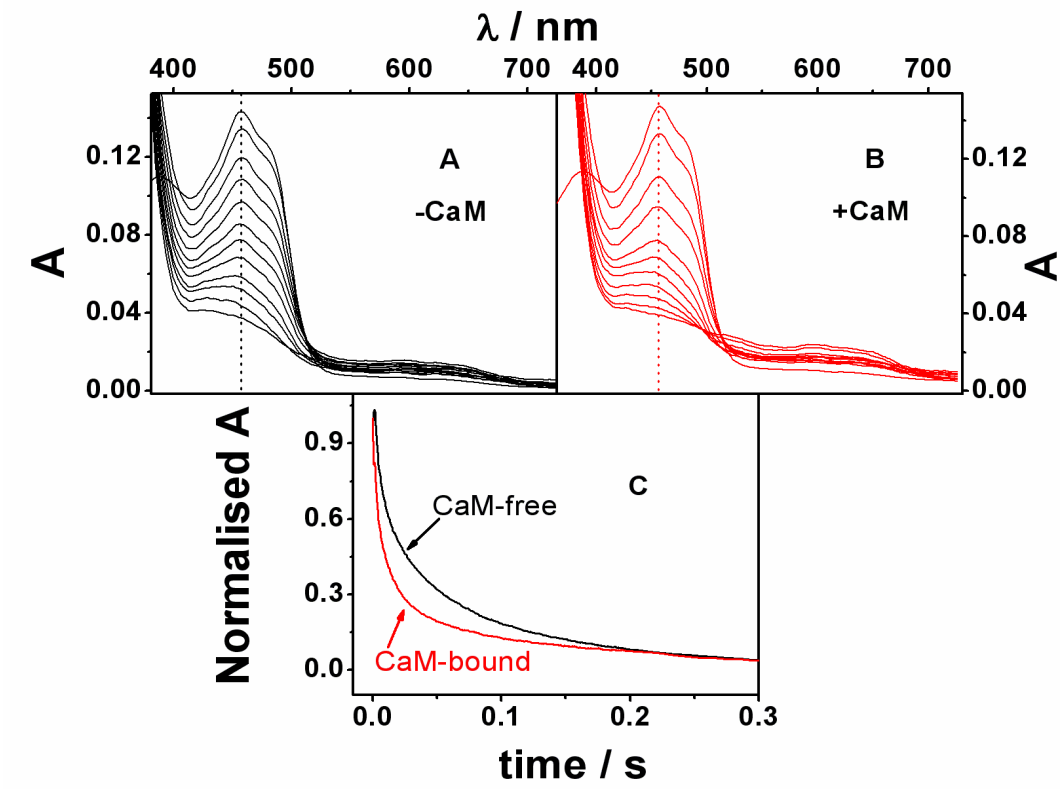

Figure 4.7 Stopped-flow reduction of fully oxidised nNOSrd (10µM) by NADPH (100µM). Diode array spectra for (A) CaM-free and (B) CaM-bound oxidised nNOSrd, taken at 2.5 ms intervals. (C) Corresponding normalised reductive traces at 457 nm.

Table 4.4 Pre-steady-state reduction of oxidised nNOSrd by NADPH

Enzyme	Ca^{2+} / CaM	k_1 / s^{-1} (**Abs**)	k_2 / s^{-1} (**Abs**)
FMN oxidised	-	65 ± 2 (**40%**)	5.9 ± 0.1 (**60%**)
	+	73 ± 2 (**79%**)	3.6 ± 0.1 (**21%**)

Figure 4.8 plots the time-courses at 592 nm for the same reactions as in figure 4.7. These show the appearance and the disappearance of the FMN semiquinone, where for the CaM-free enzyme FMN receives a first electron from FAD rapidly

(semiquinone forms and absorbance increases) followed by a second electron (semiquinone becomes hydroquinone and absorbance decreases). The gradual rise after 1 s is due to disproportionation with other enzyme molecules. The process is essentially the same for the CaM-bound enzyme, with each step occurring more rapidly and further disproportionation towards the end of the time-course.

Looking at the reaction as a whole, the fast initial decrease in absorbance at 457 nm indicates that hydride transfer (the first step in Figure 4.6) is rapid. The initial increase at 592 nm is also fast which would indicate that the first interflavin electron transfer (the second step in Figure 4.6) is also rapid, but this is not a catalytically relevant step. The next interflavin electron transfer (the third step in Figure 4.6) is slow in the absence of CaM and the rate is increased by CaM binding, indicating that this is the rate-determining step in the flavin reduction of nNOSrd.

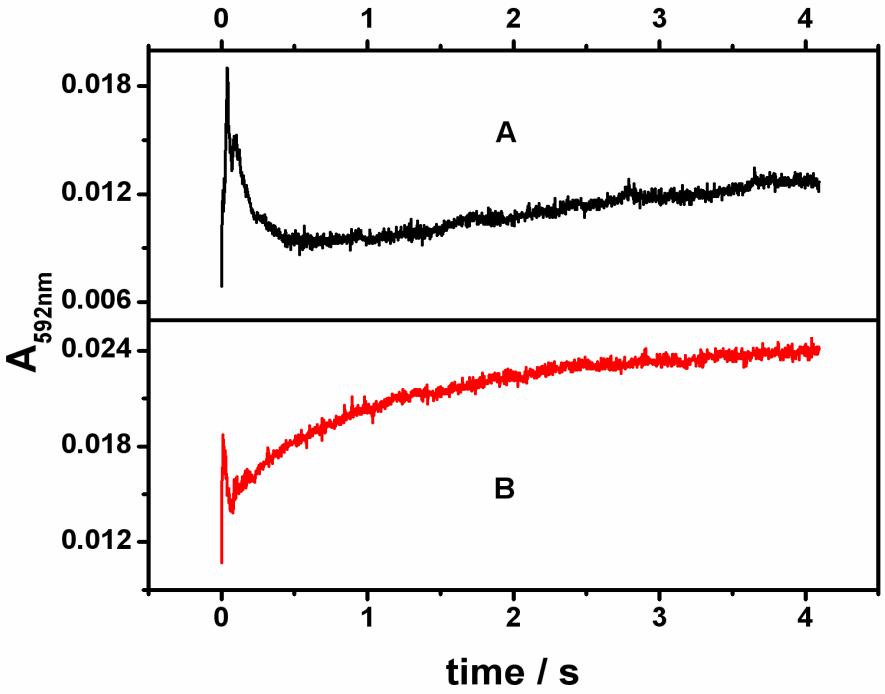

Figure 4.8 Stopped-flow reduction of fully oxidised nNOSrd (10µM) by NADPH (100µM). Traces at 592 nm from the same data as Figure 4.7 for (A) CaM-free and (B) CaM-bound oxidised nNOSrd.

The reaction between the one-electron reduced form of nNOSrd and NADPH is the natural reaction that will occur *in vivo* during nNOS catalysis. Only one equivalent of NADPH should react in this case, and the absorbance change at 457 nm should involve a single hydride transfer phase constituting the majority of the amplitude,

during which the FAD is reduced to the hydroquinone form. The transfer of an electron to the FMN should have minimal effect on the absorbance. Figure 4.9, panels A and B, shows the one-electron reduced wild-type nNOSrd reacting with NADPH in the absence and presence of CaM, respectively. The resultant time-courses at 457nm are shown in panel C, where a comparison with Figure 4.7 reveals that one-electron reduced nNOSrd has a much slower CaM-free reaction profile. The binding of CaM has a much larger effect on this enzyme form. As before, the traces were fitted to double-exponential fitting functions over 1 second and the derived parameters are listed in Table 4.5., in comparison to the values obtained for the oxidised enzyme.

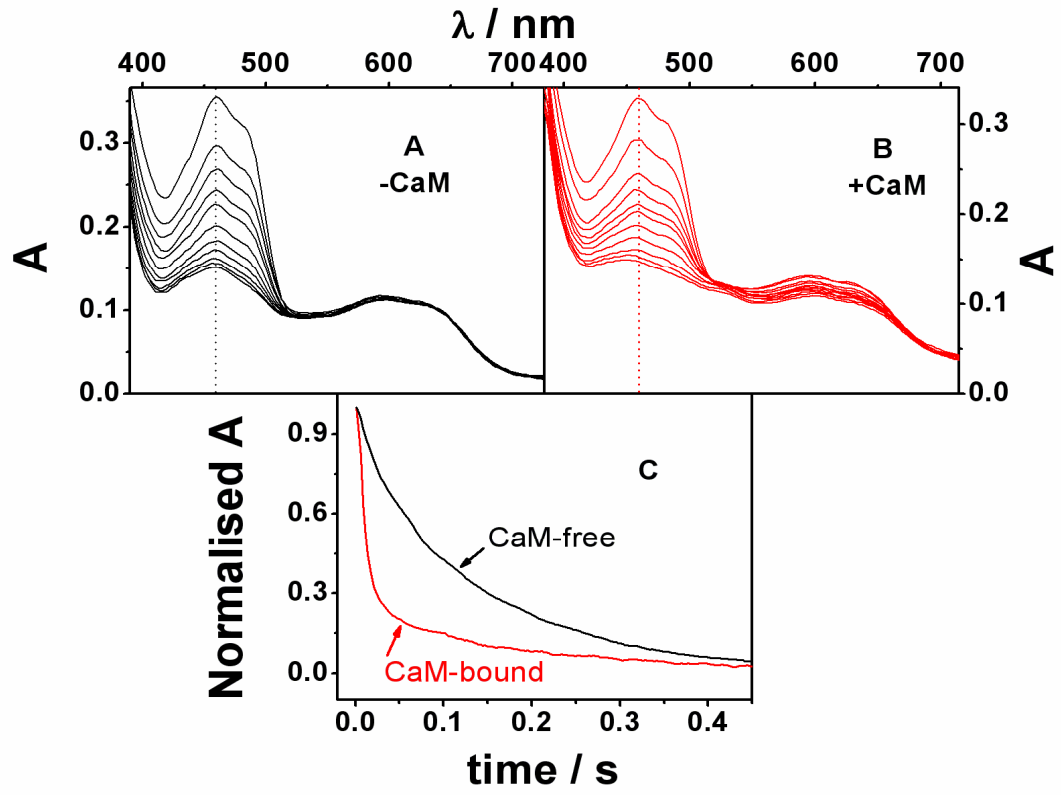

Figure 4.9 Stopped-flow reduction of one-electron reduced nNOSrd (20μM) by NADPH (100μM). Diode array spectra for (A) CaM-free and (B) CaM-bound nNOSrd, collected at 2.5 ms intervals. (C) Corresponding normalised reductive traces at 457 nm.

Table 4.5 Pre-steady-state reduction of nNOSrd by NADPH

Enzyme	Ca^{2+} / CaM	k_1 / s^{-1} (**Abs**)	k_2 / s^{-1} (**Abs**)
FMN oxidised	-	65 ± 2 (**40%**)	5.9 ± 0.1 (**60%**)
	+	73 ± 2 (**79%**)	3.6 ± 0.1 (**21%**)
FMN semiquinone	-	35 ± 1 (**20%**)	6.5 ± 0.1 (**80%**)
	+	93 ± 2 (**78%**)	5.2 ± 0.1 (**22%**)

The CaM-free enzyme is reduced by NADPH in a biphasic process with a large slow phase of rate constant 6.5 s^{-1}. This correlates with the steady-state rate constant for cytochrome *c* reduction (10.4 s^{-1}), meaning that hydride transfer may be the overall rate-limiting step. However, the small fast phase indicates that 20% of the enzyme molecules react with NADPH at a faster rate than the remainder. After FAD reduction a semiquinone form of the enzyme persists, and further reduction appears to be prevented by the inability of the enzyme to transfer electrons between molecules. This is consistent with the theory that NADPH-binding "locks" the FMN into an inaccessible position in this enzyme form [119]. The effect of CaM is much more pronounced for this enzyme form than for the oxidised; CaM-bound one-electron reduced nNOSrd is rapidly reduced by hydride transfer from NADPH at a rate that again correlates with the turnover of electrons in the cytochrome *c* reduction experiments (93 s^{-1} vs 104 s^{-1}). This is followed by further slow reduction initiated by intermolecular electron transfer and disproportionation of flavin semiquinones, observed as a decrease in absorbance at 592nm in Figure 4.9, panel B.

4.3.2 Ionic strength effects

In order to investigate the biphasic nature of the CaM-free reduction observed for the one-electron reduced form of nNOSrd, the stopped-flow experiment with NADPH was repeated with varying concentrations of salt in the assay buffer. Figure 4.10 plots the diode array spectra and reductive traces for a range of salt concentrations; the original 100mM NaCl along with two of higher ionic strength. All of the traces have a similar profile to the original experiment where one equivalent of NADPH causes a decrease at 457 nm with no reduction of the FMN semiquinone. The traces were again fitted to a double-exponential equation over 1 s and the resulting parameters are listed in Table 4.6. These show that the rate constants for each ionic strength show little change, but an increase in ionic strength causes a greater fraction of the reduction to take place in the fast phase. This is an indication that the enzyme may exist in two conformations that undergo hydride transfer at differing rates, and that the equilibrium between the two conformations can be altered by electrostatic interference associated with the increasing ionic strength in the surrounding environment.

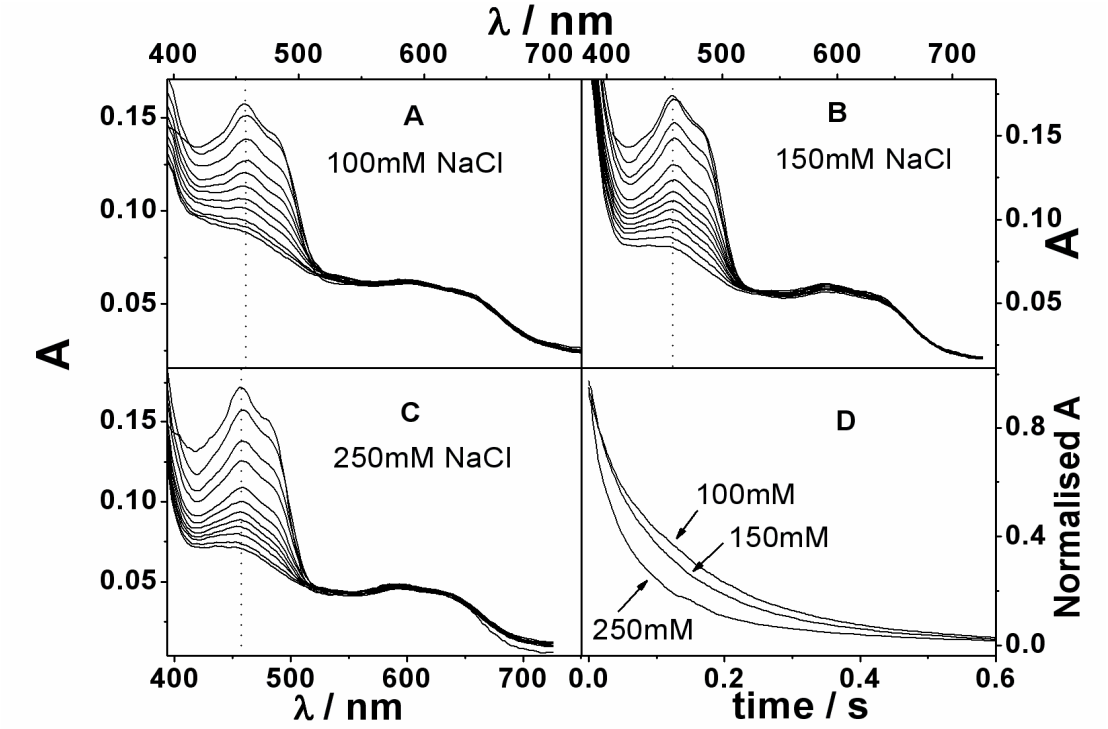

Figure 4.10 Stopped-flow reduction of nNOSrd (10μM) by NADPH (100μM) at varying ionic strength. Diode array spectra for (A) 100 mM NaCl buffer, (B) 150 mM NaCl buffer, (C) 250 mM NaCl buffer. (D) Corresponding reductive traces at 457 nm.

Table 4.6 Ionic-strength effect on pre-steady-state reduction of nNOSrd by NADPH

Enzyme	Ca^{2+} / CaM	k_1 / s^{-1} (**Abs**)	k_2 / s^{-1} (**Abs**)
wild-type – FMN semiquinone + 100mM NaCl	-	41 ± 4 (**16%**)	6.3 ± 0.1 (**84%**)
+ 150mM NaCl	-	35 ± 2 (**30%**)	6.7 ± 0.1 (**70%**)
+ 250mM NaCl	-	30 ± 1 (**60%**)	5.7 ± 0.1 (**40%**)

4.3.3 Kinetic isotope effects

To further investigate the hydride transfer event, stopped-flow flavin reduction experiments were performed with NADPD as the reductant. Figure 4.11 shows the data collected for both the fully oxidised and the 1-electron-reduced enzymes. In comparison to Figures 4.7 and 4.9, the general profile of each experiment has similar spectral changes and similar amplitudes for fast and slow phases. The only important difference is the length of time for reduction in panels C and D, which is reflected in the slower rate constants for both the fast and slow phases, Table 4.7. It is apparent that isotopic substitution affects the rate of FAD reduction through the slowing of hydride transfer. For the one-electron reduced enzyme, comparison of the values for NADPD vs. NADPH gives a kinetic isotope effect of approximately 1.5 for both phases in the presence and absence of CaM. The fully oxidised enzyme gives a slightly larger value of approximately 2 in the fast phase which is consistent with a previous report [137].

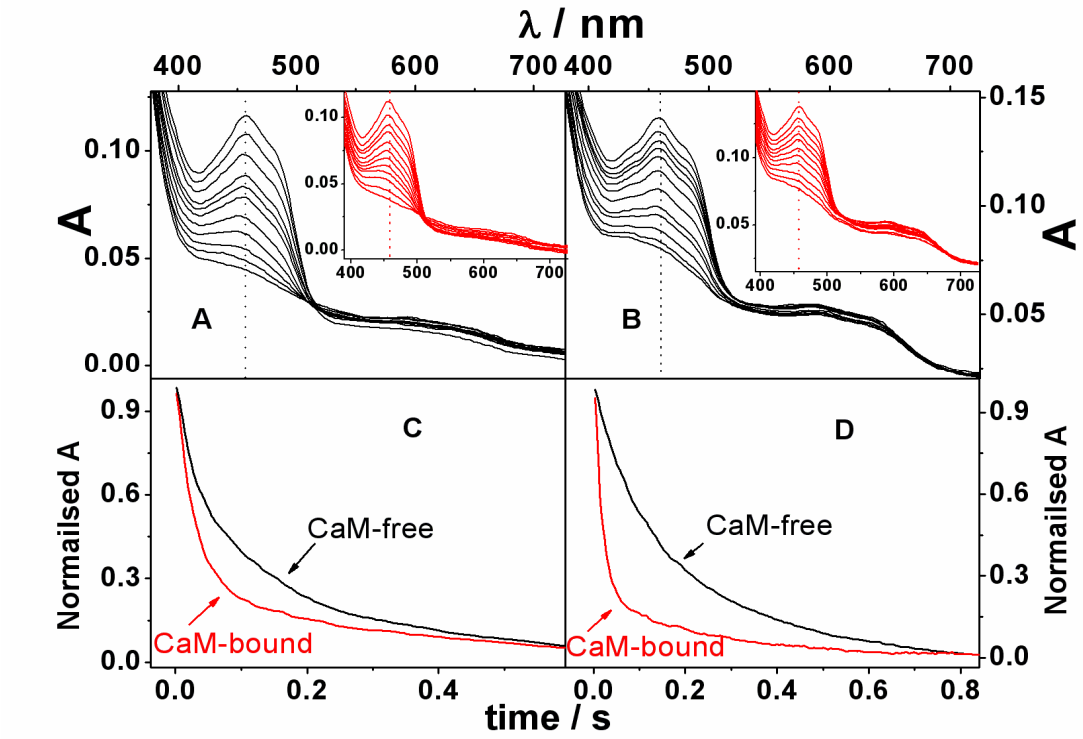

Figure 4.11 Stopped-flow reduction of nNOSrd (10μM) by NADPD (100μM). Diode array spectra for (A) oxidised CaM-free and (inset) CaM-bound, and (B) 1-electron reduced CaM-free and (inset) CaM-bound. Corresponding reductive traces at 457 nm for (C) oxidised and (D) 1-electron reduced.

Table 4.7 Pre-steady-state reduction of nNOSrd by NADPH and NADPD

Enzyme	Substrate	Ca^{2+} / CaM	k_1 / s^{-1} (*K.I.E*) (**Abs**)	k_2 / s^{-1} (*K.I.E*) (**Abs**)
FMN oxidised	NADPH	-	65 ± 2 (**40%**)	5.9 ± 0.1 (**60%**)
		+	73 ± 2 (**79%**)	3.6 ± 0.1 (**21%**)
	NADPD	-	26 ± 1 (*2.5*) (**49%**)	3.7 ± 0.1 (*1.6*) (**51%**)
		+	35 ± 1 (*2.1*) (**73%**)	2.2 ± 0.1 (*1.6*) (**27%**)
FMN semiquinone	NADPH	-	35 ± 1 (**20%**)	6.5 ± 0.1 (**80%**)
		+	93 ± 2 (**78%**)	5.2 ± 0.1 (**22%**)
	NADPD	-	24 ± 1 (*1.5*) (**30%**)	4.3 ± 0.1 (*1.5*) (**70%**)
		+	60 ± 1 (*1.6*) (**80%**)	4.0 ± 0.1 (*1.3*) (**20%**)

The primary kinetic isotope effects here are very similar to those observed in the steady-state reduction of cytochrome *c* (section 4.2.3). Again the binding of CaM has very little effect, in either the fast or slow phase that was measured. The largest isotope effect is seen in the fast phase of the oxidised enzyme, so hydride transfer has greater influence in this enzyme form. However, the values are still low compared to those that would be determined for a rate-limiting step, indicating that the rate of hydride transfer is not the slowest step in the catalytic cycle of nNOSrd.

4.4 Spectroelectrochemistry

Potentiometric studies of nNOSrd have previously shown that the FAD is reduced in two one-electron steps of similar potential (approximately -300 mV) and that the FMN is reduced in two one-electron steps with very different potentials (approximately -300 mV and -100 mV) [86]. The FMN semiquinone is thermodynamically stabilised towards oxidation (see Table 1.3), and it has considerable kinetic stability enabling the FMN to retain the semiquinone oxidation state during purification. Similar reduction potentials have been observed in the presence and absence of CaM and even in the isolated FAD and FMN domains [88]. The exception to this is that the FMN semiquinone loses some thermodynamic stability in the isolated domain and shifts to a lower potential. Given that the FMN does not cycle through the semiquinone-oxidised redox states during catalysis, this is not functionally important. However, it does indicate that the presence of the FAD domain affects the properties of the FMN.

In order to examine recent reports suggesting that the binding of CaM shifts the reduction potential of both FMN transitions along with the FAD ox/sq transition by approximately 100mV more negative [142], the potentiometric titration of CaM-free wild-type nNOSrd was repeated using the OTTLE method (Fig. 4.12). Previously, this was conducted by chemical reduction [86]. Panel A shows the UV-Visible spectra produced by stepwise reduction of the enzyme by incremental decreases of 30 mV in the electrode potential. The resultant plots of the absorbance at both 456 nm and 592 nm versus the applied potential (Panel B) were fitted using Equation 2.1, simultaneously fitting both sets of data, and yielding the midpoint reduction potentials given in Table 4.8. The results are very similar to those reported previously, although equilibration of this enzyme was particularly slow, requiring 2 hours for each potential step.

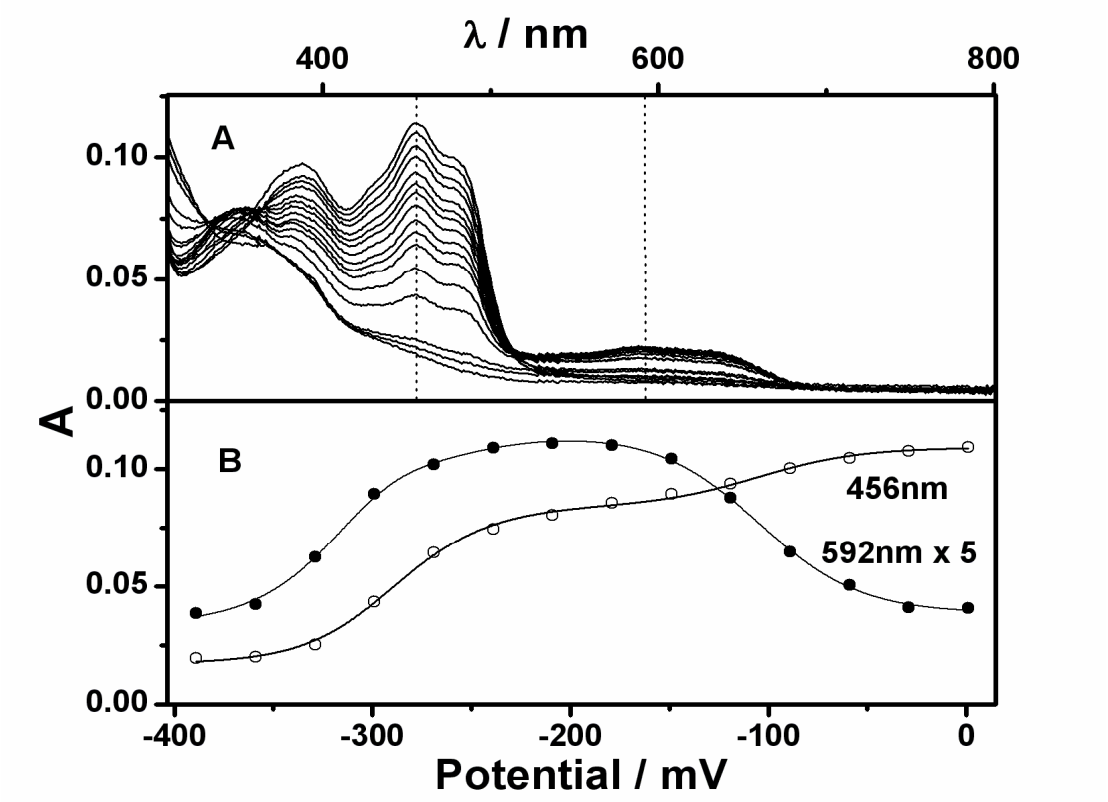

Figure 4.12 OTTLE potentiometry of wild-type nNOSrd in the absence of CaM. Spectroelectrochemistry was carried out in 100mM Tris pH 7.5, 500mM KCl with mediators added. (A) Spectra recorded at 30mV intervals. (B) Corresponding absorbance at 456 nm and 592 nm plotted against applied potential and fitted to a modified Nernst equation (Equation 2.1).

Table 4.8 Midpoint reduction potentials of nNOSrd / mV

Enzyme	FMN ox/sq	FMN sq/hq	FAD ox/sq	FAD sq/hq
Isolated Domains [88]	-179 ± 3	-314 ± 3	-291 ± 3	-326 ± 3
Wild-type (+CaM) [88]	-98 ± 5	-300 ± 8	-296 ± 6	-320 ±10
Wild-type (-CaM)	-101 ± 4	-271 ± 6	-289 ± 6	-301 ± 7

4.5 Discussion

The fundamental step in the activation of nNOS is the binding of CaM, which is believed to induce motion of the FMN-binding domain away from the FAD-binding domain to enable the transfer of electrons to the heme. Each of the three catalytic events in nNOSrd has been reported to be activated by CaM [76, 90, 119], however it is unclear which is the rate-limiting step. From the steady-state cytochrome *c* reduction experiments (Table 4.1), it would appear that the CaM-free turnover is limited by a step that is dependent on ionic strength, while the rapid reduction of ferricyanide (Figure 4.4) indicates that hydride transfer is not rate-limiting but that the transfer of electrons between the flavin cofactors is the slowest step.

By probing the hydride transfer from NADPH to FAD as an isolated event, further insight can be gained about this first catalytic step. The hydride transfer to the fully oxidised enzyme is clearly activated by CaM (Table 4.4) but this is observed as a shift in the phases of reduction. The rate constants retain approximately the same values either CaM-free or CaM-bound, but the fast phase in the CaM-free reaction makes up 40% of the reduction. This is enhanced to 80% in the CaM-bound state and would indicate that CaM increases the rate of flavin to flavin electron transfer, allowing two hydride transfers to occur in rapid succession. This can also be observed as a faster appearance and decay of the FMN semiquinone (Figure 4.8).

The transfer of hydride to the one-electron reduced enzyme better reflects on the events occurring during turnover, where only a single hydride transfer takes place. The data from these reactions (Table 4.5) indicate that hydride transfer is slow in the absence of CaM and fast with CaM-bound. The paradoxical biphasic nature of the CaM-free reaction was initially thought to be due to partly truncated or damaged enzyme samples, however the effects were seen across a range of protein preparations. The ionic strength dependence of the CaM-free hydride transfer (Table 4.6) suggests that the enzyme adopts two conformations in solution; one that reacts rapidly with NADPH and the other that either reacts slowly, or is unreactive and therefore must undergo a slow conformational change to convert to the active form. These two conformations must be linked by an equilibrium that is dependent upon ionic-strength. The effect of increasing the salt concentration on the pre-steady-state reduction kinetics of nNOSrd is similar to, but not as pronounced as, the effect of

binding CaM. It would seem logical therefore that the active conformational form of CaM-free nNOSrd is related to the CaM-bound form and that CaM-binding affects the same conformational equilibrium. This is represented in Figure 4.13 for a model of "closed" and "open" nNOSrd, where the conformational change is effectively the opening and closing of the hinge that connects the FAD- and FMN- binding domains.

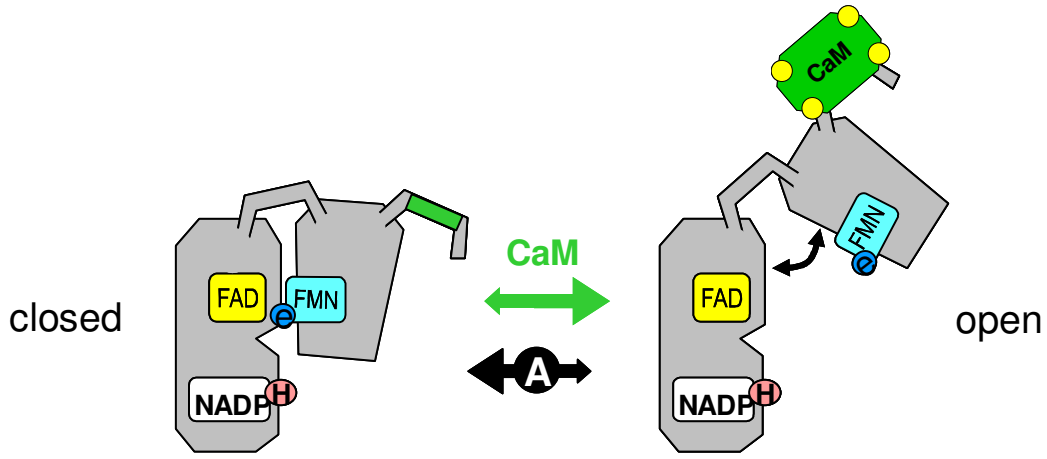

Figure 4.13 Proposed scheme for the mechanism of CaM-activation of nNOSrd. Binding of CaM alters the position of equilibrium A between the hinged-open and hinged-closed forms of the enzyme.

If only the hinged-open form is able to undergo rapid NADPH to FAD hydride transfer, then the pre-steady-state reduction kinetics would be biphasic, with the amplitudes of the two phases corresponding to the position of the conformational equilibrium, provided that the hinge-opening process (A) is slow. The hinged closed form can conceivably be considered to be the same as the "locked" form of nNOSrd, the conformation that does not transfer electrons to cytochrome *c* in the presence of NADPH and the absence of CaM [119]. The kinetic behaviour of fully oxidised nNOSrd can be rationalised from the model in Figure 4.13, where presumably the fully closed form relies on the presence of the FMN semiquinone state, so the oxidised enzyme will be more open in the absence of CaM. It is still activated by CaM, which pulls the equilibrium fully to the open form, but the effect is less pronounced.

The kinetic isotope effects observed for nNOSrd are small, in both the steady-state and pre-steady-state experiments. Values of between 1 and 2 indicate that the rate of hydride transfer from NADPH to FAD is slowed slightly due to the larger mass of

deuterium but kinetic isotope effects on hydride transfer can be as high as 8. Therefore it is unlikely that the hydride transfer step is entirely rate-determining in this case. A step prior to the actual hydride transfer event probably influences the rate of FAD reduction, a conformational change occurring after NADPH binding. The lack of a CaM effect on the kinetic isotope effect indicates that the transition state for hydride transfer is similar in both cases. In other words, CaM does not increase the rate of FAD reduction by altering the affinity of FAD for the hydride, or the orientation of nicotinamide stacking above the FAD. The logical conclusion is that CaM increases the rate at which NADPH can adopt the appropriate orientation for hydride transfer, i.e. the rate of conformational change.

Chapter 5
R1229E: Disrupting the domain-domain interface

5.1 Introduction

The regulation of electron-transfer activity through nNOSrd is achieved by the binding of CaM, along with the presence of a number of structural regulatory features (see section 1.7). The SI, AI, CT and phosphorylation sites can all feasibly be found at the FAD/FMN interface, where the flavin cofactors come into contact to transfer electrons in the "hinged-closed" state. This interface in nNOSrd was affected in Chapter 4 by the redox state of the FMN cofactor; the fully oxidised enzyme did not form a completely "locked" state and was consequently only slightly regulated by CaM in pre-steady-state flavin reduction experiments. The one-electron reduced enzyme is the catalytically relevant form and exhibited a more pronounced effect on hydride transfer upon CaM binding, which correlated with the activation step in the steady-state reduction of cytochrome *c*, attributed to conformational change.

Another feature of the interface is a salt-bridge between Arg1229 and Glu762. This is on the opposite side of the enzyme to the hinge (Figure 5.1) and close to the edge of the FAD cofactor. Furthermore, there are two more glutamate residues close to Glu762 in the crystal structure [74], also highlighted in Panel B of Figure 5.1, which could form the salt bridge. This indicates that the electrostatic attraction is an important interface interaction.

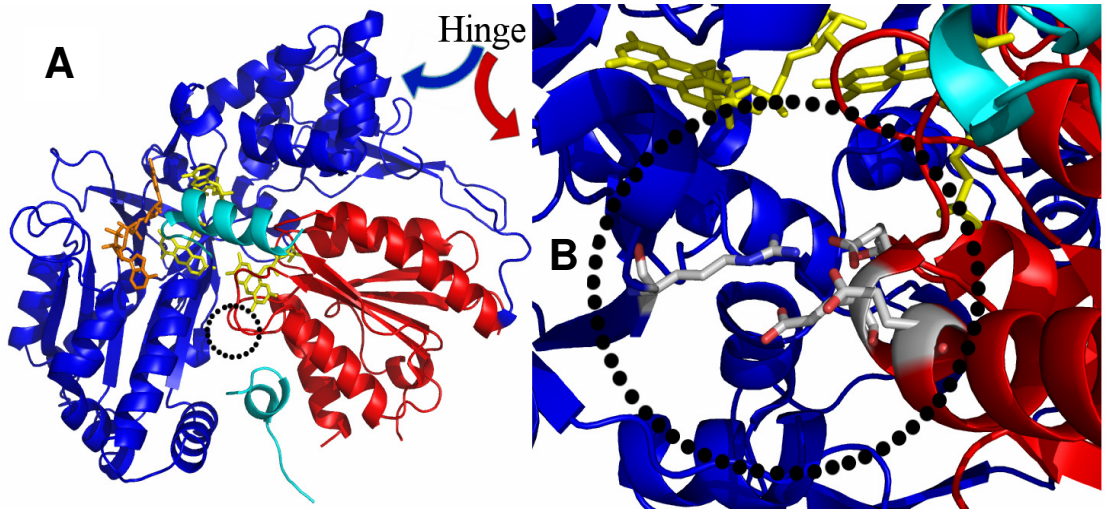

Figure 5.1 Crystal structure of nNOSrd (PDB code 1TLL). (A) Overall structure showing the position of the double salt bridge opposite to the hinge (black circles). (B) Close-up on the interaction between Arg1229 and Glu762, Glu816, Glu819. Bound flavin cofactors are coloured yellow, NADPH orange, FMN-binding domain red, other domains blue. AI and CT are coloured cyan.

To break this salt-bridge, Arg1229 on the FAD-side was substituted by glutamate. The resulting R1229E mutant should retain the overall shape near to the bound FAD cofactor, as the two amino acids are similar in size, but introduce charge repulsion between the two halves of the interface. This is likely to destabilise the hinge-closed form and be regulated by CaM differently to wild-type nNOSrd, represented in Appendix I. This chapter presents the kinetic and thermodynamic analysis of R1229E nNOSrd in comparison to the wild-type enzyme for steady-state turnover reactions, pre-steady state hydride and electron transfer, and the effect of CaM binding throughout.

5.2 Steady-state turnover

5.2.1 Cytochrome *c* reduction

The turnover of electrons through nNOSrd to cytochrome *c* is a characteristic measurement that is activated by CaM, as observed in section 4.2.1, by a 10-fold enhancement effect. Rate constants for the steady-state reduction of cytochrome *c* by R1229E nNOSrd are plotted in Figure 5.2, in comparison to the wild-type enzyme (Panel A vs. Panel B). In the CaM-free R1229E assay, the rate initially increases with the concentration of cytochrome *c*, to a maximum of 7.5 s^{-1}, however it then decreases at concentrations of cytochrome *c* greater than 20μM. This indicates that excess cytochrome *c* is inhibiting catalytic turnover. When CaM is present the rate of cytochrome *c* reduction is much lower (< 2 s^{-1}), and the inhibition is apparent at cytochrome *c* concentrations as low as 2μM. The CaM-free data fit well to a model for substrate inhibition in which the substrate (here cytochrome *c*) binds to an unproductive form of the enzyme (Equation 10, Appendix I). Inhibition occurs with the CaM-bound mutant even at low concentrations of cytochrome *c*, so these data are fitted to a simpler inhibition equation (Equation 11), and all of the derived kinetic parameters are listed in Table 5.1. The difficulty in obtaining accurate rate constants at low concentrations of cytochrome *c* compromises the accuracy of these data; however it is clear that the rate of reduction is markedly slower for R1229E nNOSrd

when CaM is bound, an occurrence not seen in other reductase domain mutants. The overall effect of this single mutation is particularly large; a decrease from 100 s^{-1} to around 2 s^{-1}. The mutation therefore appears to induce two separate effects; it decreases the rate of electron transfer through the CaM-bound enzyme and introduces substrate inhibition at high cytochrome *c* concentrations. Both of these may be due to changes in the electrostatic interactions within the domain interface.

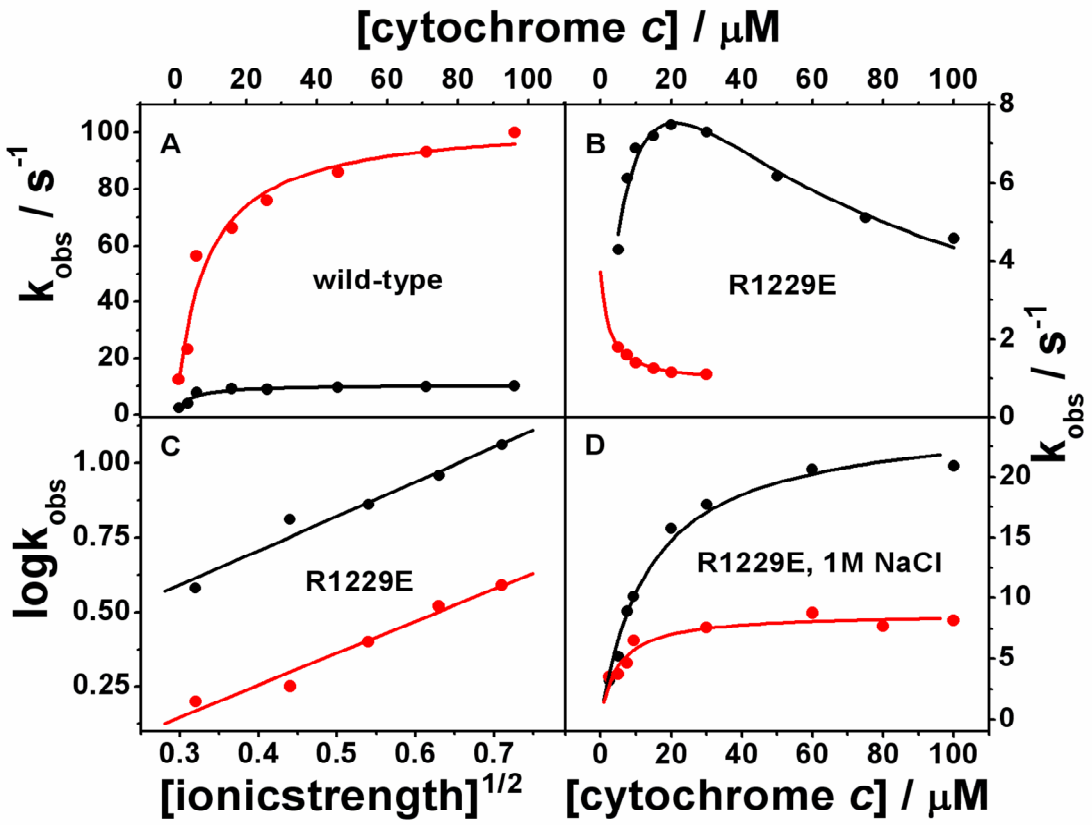

Figure 5.2 Steady-state cytochrome *c* reduction by R1229E nNOSrd, in the absence (black points) and presence (red points) of CaM. Assays were performed at 25°C in 50mM Tris, pH 7.5. (A) wild-type turnover in buffer + 100mM NaCl (B) R1229E turnover in buffer + 100mM NaCl (C) R1229E turnover with varying ionic strength (D) R1229E turnover in buffer + 1 M NaCl.

In order to test this theory, the assay was repeated at varying levels of ionic strength, i.e. increased NaCl concentration in the assay buffer. Panel C of Figure 5.2 shows a linear dependence of the log of the rate constant of cytochrome *c* reduction at 15μM versus the square root of ionic strength. According to Debye-Huckel theory (equation 14, Appendix I), the primary kinetic salt effect obtained from the gradient of the plot gives the ionic charge interaction involved. For both the CaM-free and CaM-bound

mutant there is a net unit charge interaction of 1. It seems likely therefore that the high salt concentrations can compensate for the negative-negative repulsion across the interface caused by the mutated residue and increase the rate of interflavin electron transfer. As expected, the electrostatic component of the interaction is unaltered by the binding of CaM.

When the salt concentration was increased to 1 M (Panel D of Figure 5.2), the steady-state kinetic data for R1229E nNOSrd fitted to the Michaelis-Menten equation, giving catalytic turnover rates of 24 s^{-1} (CaM-free) and 9 s^{-1} (CaM-bound). It is interesting to note that the activity of the enzyme is still decreased by more than 2-fold upon binding of CaM, which is opposite to the effect seen in the wild-type enzyme. Also, the CaM-free activity of R1229E nNOSrd is not activated relative to the wild-type enzyme, as the same activity was observed in Figure 4.3 for CaM-free nNOSrd with only 250 mM NaCl causing the effect.

Table 5.1 Steady-state cytochrome *c* reduction by R1229E nNOSrd

Enzyme	Ca^{2+}/ CaM	k_{cat} / s^{-1}	K_m^{cytc} / μM	K_i / μM
wild-type	-	10.4 ± 0.4	3 ± 1	n/a
	+	104 ± 6	8 ± 2	
wild-type + 250mM NaCl	-	23 ± 1	12 ± 2	n/a
	+	95 ± 6	12 ± 3	
R1229E	-	14.8 ± 1.8	10 ± 2	44 ±9
	+	3.4 ± 1.8	n/a	2 ± 2
R1229E + 1M NaCl	-	24.3 ± 1.4	14 ± 2	n/a
	+	8.8 ± 0.5	5 ± 1	

5.2.2 Ferricyanide reduction

The reduction of ferricyanide by nNOSrd occurs at both the FAD and FMN cofactors, leading to faster rates of turnover and a smaller CaM-mediated activation step, as

observed in section 4.2.2. Rate constants for the steady-state reduction of ferricyanide by R1229E nNOSrd are plotted in Figure 5.3, in comparison to wild-type. The gradients of the straight-line fits, i.e. catalytic efficiency, and the y-intercepts are listed and compared in Table 5.2.

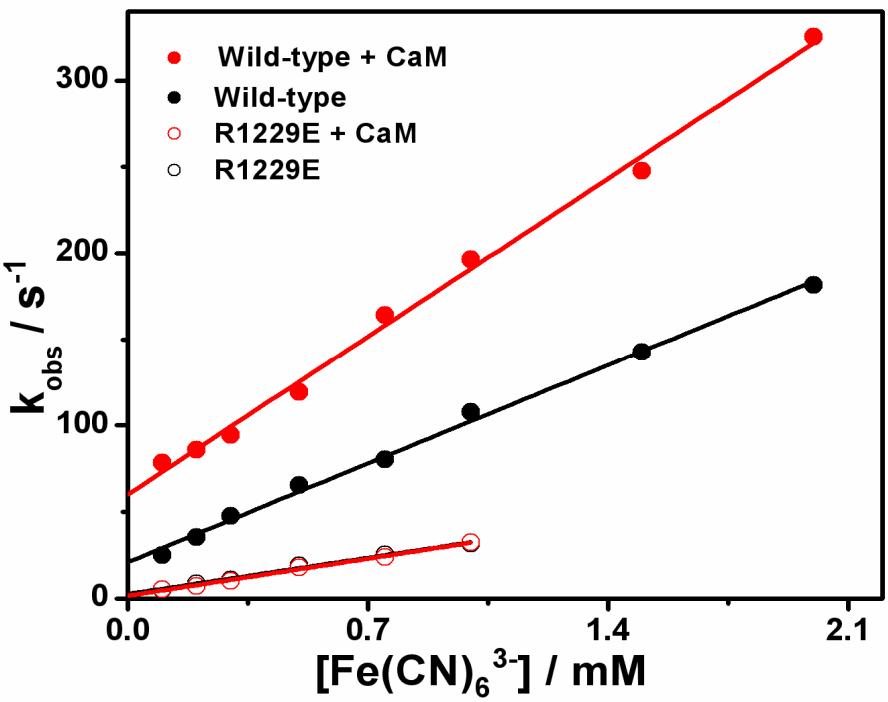

Figure 5.3 Steady-state ferricyanide reduction by R1229E nNOSrd. Assays were performed at 25°C in 50mM Tris buffer, pH 7.5 + 100mM NaCl. Data points were fitted to a straight-line equation.

Table 5.2 Steady-state ferricyanide reduction by R1229E nNOSrd

Enzyme	Ca^{2+} / CaM	gradient / $mM^{-1}s^{-1}$	y-intercept / s^{-1}
wild-type	-	81 ± 2	21 + 2
	+	131 ± 4	60 ± 4
R1229E	-	30 ± 1	2.6 ± 0.7
	+	31 ± 1	1.6 ± 0.6

The R1229E mutant turns over at a much lower catalytic efficiency than wild-type nNOSrd, approximately 2.5-fold, CaM-free. This can be rationalised by the proximity of the mutation site to a site where ferricyanide would have to bind to receive electrons from FAD, where glutamate is less favourable than arginine (in

wild-type) in interacting with the negative ferricyanide ion. The y-intercept is also decreased considerably, to 2 s^{-1}, which can be interpreted as a severe decrease in electron flux through the mutant enzyme. It is also of note that the binding of CaM does not have any effect on the mutant's rate of turnover. This indicates that the destabilisation at the interface allows the ferricyanide access to the FAD site to perform electron transfer in the absence of CaM, but this is retarded by the presence of the negative glutamate residue. Furthermore, the binding of CaM does not allow any greater access for the ferricyanide, nor does it increase the rate of interflavin electron transfer.

5.2.3 NO synthesis

Full-length nNOS, both wild-type and the R1229E mutant, were assayed for NOS activity and the results are summarised in Table 5.3. There was no CaM-free activity observed for R1229E nNOS, and the CaM-bound activity was reduced compared to the wild-type by approximately 5-fold. NADPH consumption was reduced by less than the NOS activity, approximately 2.5-fold, indicating that R1229E nNOS has a greater degree of uncoupled NADPH oxidation. Overall it is clear that R1229E nNOS is less efficient than the wild-type holoenzyme, which means that destabilisation at the interface does not activate electron transfer to the oxygenase domain of holo-nNOS. A partially hinged-open state would mean that the flavin cofactors have more access to solvent and therefore oxygen, which would explain the relative increase in the rate of NADPH oxidation. These results are in good agreement with substitutions of the acidic residues on the FMN-binding domain at the interface in nNOS [81].

Table 5.3 Steady-state NO synthesis by R1229E nNOS

Enzyme	Ca^{2+} / CaM	NO synthesis / min^{-1}	NADPH oxidation / min^{-1}
wild-type	-	no activity	
	+	10.2 ± 0.6	27 ± 2
R1229E	-	no activity	
	+	2.0 ± 0.4	9.3 ± 0.4

5.3 Pre-steady-state kinetics

Wild-type nNOSrd is regulated by CaM for each of the three steps in turnover; hydride transfer (NADPH to FAD), interflavin electron transfer (FAD to FMN) and the transfer of an electron from FMN to heme. This occurs through the adoption of two distinct conformations; open and closed. These conformations should be present in the R1229E mutant and affected by the change at the interface. Furthermore, the inhibition effect observed during steady-state cytochrome *c* reduction can be investigated in each of the catalytic events, in order to ascertain which individual step or steps are affected in the mutant's turnover reactions.

5.3.1 Cytochrome *c* reduction

The transfer of an electron from hydroquinone FMN to cytochrome *c* is the final step in the turnover of nNOSrd, and provides a measure of the accessibility of the bound FMN. It is measured by the stopped-flow mixing of chemically reduced enzyme with a sub-stoichiometric amount of cytochrome *c*, in the presence and absence of CaM and NADPH. This experiment has previously been used to reveal that the CaM-free NADPH-bound wild-type enzyme is in a "locked" FMN-inaccessible conformation, where the binding of NADPH causes the second-order rate-constant to drop from $15\mu M^{-1}s^{-1}$ to $1\mu M^{-1}s^{-1}$, while the binding of CaM enhances it to $>35\mu M^{-1}s^{-1}$, releasing the lock and allowing the rapid transfer of an electron from FMN to cytochrome *c* [119]. Furthermore, analysis of the isolated FMN domain under the same conditions highlighted the similarity in accessibility between FMN bound to this single domain and that bound to CaM-activated nNOSrd [120].

Figure 5.4 plots the stopped-flow traces associated with cytochrome *c* reduction by R1229E nNOSrd under the same conditions.

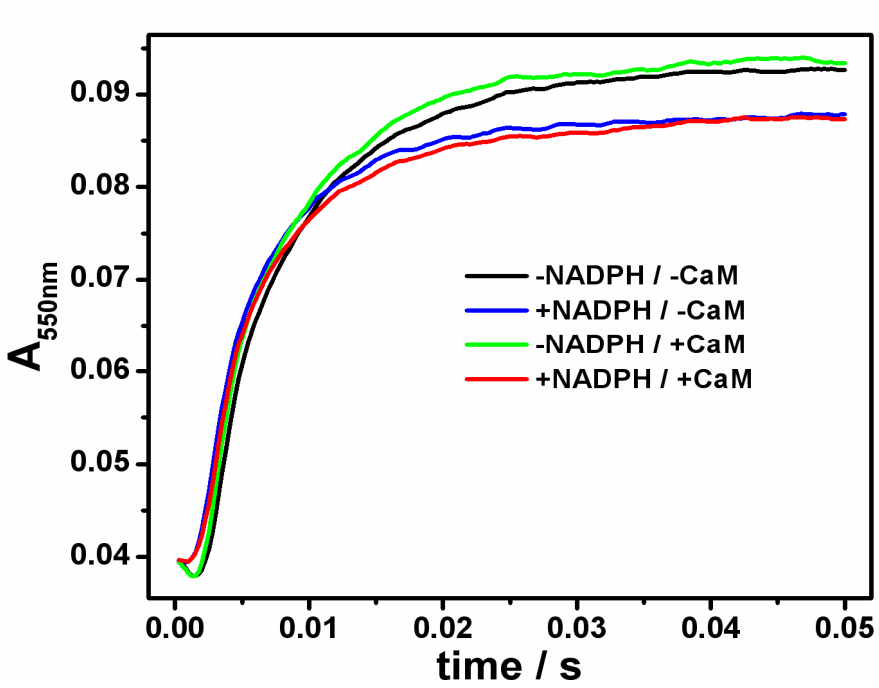

Figure 5.4 Pre-steady-state reduction of cytochrome *c* by R1229E nNOSrd. Stopped-flow mixing of pre-reduced enzyme (10μM) with ferric cytochrome *c* (4μM) was carried out at 25°C in the absence and presence of NADPH and CaM.

In all cases, in the presence or absence of NADPH and CaM, the reduction of cytochrome *c* occurs rapidly. The associated rate constants were obtained by fitting the traces to a single exponential function and found to be dependent on the concentration of R1229E nNOSrd, as for wild type. This is presented in Figure 5.5, where the rate of cytochrome *c* reduction by R1229E nNOSrd at a range of concentrations with the addition of NADPH is plotted.

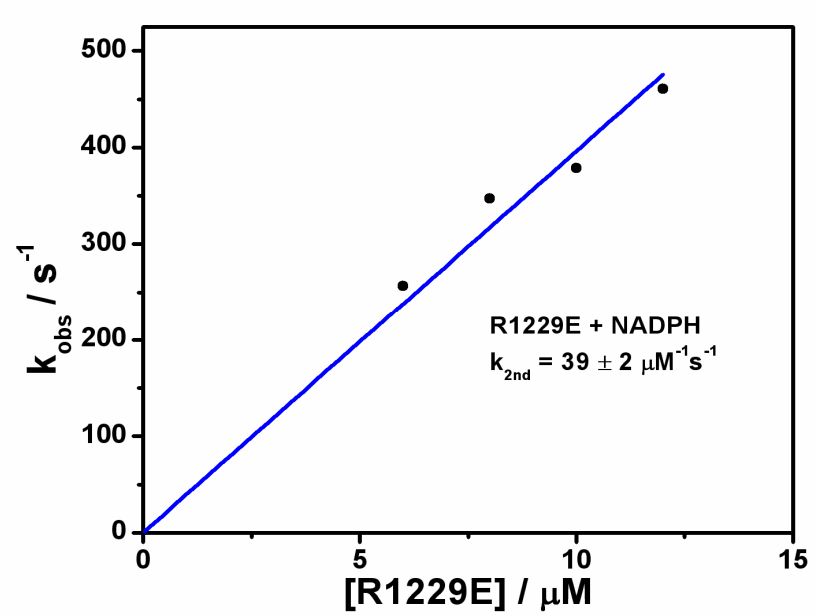

Figure 5.5 Concentration dependence of pre-steady-state reduction of cytochrome *c* by R1229E nNOSrd. Stopped-flow mixing of pre-reduced enzyme (6-12μM) with ferric cytochrome *c* (4μM) was carried out at 25°C with NADPH bound in each case.

The second-order rate-constant for the mutant is 39 $\mu M^{-1}s^{-1}$, which is analogous to activated wild-type enzyme (38 $\mu M^{-1}s^{-1}$, [119]) and the isolated FMN-binding domain [120] and indicates that the bound FMN in R1229E nNOSrd is always accessible to cytochrome *c*. The presence of NADPH in the absence of CaM is unable to induce a "locked" conformation in the mutant.

In order to investigate the self-inhibition of cytochrome *c* during turnover reactions (section 5.2.1), the pre-steady-state reduction was repeated in the presence of 10μM ferrous cytochrome *c*. This species would be present in the steady-state assays and could inhibit the reduction of further molecules of ferric cytochrome *c*. The traces associated with this experiment are plotted in Figure 5.6 and the rapid reduction under all conditions is again apparent, with no inhibition effect observed in this part of the catalytic turnover of the mutant enzyme. This indicates that ferrous cytochrome *c* does not inhibit the direct transfer of electrons to ferric cytochrome *c* during steady-state turnover.

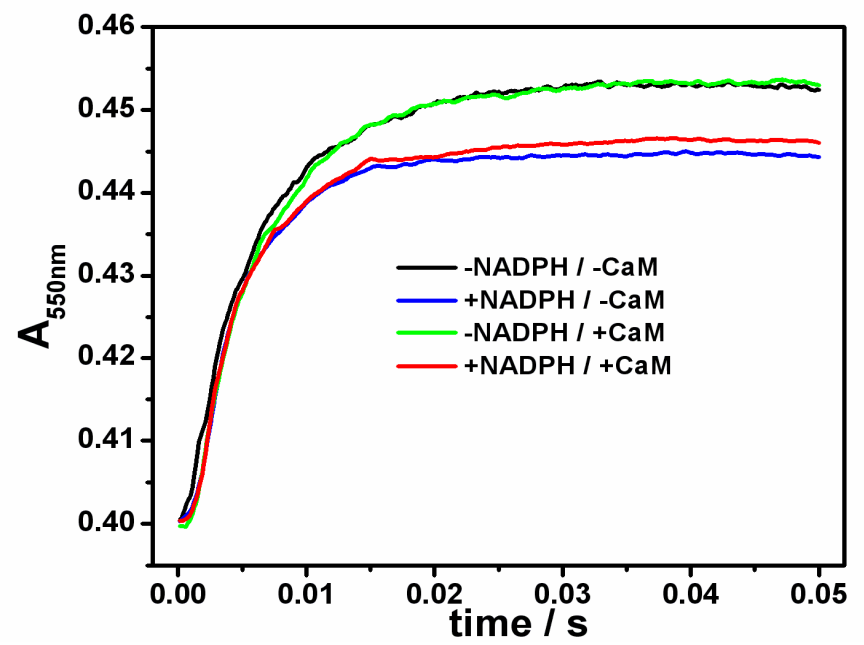

Figure 5.6 Pre-steady-state reduction of cytochrome *c* by R1229E nNOSrd in the presence of ferrous cytochrome *c*. Stopped-flow mixing of pre-reduced enzyme (10µM) with ferric cytochrome *c* (4µM) + ferrous cytochrome *c* (10µM) was carried out at 25°C in the absence and presence of NADPH and CaM.

5.3.2 Flavin reduction

The hydride transfer step in wild-type nNOSrd (section 4.3) was found to be regulated by CaM in the fully oxidised form of the enzyme, but there was a more pronounced effect in the one-electron reduced (FMN semiquinone) state. These experiments were repeated for R1229E nNOSrd; Figure 5.7 shows the fully oxidised version, with Panels A and B representing the CaM-free and CaM-bound forms respectively. The resulting time-dependent reduction traces are plotted in Panel C, where they are compared to the wild-type traces from Figure 4.7. The data were fitted to the same double exponential function over 1 s and the derived kinetic parameters are listed in Table 5.4, in comparison to wild-type values from Table 4.4.

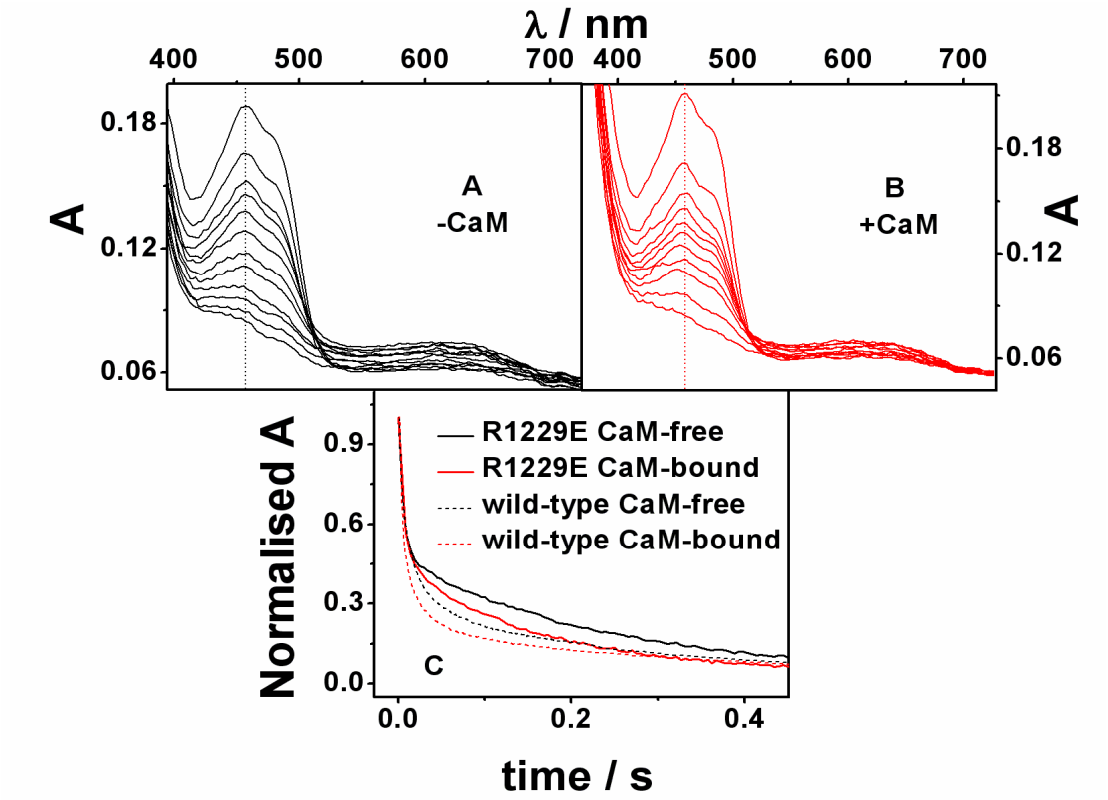

Figure 5.7 Stopped-flow reduction of fully oxidised R1229E nNOSrd (10µM) by NADPH (100µM). Diode array spectra for (A) CaM-free and (B) CaM-bound oxidised R1229E nNOSrd. (C) Corresponding normalised reductive traces at 457 nm compared to wild-type, from Figure 4.7.

Table 5.4 Pre-steady-state reduction of oxidised R1229E nNOSrd by NADPH

Enzyme	Ca^{2+} / CaM	k_1 / s^{-1} (**Abs**)	k_2 / s^{-1} (**Abs**)
wild-type – FMN oxidised	-	65 ± 2 (**40%**)	5.9 ± 0.1 (**60%**)
	+	73 ± 2 (**79%**)	3.6 ± 0.1 (**21%**)
R1229E – FMN oxidised	-	169 ± 5 (**52%**)	4.0 ± 0.1 (**48%**)
	+	156 ± 6 (**57%**)	5.6 ± 0.1 (**43%**)

It is apparent that the traces for CaM-free and CaM-bound R1229E nNOSrd are very similar and are divided into two phases of almost equal amplitude. The first one is

presumably the first hydride transfer and occurs more rapidly than that for the wild-type enzyme, while the slower second step leads to an obvious change in the kinetic trace (Panel C). This implies that the enzyme is unable to perform rapid interflavin electron transfer, which can be further observed from the semiquinone build-up and decay at 592 nm. This is shown as a time-course in Figure 5.8, with Panels A and B replicated from Figure 4.8 for the wild-type experiments, and Panel C from the same CaM-free R1229E reaction as Figure 5.7 (A). In the wild-type enzyme, the FMN rapidly receives a first and second electron from FAD and then disproportionates with other enzyme molecules, observed as a slow build up of semiquinone. The R1229E mutant proceeds much more slowly, with the slow appearance and even slower disappearance of the semiquinone band occurring over a 4 s period. Referring back to the scheme of electron transfer in Figure 4.6, this means that the first step, hydride transfer, is accelerated but the subsequent interflavin electron transfers are slowed.

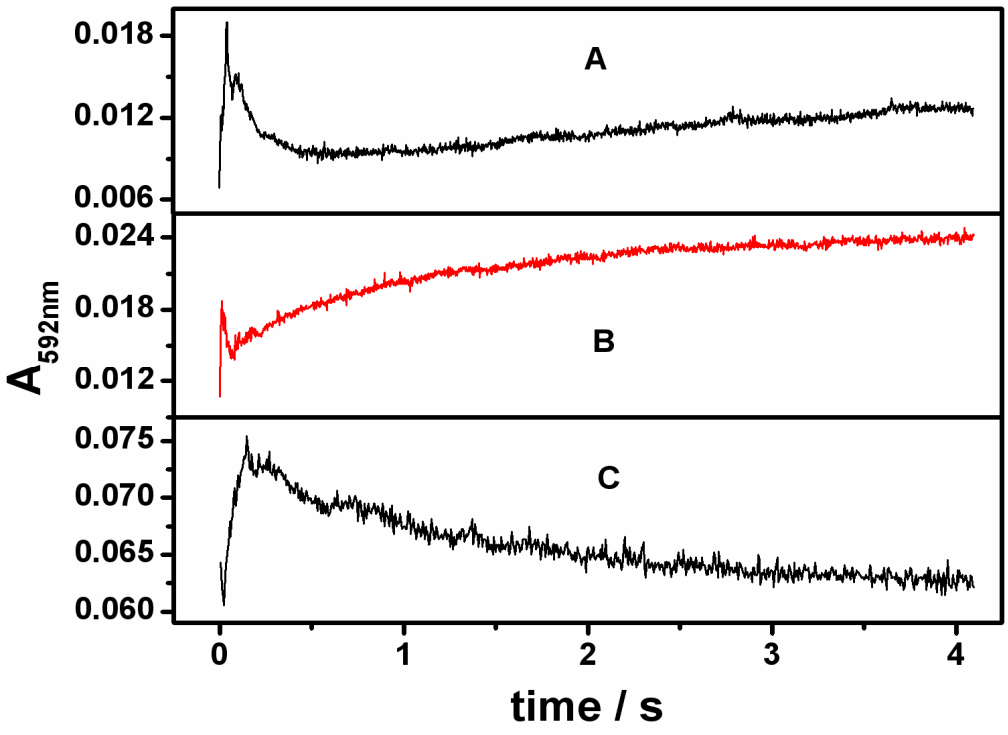

Figure 5.8 Stopped-flow reduction of fully oxidised R1229E nNOSrd (10µM) by NADPH (100µM). Traces at 592 nm are replicated from Figure 4.8 for (A) CaM-free and (B) CaM-bound wild-type. (C) R1229E from the same data as Figure 5.7, Panel A.

The stopped-flow reaction for one-electron reduced R1229E nNOSrd is plotted in Figure 5.9, with Panels A and B showing the CaM-free and CaM-bound reduction

respectively. The resultant traces, in Panel C, are compared to wild-type equivalents from Figure 4.9 and the derived rate constants from these are listed in Table 5.5.

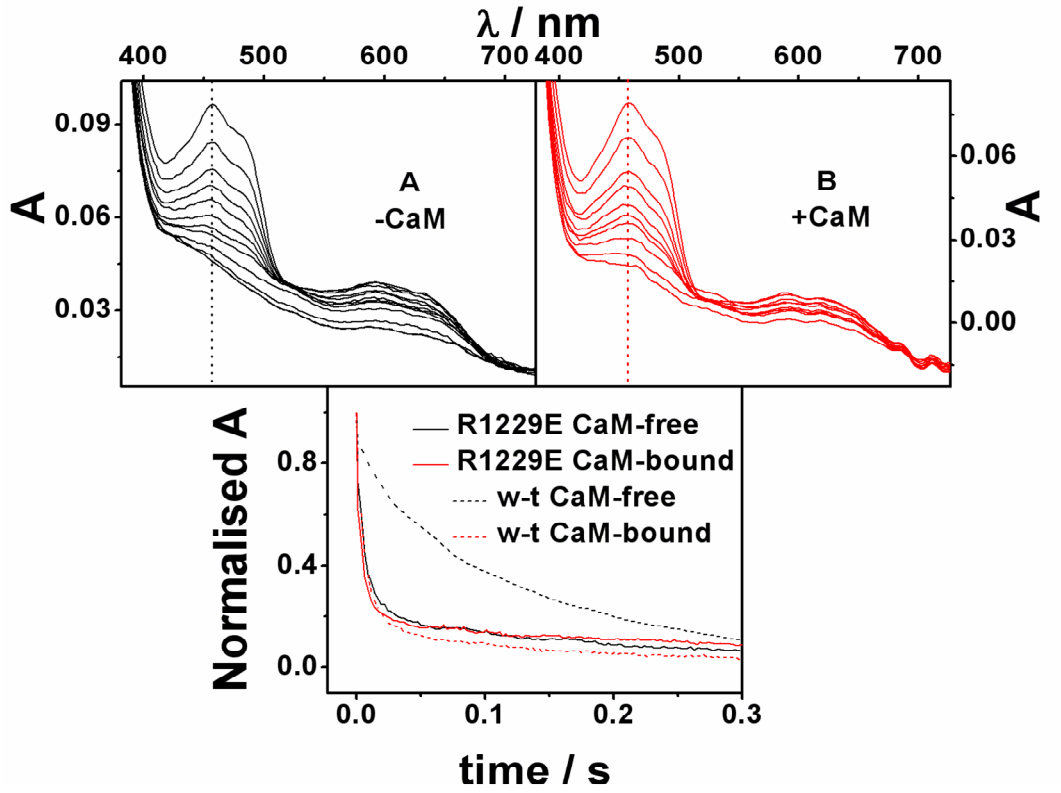

Figure 5.9 Stopped-flow reduction of one-electron reduced R1229E nNOSrd (10μM) by NADPH (100μM). Diode array spectra for (A) CaM-free and (B) CaM-bound R1229E nNOSrd. (C) Corresponding normalised reductive traces at 457 nm compared to wild-type, from Figure 4.9.

Table 5.5 Pre-steady-state reduction of 1-electron-reduced R1229E nNOSrd by NADPH

Enzyme	Ca^{2+} / CaM	k_1 / s^{-1} (**Abs**)	k_2 s^{-1} (**Abs**)
wild-type – FMN semiquinone	-	35 ± 1 (**20%**)	6.5 ± 0.1 (**80%**)
	+	93 ± 2 (**78%**)	5.2 ± 0.1 (**22%**)
R1229E – FMN semiquinone	-	138 ± 3 (**73%**)	5.6 ± 0.1 (**27%**)
	+	162 ± 4 (**80%**)	4.3 ± 0.1 (**20%**)

It is apparent that the hydride transfer occurs rapidly in both the CaM-free and CaM-bound states, with the kinetic profile resembling that of the CaM-bound, activated form of the wild-type enzyme; fast flavin reduction is followed by further disproportionation events. This means that the R1229E mutant has activated hydride transfer in the CaM-free state.

All of the flavin reduction experiments with the R1229E mutant were repeated in the presence of ferrous cytochrome *c*, in order to investigate the possibility of inhibition in the steady-state turnover assays. Figure 5.10 plots the stopped-flow mixing of oxidised R1229E nNOSrd, augmented with 10 µM ferrous cytochrome *c*, vs. NADPH. A significant part of the absorbance trace is taken up by the more intense absorption of cytochrome *c* (Panel A); however the reduction of the flavin band at 457 nm can still be observed (Panel B).

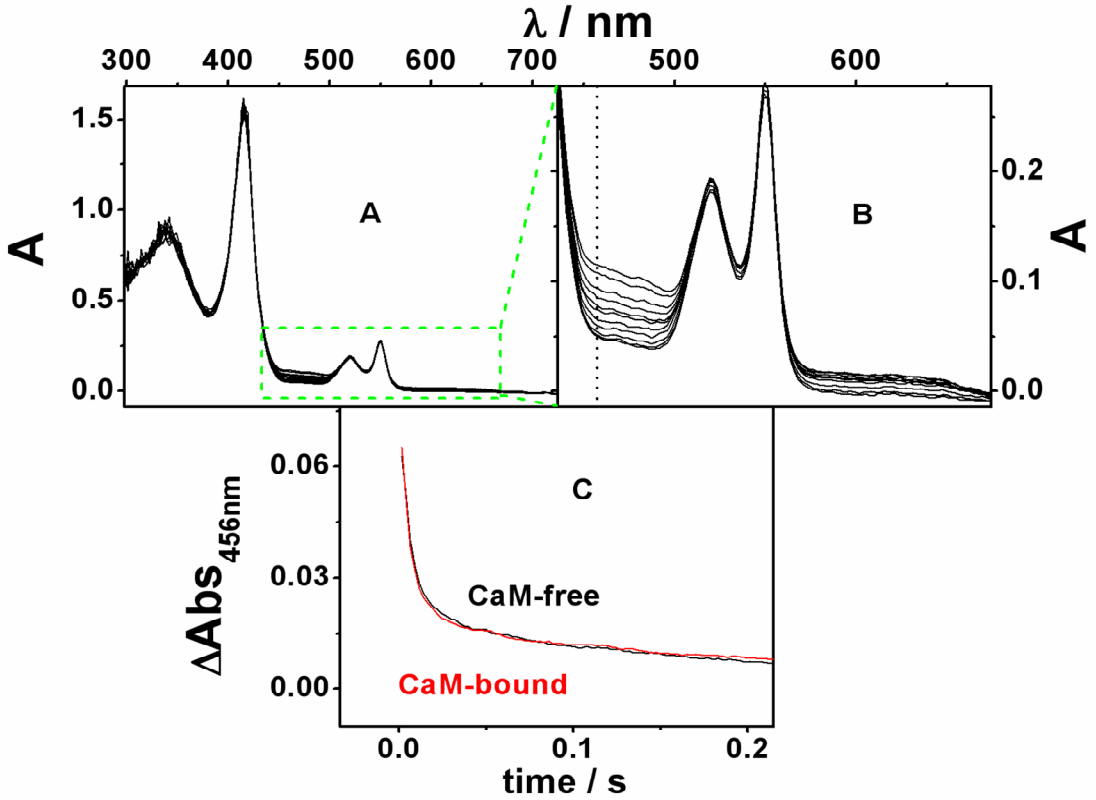

Figure 5.10 Stopped-flow reduction of oxidised R1229E nNOSrd (10µM), in the presence of cytochrome *c* (10µM), by NADPH (100µM). Diode array spectra for the CaM-free reaction are shown in (A) broad-range and (B) close-up wavelengths to highlight the flavin reduction occurring at 457 nm. (C) Traces for time-courses of flavin reduction.

The absorbance change in this experiment was only half of the magnitude of the analogous change in Figure 5.7 (0.06 vs. 0.125), although the concentration of enzyme was the same in both reactions. This indicates that only the first hydride transfer occurred which means that the kinetic profile (Panel C) and the derived parameters (Table 5.6) of the oxidised enzyme are now similar to those obtained in the experiments with the one-electron reduced R1229E mutant where a single hydride transfer also occurs. The fast rate constant in the initial reduction is retained, but the presence of cytochrome *c* clearly inhibits the inter-flavin electron transfer from FAD to FMN.

Table 5.6 Summary of pre-steady-state reduction of R1229E nNOSrd by NADPH

Enzyme	Ca^{2+} / CaM	k_1 / s^{-1} (**Abs**)	k_2 / s^{-1} (**Abs**)
R1229E – FMN oxidised	-	169 ± 5 (**52%**)	4.0 ± 0.1 (**48%**)
	+	156 ± 6 (**57%**)	5.6 ± 0.1 (**43%**)
R1229E – FMN oxidised + cytochrome c^{2+}	-	128 ± 2 (**71%**)	4.5 ± 0.1 (**29%**)
	+	141 ± 2 (**74%**)	3.6 + 0.1 (**26%**)
R1229E – FMN semiquinone	-	138 ± 3 (**73%**)	5.6 ± 0.1 (**27%**)
	+	162 ± 4 (**80%**)	4.3 ± 0.1 (**20%**)
R1229E – FMN semiquinone + cytochrome c^{2+}	-	139 ± 3 (**80%**)	5.4 ± 0.2 (**20%**)
	+	160 ± 6 (**89%**)	3.8 ± 0.4 (**11%**)

5.4 Spectroelectrochemistry

The thermodynamic stability of the flavin cofactors was shown in section 4.4 not to be affected by CaM-binding to nNOSrd. There was an effect observed, however, in a previous study of the isolated FMN-binding domain [88]. There, the FMN oxidised/semiquinone couple was more stabilised in nNOSrd (-100 vs -180 mV), indicating that the presence of the other binding domains has an effect on the stability of the bound FMN cofactor. The R1229E mutant may have a related effect due to the change at the FAD/FMN interface region, but the residue is also in close proximity to the bound FAD cofactor so could affect more than one reduction potential.

R1229E nNOSrd was analysed under identical conditions to the wild-type enzyme using OTTLE potentiometry. Figure 5.11, Panel A, shows the UV-visible spectra obtained during the stepwise reduction of the mutant by 30 mV increments. The spectra are very similar to those obtained for the wild-type enzyme in Figure 4.12. The resultant plots of the absorbance at 456 nm and 592 nm vs. applied potential (Panel B) were fitted simultaneously to Equation 2.1, yielding the midpoint reduction potentials listed in Table 5.7.

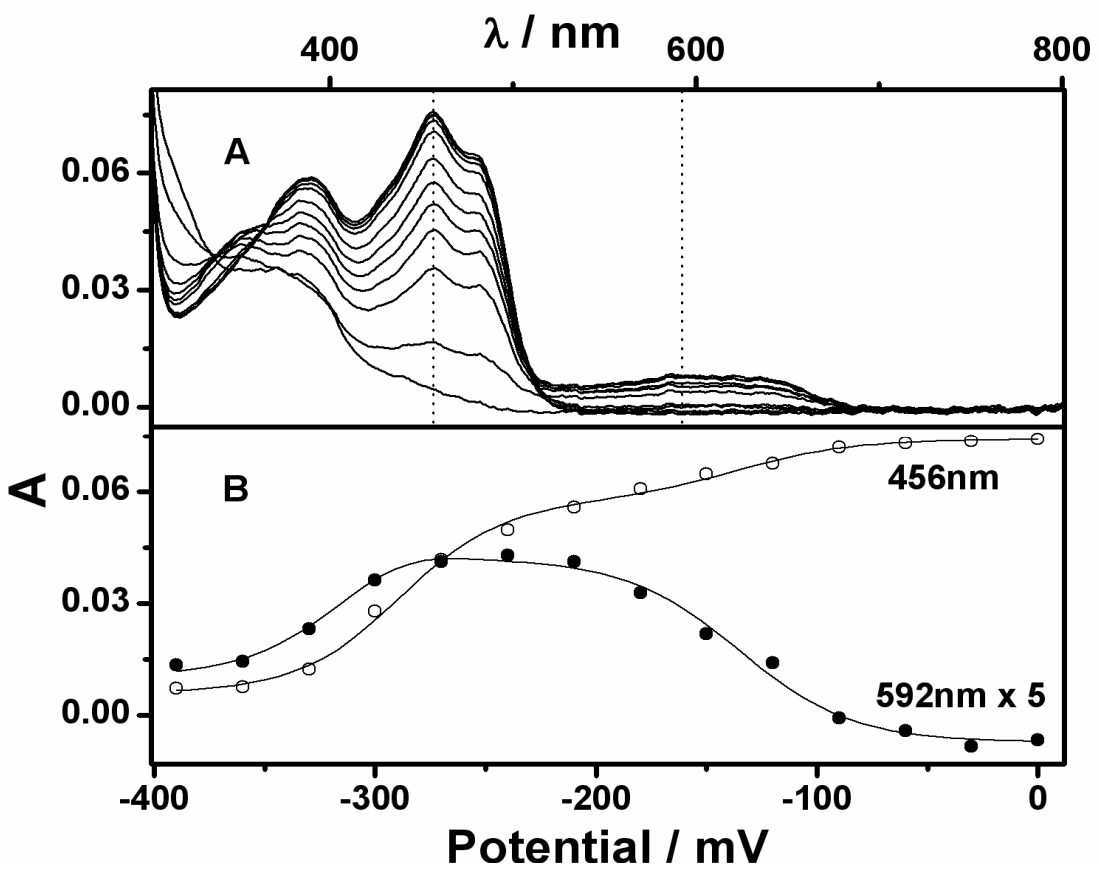

Figure 5.11 OTTLE potentiometry of R1229E nNOSrd in the absence of CaM. Spectroelectrochemistry was carried out in 100mM Tris pH 7.5, 500mM KCl with mediators added. (A) Spectra recorded at 30mV intervals. (B) Corresponding absorbance at 456 nm and 592 nm plotted against applied potential and fitted to a modified Nernst equation (Equation 2.1).

Table 5.7 Midpoint reduction potentials of nNOSrd / mV

Enzyme	FMN ox/sq	FMN sq/hq	FAD ox/sq	FAD sq/hq
Isolated Domains [88]	-179 ± 3	-314 ± 3	-291 ± 3	-326 ± 3
Wild-type (+CaM) [88]	-98 ± 5	-300 ± 8	-296 ± 6	-320 ±10
Wild-type (-CaM)	-101 ± 4	-271 ± 6	-289 ± 6	-301 ± 7
R1229E (-CaM)	-135 ± 4	-278 ± 9	-283 ± 9	-300 ± 9
R1229E (+CaM)	-140 ± 4	-246 ± 8	-268 ± 8	-270 ± 8

Clearly none of the redox-active reduction potentials, i.e. the FMN semiquinone / hydroquinone pair or either of the FAD transitions, are affected by the introduction of the R1229E mutation, which indicates that the steady-state inhibition of electron

transfer is not caused by a thermodynamic change in the flavin cofactors. Furthermore, thermodynamic effects alone would not explain the activation of hydride transfer and electron transfer in the pre-steady-state experiments. It is intriguing that a mutation close to the site of the bound FAD cofactor affects exclusively the reduction potential of the bound FMN cofactor; only the FMN oxidised/semiquinone couple is altered, just as for the isolated FMN-binding domain. The value for the R1229E mutant falls midway between the reductase domain and the FMN-binding domain, indicating that the interface is open such that the FMN cofactor is exposed relative to wild-type nNOSrd.

5.5 Discussion

The reduction of cytochrome *c* by nNOSrd is the measurement by which the electron transfer activity is most frequently studied. Alteration of any of the structural regulatory features in nNOSrd activates this electron transfer through the CaM-free enzyme, but not necessarily to the oxygenase domain in the holoenzyme. Table 5.8 summarises previous data on the activation of steady-state cytochrome *c* reduction by CaM in nNOS mutants. The mutations do not generally affect turnover in the presence of CaM, rationalised by the fact that nNOSrd is catalytically repressed in the absence of CaM. Deletion of the CT, however, produces a truncated mutant that turns over slightly faster than wild-type in the presence of CaM [105]. This, as well as mutation of Phe1395 [128], which facilitates the reaction between NADPH and FAD, both also activate NO synthesis in the CaM-free state. The effect of the R1229E mutation on steady-state cytochrome *c* reduction by nNOSrd is particularly severe. In the presence of CaM, the enzyme is 30-fold slower than the wild-type and 4-fold slower than in the absence of CaM. This unique shift in behaviour is particularly striking given that only a single charge reversal mutation is involved.

Table 5.8 CaM-dependent activation factors for cyt. *c* reduction in nNOSrd	
Enzyme	Ratio CaM-bound / CaM-free
wild-type	10
SI deletion [117]	4
AI deletion [102]	2.5
R1400E [124]	1.4
F1395S [128]	1.2
CT deletion [105]	0.77
R1229E	0.23 (with inhibition)
R1229E + 1 M salt	0.37

All of the mutations listed have multiple effects on the CaM-free enzyme, often characterised by increased cytochrome *c* reductase activity, faster rates of flavin reduction and decreased response to CaM. It is likely that destabilisation of the FAD/FMN interface is a common cause of these effects. Arg1229 is not part of an autoinhibitory feature, or of any other catalytic unit. Therefore, its mutation reports directly on the importance of the interface to the different steps of catalysis.

As discussed previously for the wild-type oxidised enzyme, the transfer of NADPH to FAD shows a complex CaM-effect, with two consecutive hydride transfers occurring in shifting phases. For the R1229E mutant the results are more obvious, with two exponentials of equal amplitudes, it is clear that the first hydride transfer is fast and the second is slow. The reason for this is a slow interflavin electron transfer step occurring between the two hydride transfers. Note that it is apparent from Panel C of Figure 5.7 that removing CaM from nNOSrd and introducing the R1229E mutation clearly affects different steps of the reduction process.

For the wild-type one-electron reduced enzyme, hydride transfer is slow in the absence of CaM and fast with CaM bound. This was attributed in the previous chapter to a conformational equilibrium between “hinged-open” and hinged-closed” states, reproduced in Figure 5.12. Presumably the R1229E mutant favours a hinged-open conformation in which hydride transfer is rapid and interflavin electron transfer is slowed. It is logical to consider that the converse is also true, i.e. that hydride transfer in the hinged-closed or “locked” conformation is slowed and interflavin

electron transfer is rapid (the two flavin rings are only 5 Å apart in the hinged closed state presented in the crystal structure and the $NADP^+$ is bound in an unproductive conformation). In the case of the wild-type, the stability of the domain-domain interface determines the rate of hydride transfer from NADPH to FAD by controlling the rate at which the enzyme can hinge open (approx 6.5 s^{-1} CaM-free). The rate of electron transfer from FAD to FMN in the R1229E mutant conversely depends on the rate at which the enzyme can hinge close (approx 5 s^{-1}), if it can access this state at all. The values in Table 4.6 indicate that the rate constants for both hydride and interflavin electron transfer increase by at least an order of magnitude when the appropriate conformation is stabilised.

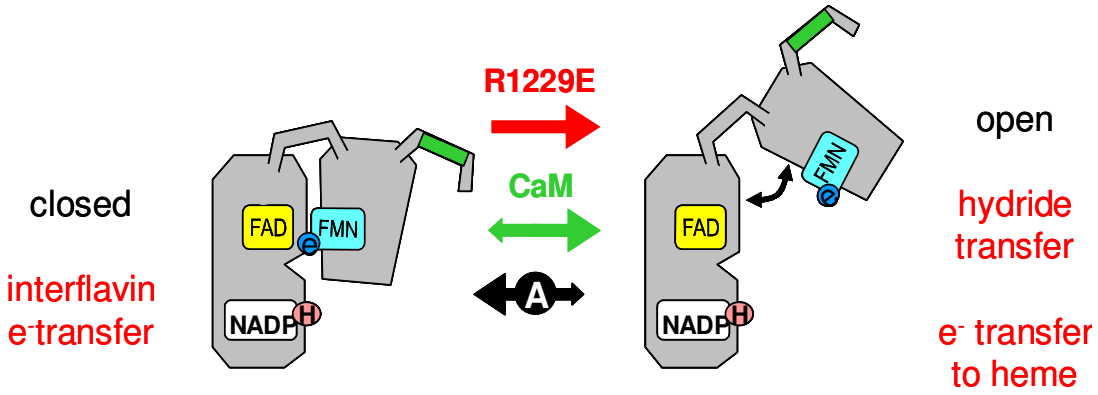

Figure 5.12 Proposed scheme for the mechanism of CaM-activation of nNOSrd. The R1229E mutation disrupts the conformational equilibrium to form a predominantly open enzyme.

The fact that cytochrome *c* is able to inhibit interflavin electron transfer in the mutant enzyme suggests that the FAD and FMN domains separate enough to allow another protein to access the interface. This indicates that the FMN domain is able to move a large distance during catalysis, which may be a feature of electron transfer to the nNOS heme in the holoenzyme. In fact, the short-range nature of electrostatic interactions such as the salt bridge between R1229 and the acidic patch in nNOS means that once the contact is broken during domain-domain motion, wide separation such as that observed in the R1229E mutant is likely. The pre-steady-state reduction of cytochrome *c* by nNOSrd is a second order process dependent on the collision frequency between cytochrome *c* and the FMN. The rate constants measured for CaM-bound wild-type nNOSrd, the R1229E mutant and the isolated FMN domain are all very similar, indicating that the FMN is equally accessible in all three cases. This

indicates that CaM binding induces a mainly open form of the enzyme, in which the FMN and FAD are not usually in contact. Electron transfer from FAD to FMN in the hinged-closed form is likely to be very rapid over the 5 Å distance reported in the crystal structure, such that the hinged closed form may only need to be sampled very briefly to maintain turnover.

Mutation of the acidic patch interface residues Glu816 and Glu762 (in addition to Arg1229) has recently been shown to activate electron transfer through CaM-free nNOS and to slow the rate of electron transfer to nNOS heme [81]. It has been speculated that the same residues interact with a basic patch on the oxygenase domain, including Lys423. Mutation of this residue has also been shown to affect the rate of NO synthesis [56]. None of these mutations, or the R1229E mutant described here, result in the activation of NO synthesis in CaM-free nNOS. Thus, there is no correlation between the strength of interaction across the FAD-FMN interface and NO synthesis activity.

In summary, the R1229E mutation disrupts the FAD-FMN domain interface in nNOSrd such that there is no regulatory interaction between the two domains. Electron transfer from FAD to FMN is severely retarded and hydride transfer from NADPH to FAD is accelerated, particularly when compared to the CaM-free wild-type one-electron reduced enzyme. This is consistent with a model for catalytic action of the enzyme in which it exists in two conformational states, “closed” and “open”, with distinct kinetic events happening in each state. The “closed” form allows electron transfer from FAD to FMN, while the enzyme must be in the “open” form for both facile hydride transfer from NADPH to FAD and electron transfer from FMN to cytochrome *c* or nNOS heme. The presence of the salt-bridge at Arginine1229 is clearly essential for the successful movement of the FMN binding domain from an electron-receiving position to an electron-donating one and can be thought of as another regulatory feature in the complex structural makeup of nNOS.

Chapter 6
Residues involved in hydride transfer

6.1 Introduction

Hydride transfer from NADPH to the bound FAD cofactor in nNOSrd is enabled by the movement of the substrate's nicotinamide moiety from a non-productive to a productive conformation [125]. This is associated with the mobility of Phe1395 away from FAD, which forms part of a complex regulatory system of the subsequent electron transfer events [127, 128]. The area around the bound FAD cofactor is depicted in Figure 6.1 for the non-productive conformation in nNOSrd [74] and the productive conformation in a mutant of CPR [126]. This "FAD-active-site" includes a number of well conserved residues between FNR, CPR and the NOS isoforms.

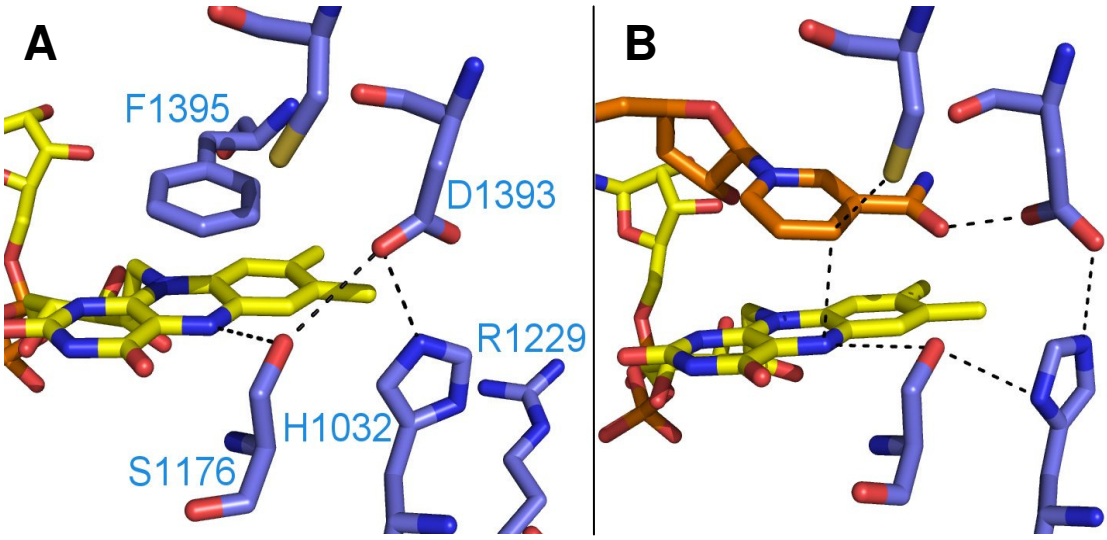

Figure 6.1 X-ray crystal structures of (A) nNOSrd (PDB code 1Tll) and (B) W677X CPR (1JAO). FAD is coloured yellow, NADPH orange, NADPH-binding domain residues blue. Key interactions are marked with black dashed lines.

Ser1176 is shown to be performing the same role in both conformations by H-bonding to the bound FAD cofactor, at the flavin N5 position where NADPH will transfer hydride to. Substitution of the serine by alanine, S1176A, has been carried out to ascertain the importance of this interaction. The alanine in place of the serine will be shorter and have no H-bonding capability.

Asp1393 appears able to form H-bonding interactions to either Ser1176 or His1032 in the non-productive conformation, and to the nicotinamide group or His1032 in the productive conformation. This implies that it may serve to position NADPH correctly, as well as stabilising the other FAD-active-site residues. In the D1393E

mutant that was made, the aspartate was replaced by a glutamate. This substitution retains H-bonding capabilities, as well as the charge and acidity, but the longer chain length of glutamate may affect the steric environment around the FAD cofactor.

His1032 forms H-bonding interactions, with either Asp1393 or Ser1176, and its properties as a base could mean that it has a role in the proton removal from the FAD cofactor. Furthermore, it is adjacent to Arg1229 which forms the salt-bridging interaction with the FMN-binding domain, meaning that it may be close to solvent exposure in the open conformation of nNOSrd. Substitutions of the histidine were made to glutamine and serine. The H1032Q mutant will retain a residue of approximately the same size, but with different H-bonding properties. The H1032S mutant, on the other hand, will affect the size of the residue and possibly the conformation of the surrounding residues, along with the removal of the basic character of the residue.

Each of the FAD-active-site mutants in this chapter has been investigated with regard to the activation step by CaM in steady-state turnover experiments and pre-steady-state kinetic measurements. The different properties of each residue in the H-bonding network are directly related to effects on catalysis and regulation.

6.2 Steady-state turnover

6.2.1 Cytochrome *c* reduction

The rate of cytochrome *c* reduction is characteristically activated by CaM binding to wild-type nNOSrd (section 4.2.1) and this effect is reversed in the R1229E mutant which is coupled with substrate inhibition effects (section 5.2.1). The same experiments were performed to assess the rate of turnover in the four other FAD-active-site mutants. Rate constants for steady-state cytochrome *c* reduction are plotted in Figure 6.2. In each case, the data exhibited normal kinetic behaviour and were fitted to the Michaelis-Menten equation (Equation 6, Appendix I). The derived values for k_{cat} and K_m are listed in Table 6.1.

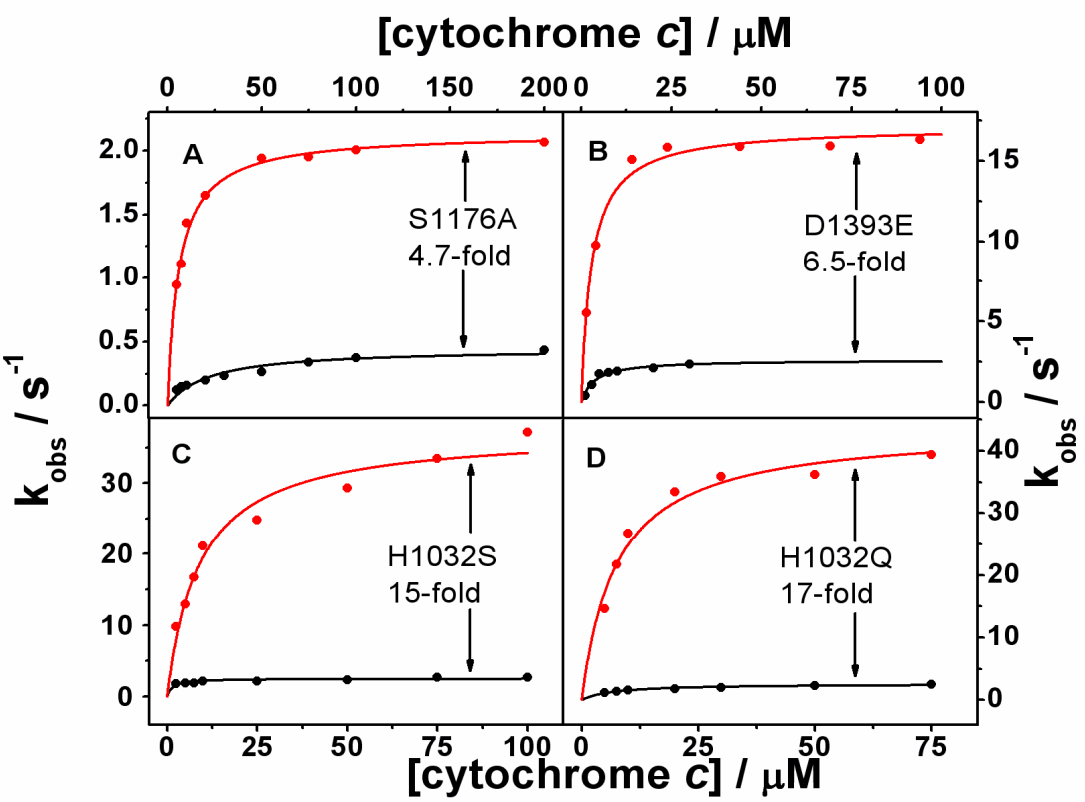

Figure 6.2 Steady-state cytochrome *c* reduction by nNOSrd mutants. Assays were performed at 25°C in 50mM Tris, pH 7.5 + 100mM NaCl. Data are compared for (A) S1176A, (B) D1393E, (C) H1032S and (D) H1032Q in the absence (black points) and presence (red points) of CaM

Table 6.1 Steady-state cytochrome *c* reduction by nNOSrd mutants

Enzyme	Ca^{2+} / CaM	k_{cat} / s-1	K_m^{cytc} / μM	CaM-effect
wild-type	- +	10.4 ± 0.4 104 ± 6	3 ± 1 8 ± 2	10-fold
S1176A	- +	0.45 ± 0.03 2.1 ± 0.1	12 ± 5 6 ± 1	4.7-fold
D1393E	- +	2.6 ± 0.2 17 ± 0.5	4 ± 1 3 ± 0.5	6.5-fold
H1032S	- +	2.5 ± 0.1 37 ± 2	1.5 ± 0.5 9 ± 1.5	14.8-fold
H1032Q	- +	2.6 ± 0.1 44 ± 2	7 ± 1 8 ± 1	16.9-fold

The activity of each of the mutants is decreased relative to wild-type nNOSrd, with the greatest effects seen in S1176A. The activity of this mutant is over 20-fold slower in the CaM-free and 50-fold slower in the CaM-bound state. From the position of Ser1176, it would appear that the rate of hydride transfer to the FAD is severely slowed, but still retains CaM sensitivity in the mutant, to a lesser extent than wild-type nNOSrd. These results for the S1176A mutant are consistent with studies in the nNOS holoenzyme [129]. Adjacent to Ser1176 is Asp1393, and the D1393E mutant had the next slowest activity, 4-fold and 6-fold slower than the wild-type enzyme in the absence and presence of CaM respectively. Again, these parameters are consistent with holo-nNOS studies [130], along with the lesser sensitivity to CaM, which implies that the D1393E mutant is affecting a similar step to S1176A nNOSrd.
The two substitutions at His1032 have a different effect on the steady-state turnover of cytochrome *c*. In the absence of CaM the rates of reduction were slowed to the same level as D1393E, however when CaM was present both H1032S and H1032Q nNOSrd transferred electrons at a rate only 2-fold slower than that of the wild-type enzyme. Furthermore the CaM-activation in both of these mutants is greater than for wild-type, a feature that is not observed in other single residue substitutions of nNOSrd. If the CaM-free activity is slowed due to a similar effect as in D1393E, then the CaM-bound enzymes must exhibit a different conformational change.

6.2.2 Ferricyanide reduction

The steady-state reactions of H1032S and H1032Q nNOSrd were further investigated using ferricyanide as the electron acceptor. This does not occur in the same way as the cytochrome *c* reduction, because the ferricyanide ion can access the FAD cofactor in addition to the bound FMN. This leads to a faster rate of reduction and a lesser CaM-mediated activation effect. The observed rate constants are plotted in Figure 6.3, where a linear increase in rate occurred over the concentration range, analogous to the wild-type experiments (section 4.2.2). The data were fitted to a straight-line function and the derived kinetic parameters are listed in Table 6.2.

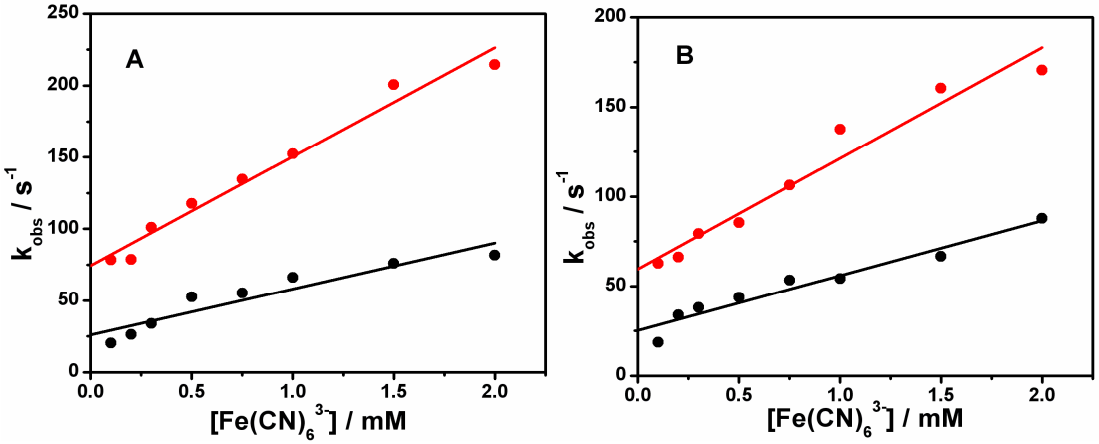

Figure 6.3 Steady-state ferricyanide reduction by (A) H1032S and (B) H1032Q nNOSrd. Assays were performed at 25°C in 50mM Tris buffer, pH 7.5 + 100mM NaCl. Data points for CaM-free (black) and CaM-bound (red) were plotted in Origin 7.5 (Microcal) and fitted to a straight line equation.

Table 6.2 Steady-state ferricyanide reduction by H1032S and H1032Q nNOSrd

Enzyme	Ca^{2+} / CaM	gradient / $mM^{-1}s^{-1}$	y-intercept / s^{-1}	CaM-effect
wild-type	-	81 ± 2	21 ± 2	1.6-fold
	+	131 ± 4	60 ± 4	
H1032S	-	32 ± 5	26 ± 5	2.4-fold
	+	76 ± 5	74 ± 5	
H1032Q	-	30 ± 3	25 ± 3	2.1-fold
	+	62 ± 5	60 ± 5	

Compared to wild-type nNOSrd, the catalytic efficiency of the mutants is slowed by 2.5-fold CaM-free and 2-fold CaM-bound, and the activation of both H1032S and H1032Q nNOSrd is again greater than the CaM-effect seen for the wild-type enzyme (1.5-fold). The y-intercept values, on the other hand, show no deviation from the corresponding wild-type values. In the wild-type enzyme these corresponded to the rate of cytochrome *c* turnover but for these mutants the CaM-free rate is significantly increased. If these rates represent the transfer of electrons from NADPH to FAD to FMN, then H1032Q and H1032S must behave differently in turnover with ferricyanide vs. turnover with cytochrome *c*. One reason for this may be that the ferricyanide oxidises the bound FMN cofactor before electrons arrive through the

enzyme, therefore the predominantly oxidised form is present which can transfer hydride at a faster rate, due to its partially open conformation.

6.3 Pre-steady-state kinetics

6.3.1 Cytochrome *c* reduction

The accessibility of the bound FMN cofactor to sub-stoichiometric amounts of cytochrome *c* is inhibited by the binding of NADPH to wild-type nNOSrd [119]. This effect is completely abolished in the R1229E mutant, section 5.3.1, and for other mutations where the suppression of CaM-free electron transfer is partially relieved, such as R1400E [124] and F1395S [128]. Figure 6.4 presents the same experiment performed with the S1176A and D1393E mutants of nNOSrd.

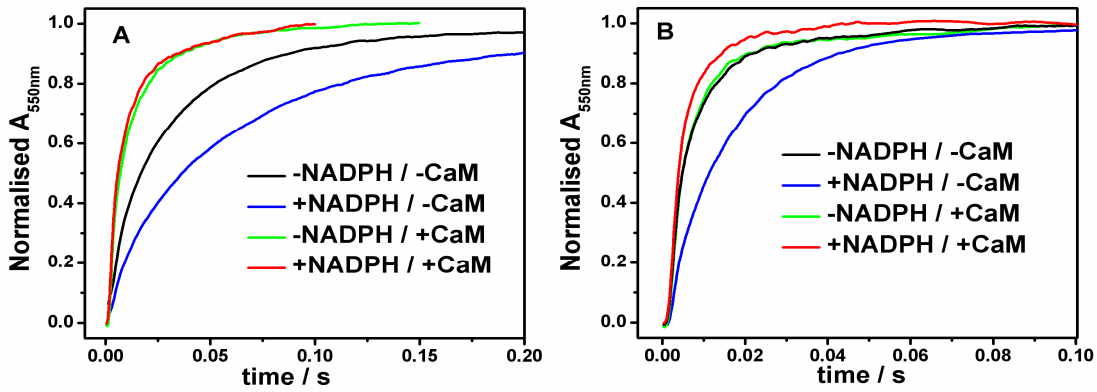

Figure 6.4 Pre-steady-state reduction of cytochrome *c* by (A) S1176A and (B) D1393E nNOSrd. Stopped-flow mixing of pre-reduced enzyme (10μM) with ferric cytochrome *c* (4μM) was carried out at 25°C in the absence and presence of NADPH and CaM.

The initial rates of reduction were measured and corrected for enzyme concentration to give second order rate constants for each state, i.e. the absence and presence of NADPH and CaM. Table 6.3 lists the derived rate constants in comparison to wild-type from a previous study [119]. S1176A nNOSrd exhibits similar behaviour to the wild-type enzyme; NADPH causes a decrease in the accessibility of the bound FMN cofactor and this is relieved by the binding of CaM. The effect is not as pronounced in the mutant however, as the uncomplexed mutant enzyme transfers electrons at a

slower rate than wild-type and the binding of NADPH only lowers the rate constant by 1.6-fold. The CaM-bound rate constant, in both the NADPH-free and NADPH-bound states, is analogous to the wild-type enzyme.

D1393E nNOSrd is not regulated by NADPH in the same way as the wild-type enzyme as the rate constant for the uncomplexed enzyme is greater in the mutant and only has a small CaM-activation effect. The binding of NADPH does slow the rate constant, but this is 10-fold faster than the corresponding wild-type value.

Table 6.3 Pre-steady-state cytochrome *c* reduction by nNOSrd mutants

Second order rate constants / $\mu M^{-1}s^{-1}$				
Enzyme	-NADPH-CaM	+NADPH-CaM	-NADPH+CaM	+NADPH+CaM
wild-type [119]	15.4	1.1	37.8	35.5
S1176A	9.4 ± 0.7	5.8 ± 0.5	35.7 ± 0.9	38.0 ± 0.9
D1393E	27.6 ± 0.7	11.7 ± 0.3	29.2 ± 0.4	36.7 ± 0.6

6.3.2 Flavin reduction

Reduction of the flavin cofactors in nNOSrd by NADPH occurs primarily as a hydride transfer from the nicotinamide group to FAD, followed by electron transfer between the flavin cofactors. This reduction was differently regulated by CaM in the fully oxidised and one-electron reduced forms (section 4.3), by way of a conformational equilibrium between hinged-open and hinged-closed states. This equilibrium was drastically affected in the hinged-open R1229E mutant, with activated hydride transfer and inhibited interflavin electron transfer (section 5.3.2).

Figure 6.5 presents the flavin reduction reactions of S1176A nNOSrd, both oxidised and one-electron reduced. From the spectral changes in Panel A, it is obvious that the reaction does not proceed as far as for the wild-type enzyme, there is no fully reduced state present after 8 seconds for the CaM-free mutant, or after 2 seconds in the presence of CaM. The traces in Panel C were normalised according to their

apparent end-point and fitted to the same double-exponential function over the corresponding time period. The associated kinetic parameters are listed in Table 6.4 and the CaM-activation effect can be seen to be analogous to that for the wild-type enzyme. There is a shift towards the fast phase of reduction, while the actual rate constants are slowed by a similar factor as that of the cytochrome *c* reduction activity. The binding of CaM to the oxidised mutant enzyme clearly activates the interflavin electron transfer, observed in the inset of Panel C. The same absorbance change occurs over 8 seconds CaM-free and 2 seconds CaM-bound. Also of note is that this is the formation of the FMN semiquinone only, a second electron is not transferred over the measured time period.

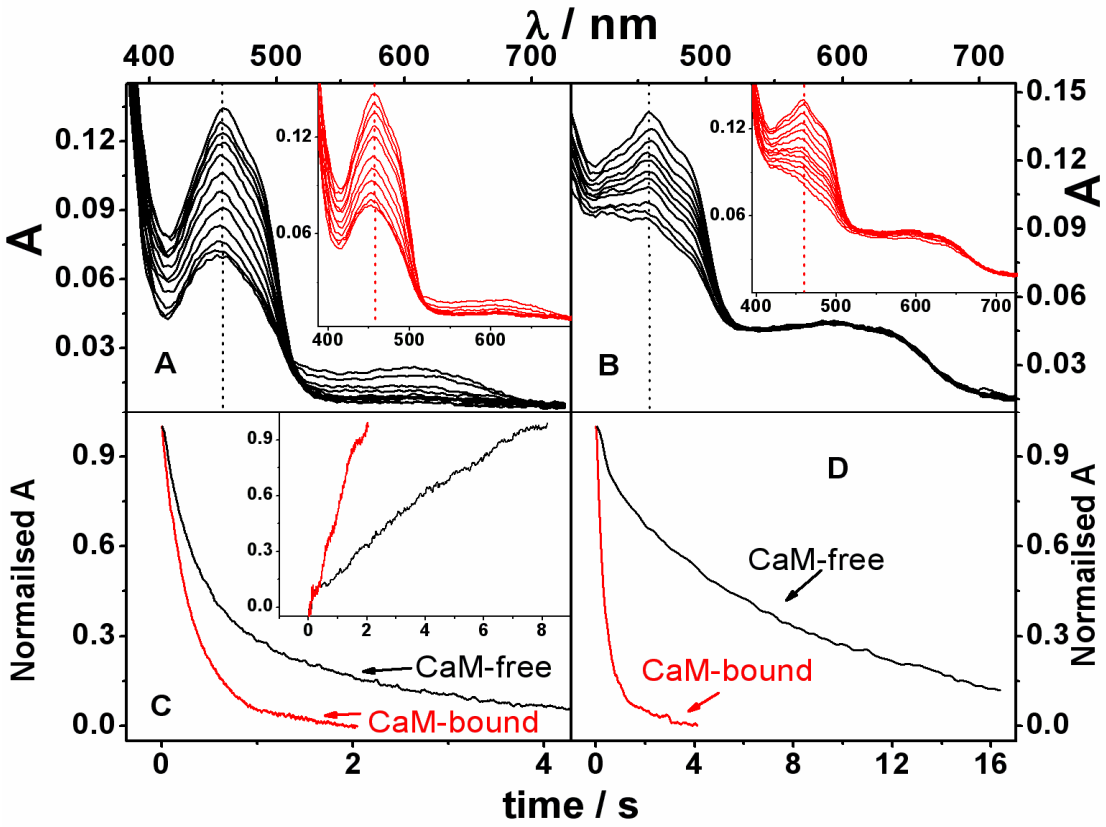

Figure 6.5 Stopped-flow reduction of S1176A nNOSrd (10µM) by NADPH (100µM). Diode array spectra for (A) oxidised CaM-free and (inset) CaM-bound, and (B) 1-electron reduced CaM-free and (inset) CaM-bound. Corresponding reductive traces for (C) oxidised at 457 and (inset) 592 nm and (D) one-electron reduced at 457 nm.

One-electron reduced S1176A nNOSrd in Panel B again proceeds very slowly, with the spectra representing 16 seconds of reaction in the absence of CaM and 4 seconds for the CaM-bound state. The time-dependent traces in Panel D were treated in the same manner as the oxidised versions, and the kinetic parameters in Table 6.4

highlight a similar pattern to the wild-type enzyme. The large slow phase of the CaM-free reduction is of a similar rate constant to the CaM-free cytochrome *c* reductase activity (0.45 s^{-1}) with a short phase at significantly faster rate. The trace in the presence of CaM has the same profile to the oxidised CaM-bound enzyme and corresponds to the activated steady-state cytochrome *c* reduction rate (2.1 s^{-1}).

Table 6.4 Pre-steady-state reduction of S1176A nNOSrd by NADPH

Enzyme	Ca^{2+} / CaM	k_1 / s^{-1} (**Abs**)	k_2 / s^{-1} (**Abs**)
S1176A – FMN oxidised	-	3.3 ± 0.1 (**59%**)	0.46 ± 0.01 (**41%**)
	+	3.5 ± 0.06 (**86%**)	0.40 ± 0.08 (**14%**)
S1176A – FMN semiquinone	-	1.9 ± 0.04 (**19%**)	0.11 ± 0.01 (**81%**)
	+	3.2 ± 0.04 (**83%**)	0.39 ± 0.03 (**17%**)

The stopped-flow reduction of D1393E nNOSrd is represented in Figure 6.6, again comparing the oxidised and one-electron reduced forms of the enzyme. The spectra in Panel A indicate that the oxidised D1393E enzyme proceeds further towards the fully-reduced state than S1176A in the oxidised form, but it does not reach the same stage as the corresponding wild-type reaction. The data for the CaM-free and CaM-bound forms here are extremely similar, and this is reflected in the traces plotted in Panel C. Both of the traces were fitted to a double exponential function over 2 seconds and the derived rate constants are compared in Table 6.5. The phases of reduction are the same in both states, with the binding of CaM here seen to speed up the actual rate, a slight deviation from the wild-type CaM-effect. Another difference is noticeable in the spectra in Panel A, where there is no apparent formation of the FMN semiquinone. This would indicate that the di-semiquinone of the mutant enzyme is unfavourable and the transfer of two electrons from FAD to FMN happens simultaneously to allow the reaction to proceed.

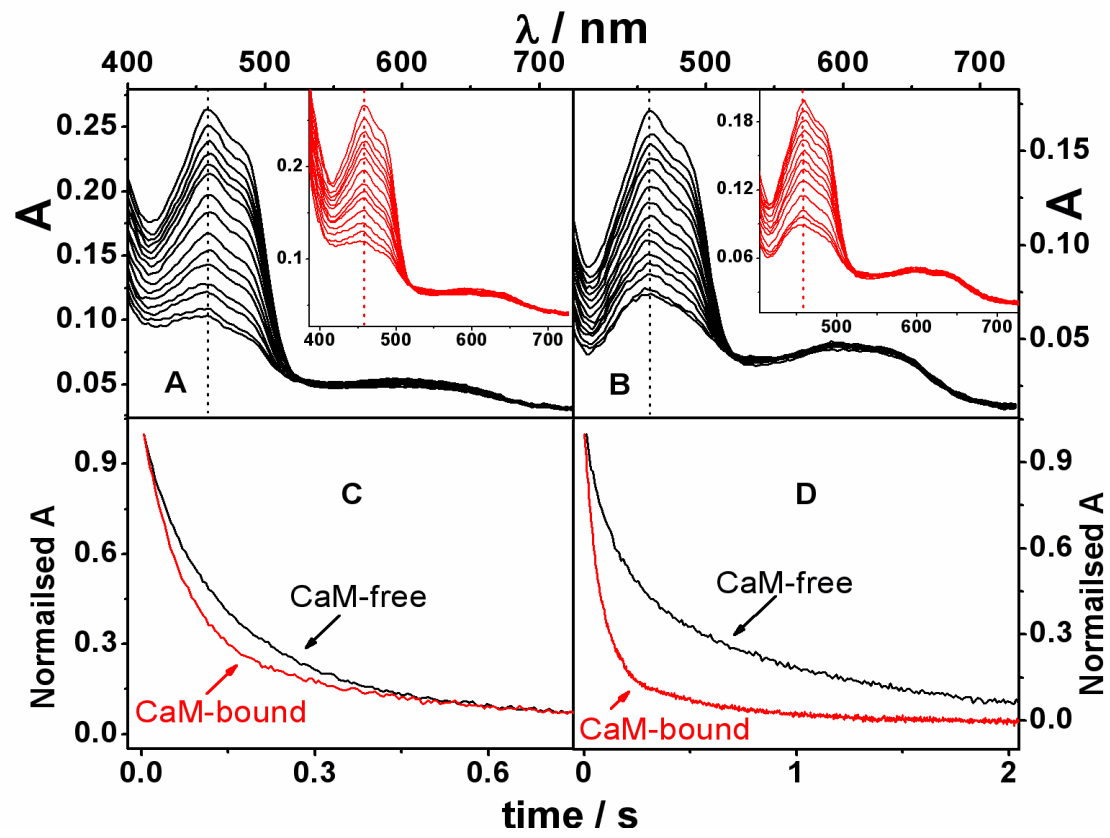

Figure 6.6 Stopped-flow reduction of D1393E nNOSrd (10μM) by NADPH (100μM). Diode array spectra for (A) oxidised CaM-free and (inset) CaM-bound, and (B) 1-electron reduced CaM-free and (inset) CaM-bound. Corresponding reductive traces at 457 nm for (C) oxidised and (D) one-electron reduced.

Panel B of Figure 6.6 shows the one-electron reduced form of D1393E nNOSrd being reduced, again to a greater extent than the corresponding S1176A experiment. The spectra for the CaM-free state occurred over 4 seconds while the CaM-bound spectra represent 2 seconds. The traces in Panel D were normalised and fitted to the same function as for the previous reactions, and the pattern of the rate constants again deviates slightly from that observed for the other enzymes (Table 6.5). There is still a larger slower phase, however this comprises only 54% of the reduction here compared to 80% for wild-type and S1176A nNOSrd. The rate constant of the slow phase is comparable to the cytochrome *c* reductase activity (2.6 s^{-1}), as is the fast rate constant that makes up most of the CaM-bound reduction (17 s^{-1}). Another feature that is retained is that the CaM-bound traces for both oxidised and one-electron reduced D1393E nNOSrd have the same kinetic profile, i.e. the relative rates and magnitude of the phases of reduction are the same in both activated forms.

Table 6.5 Pre-steady-state reduction of D1393E nNOSrd by NADPH

Enzyme	Ca^{2+} / CaM	k_1 / s^{-1} (**Abs**)	k_2 / s^{-1} (**Abs**)
D1393E – FMN oxidised	-	8.7 ± 0.05 (**73%**)	1.9 ± 0.08 (**27%**)
	+	14.1 ± 0.1 (**74%**)	1.7 ± 0.05 (**26%**)
D1393E – FMN semiquinone	-	7.7 ± 0.1 (**46%**)	1.0 ± 0.02 (**54%**)
	+	14.5 ± 0.1 (**79%**)	2.1 ± 0.1 (**21%**)

The reaction of H1032S nNOSrd with excess NADPH is plotted in Figure 6.7. The spectral changes in Panel A for the fully oxidised enzyme are similar to those recorded for the D1393E mutant, but in this case both the CaM-free and CaM-bound reactions took place over 1 second. The corresponding traces in Panel C were normalised and fitted to a double exponential equation over 1 second and the kinetic parameters are listed in Table 6.6. The rate constants for the oxidised H1032S enzyme are approaching the value of those for wild-type nNOSrd, with the CaM-effect shifting more of the reduction into the fast phase in a similar manner. As with the oxidised D1393E mutant there was very little formation of FMN semiquinone observed at 592 nm.

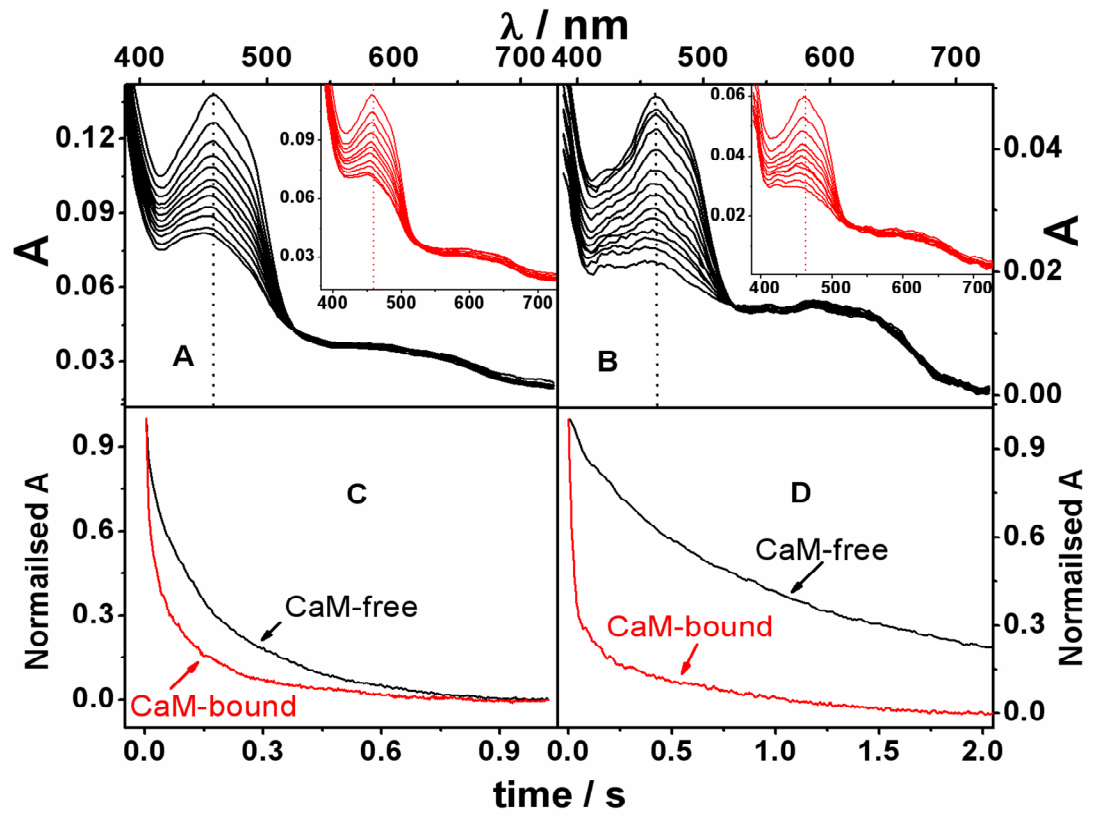

Figure 6.7 Stopped-flow reduction of H1032S nNOSrd (10μM) by NADPH (100μM). Diode array spectra for (A) oxidised CaM-free and (inset) CaM-bound, and (B) 1-electron reduced CaM-free and (inset) CaM-bound. Corresponding reductive traces at 457 nm for (C) oxidised and (D) one-electron reduced.

CaM-free one-electron reduced H1032S nNOSrd (Panel B) reacted very slowly with NADPH compared to the oxidised form, with the spectral changes taking place over 8 seconds, while the CaM-bound reaction was completed within 2 seconds. The time-dependent reductive traces in Panel D were analysed as for the other enzymes, and the kinetic parameters from Table 6.6 show a similar pattern to those observed previously. The size of the larger, slower CaM-free phase is midway between the percentages for the wild-type and D1393E enzymes, indicating an intermediate effect on the conformational equilibrium. The value of the rate constant in this case does not exactly concur with the rate of CaM-free cytochrome *c* reduction, but is of the same order of magnitude. The kinetic profile in the presence of CaM was as expected from the wild-type activation effect.

Table 6.6 Pre-steady-state reduction of H1032S nNOSrd by NADPH

Enzyme	Ca^{2+} / CaM	k_1 / s^{-1} (**Abs**)	k_2 / s^{-1} (**Abs**)
H1032S – FMN oxidised	-	43 ± 2 (**29%**)	4.6 ± 0.1 (**71%**)
	+	51 ± 2 (**59%**)	6.1 ± 0.1 (**41%**)
H1032S – FMN semiquinone	-	2.4 ± 0.1 (**36%**)	0.5 ± 0.02 (**64%**)
	+	47 ± 1 (**74%**)	1.7 ± 0.1 (**26%**)

Figure 6.8 plots the reaction between H1032Q nNOSrd and NADPH, where the spectra for the fully oxidised enzyme in Panel A are comparable to those for the fully oxidised H1032S enzyme. Again, the reduction was completed over 1 second for both CaM-free and CaM-bound with very little absorbance change for the FMN semiquinone at 592 nm. The traces in Panel C are also comparable to those for H1032S nNOSrd, as are the kinetic parameters in Table 6.7. The only difference between the two sets of numbers is that the percentage of absorbance change occurring in the CaM-free fast phase is higher for the H1032Q enzyme.

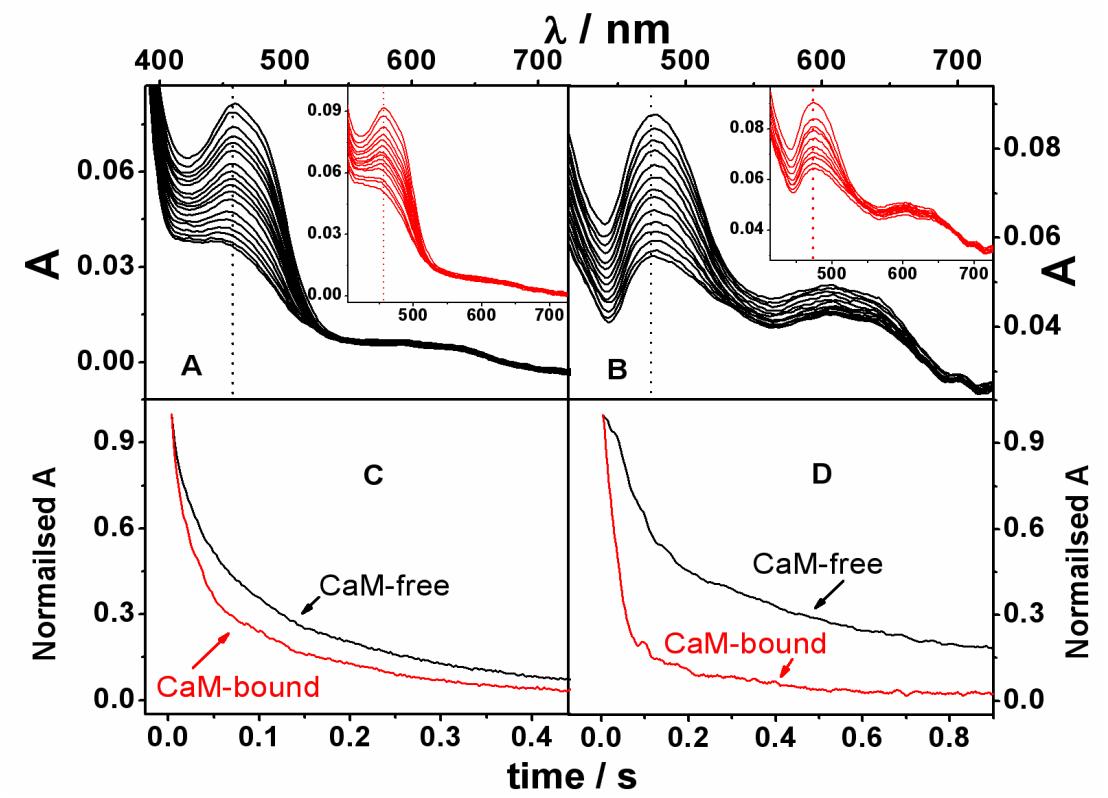

Figure 6.8 Stopped-flow reduction of H1032Q nNOSrd (10μM) by NADPH (100μM). Diode array spectra for (A) oxidised CaM-free and (inset) CaM-bound, and (B) 1-electron reduced CaM-free and (inset) CaM-bound. Corresponding reductive traces at 457 nm for (C) oxidised and (D) one-electron reduced.

Spectra collected for the stopped-flow reaction of one-electron reduced H1032Q, in Panel B of Figure 6.8, appear to exhibit a change in the absorbance profile at 457 nm, however this was not observed during the preparation of the samples and may indicate the presence of a contaminant within the apparatus. This did not have any effect on the rate of reduction, as the CaM-free reaction with NADPH took place over 4 seconds, and 2 seconds in the presence of CaM. The traces in Panel D were affected by a high signal-to-noise ratio, but fitted well to a double exponential function and yielded a set of kinetic parameters comparable to all of the other enzymes. Here, the CaM-free slow phase is now slightly smaller than the fast phase, however this is consistent with the oxidised H1032Q experiment, which reflects on a subtle conformational change between the glutamine and serine residues. One common feature of the two substitutions of His1032 is that the CaM-bound traces for the oxidised vs. one-electron reduced forms do not exactly match with each other. There is a lesser proportion in the fast phase for the fully oxidised enzyme, which may be an

indication that the conformational equilibrium is differently modified by CaM in these mutants relative to the wild-type enzyme.

Table 6.7 Pre-steady-state reduction of H1032Q nNOSrd by NADPH

Enzyme	Ca^{2+} / CaM	k_1 / s^{-1} (**Abs**)	k_2 / s^{-1} (**Abs**)
H1032Q- FMN oxidised	-	30 ± 1 (**49%**)	4.6 ± 0.1 (**51%**)
	+	49 ± 1 (**59%**)	6.1 ± 0.1 (**41%**)
H1032Q – FMN semiquinone	-	10 ± 0.1 (**57%**)	1.0 ± 0.1 (**43%**)
	+	33 ± 0.3 (**84%**)	3.8 ± 0.2 (**16%**)

6.4 Spectroelectrochemistry

The effect of CaM-binding on the midpoint reduction potentials of the bound flavin cofactors in nNOSrd is negligible, as highlighted in section 4.4, while destabilisation of the FAD/FMN interface (section 5.4) destabilises only the non-catalytically-active FMN oxidised/semiquinone couple. The FAD-active-site substitutions at Ser1176 and Asp1393 affect electron transfer in nNOSrd in differing ways to the R1229E mutant so could feasibly have an effect on any of the thermodynamic parameters.

OTTLE potentiometry was utilised to assess the midpoint reduction potentials in S1176A and D1393E nNOSrd, as shown in Figure 6.9. Panel A and C represent the incremental potential decrease and resulting plots for S1176A, while Panel B and D correspond to the D1393E mutant. Simultaneous fitting to equation 2.1 in both cases yielded the values listed in Table 6.8.

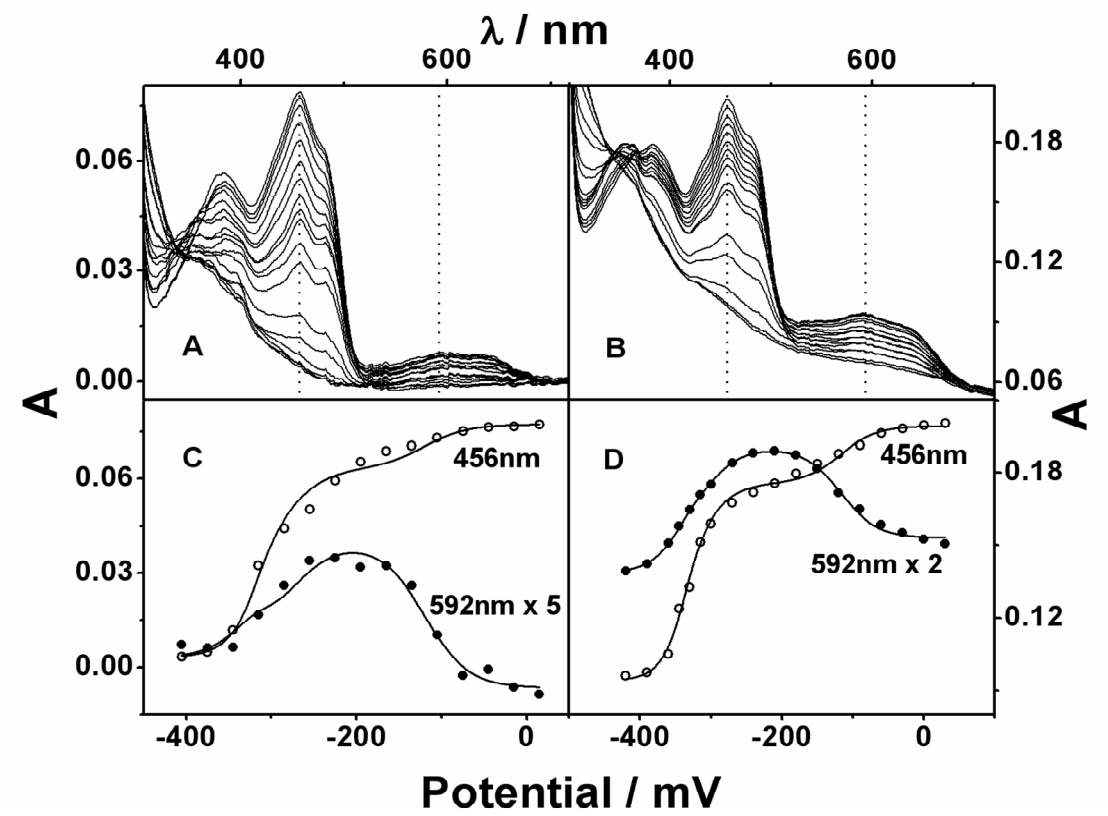

Figure 6.9 OTTLE potentiometry of (A) S1176A and (B) D1393E nNOSrd in the absence of CaM. Spectroelectrochemistry was carried out in 100mM Tris pH7.5, 500mM KCl with mediators added. Spectra were recorded at 30mV intervals and corresponding traces for absorbance at 456 nm and 592 nm were plotted against applied potential for (C) S1176A and (D) D1393E and fitted to a modified Nernst equation (Equation 2.12)

Table 6.8 Midpoint reduction potentials of nNOSrd / mV

Enzyme (-CaM)	FMN ox/sq	FMN sq/hq	FAD ox/sq	FAD sq/hq
wild-type	-101 ± 4	-271 ± 6	-289 ± 6	-301 ± 7
R1229E	-135 ± 4	-278 ± 9	-283 ± 9	-300 ± 9
S1176A	-125 ± 6	-280 ± 7	-339 ± 13	-298 ± 15
D1393E	-117 ± 3	-307 ± 3	-350 ± 7	-316 ± 7

The potential for the FMN oxidised/semiquinone transition is negatively shifted compared to wild-type nNOSrd in both the S1176A and the D1393E mutants. This effect is not as large as for the hinged-open R1229E mutant but it is again intriguing that residues extremely close to the bound FAD cofactor can affect the stability of the FMN cofactor. The biggest change in both sets of data, however, is in the FAD

oxidised/semiquinone transition which is also negatively shifted relative to wild-type nNOSrd. This means that the FAD semiquinone species is destabilised which in turn means that the enzyme is more likely to transfer 2 electrons from FAD to FMN at the same time. This was observed in the flavin reduction experiments of the D1393E mutant but not in S1176A nNOSrd. Clearly the thermodynamic properties of the cofactor are only one aspect of the catalytic cycle and the S1176A mutant is kinetically hindered during turnover. Furthermore, the two electron couple for the FAD cofactor (the average of the two values) is more negative in both cases indicating that it is more difficult thermodynamically for NADPH to reduce the FAD, which is clearly the case in both mutants. The S1176A mutant appears to affect solely the FAD ox/sq transition, where as the D1393E mutant shifts the other potentials which would correlate with Asp1393 having multiple roles to play in the regulation of electron transfer.

These findings are in contrast to other reports of reduction potentials for similar mutations. S1176A was previously characterised in holo-nNOS [129], where the chemical titration data indicated that the FMN oxidised/semiquinone was positively shifted to greater than +40mV. Furthermore the FAD semiquinone state could not be fitted from the experimental data, and the two electron transition from oxidised to hydroquinone was also reported to be positively shifted. The different environments in nNOSrd and the holoenzyme may result in the broad shifts reported, however the positive shift was not observed in these spectroelectrochemical studies.

The thermodynamics of the D1393N mutant in nNOSrd were assessed in the FAD and NADPH-binding domains only, the construct that resembles FNR [80]. This mutant had very similar kinetic properties to the D1393E mutant in the holoenzyme [130] and the chemical titration of the D1393N FAD cofactor showed a destabilisation in the semiquinone state such that a two electron transition from oxidised to hydroquinone was reported. This was negatively shifted by approximately 20 mV, a similar change to that observed in Table 6.8.

6.5 Discussion

The transfer of a hydride from NADPH to the bound FAD cofactor is activated by the binding of CaM to both holo-nNOS and the isolated nNOSrd [76]. In the previous chapters of this thesis, hydride transfer was shown to be differently regulated in the fully oxidised vs. one-electron reduced forms of the reductase domain, occurring rapidly when the enzyme is in the hinged-open conformational form. Following the hydride transfer step, electrons can be passed directly from FAD to FMN as the cofactors are only 5 Å apart in the crystal structure [74]. This leaves a proton to be removed from the flavin N5 of the FAD cofactor which is not solvent accessible, and instead requires a conserved H-bonding network at its *si*-face to carry out this event.

The alteration of this network to slightly change the H-bonding properties of the residues decreased the turnover activity in each of the mutants studied. The data in Table 6.1 indicate that increased proximity to the FAD cofactor had a larger effect on steady-state cytochrome *c* reduction, but that each activity was enhanced by CaM binding. S1176A nNOSrd had the slowest rate of steady-state electron transfer to cytochrome *c*, which correlates with its slow hydride transfer reactions observed in the pre-steady-state experiments (Table 6.4). Here, the size of the kinetic phases was affected by CaM binding in the same way as wild-type nNOSrd, with the decreased magnitudes of the rate constants matching that of the activity relative to the wild-type enzyme. There was no drastic effect on the pre-steady state reduction of cytochrome *c* for the S1176A mutant (Table 6.3), so the role of Ser1176 appears to be centred on stabilising the reduced forms of FAD and facilitating hydride transfer, rather than affecting subsequent electron transfer events.

The D1393E mutant had reduced activity and a decreased CaM-mediated activation effect compared to wild-type nNOSrd, but not as pronounced as that in the S1176A mutant (Table 6.1). This can be interpreted as causing an analogous effect through H-bonding to the FAD cofactor via Ser1176. In the pre-steady-state experiments, however, D1393E nNOSrd showed slightly different CaM-mediated regulation. In Table 6.5, the shift in phases of the one-electron reduced enzyme is less than that of wild-type nNOSrd and the S1176A mutant, indicating that more of it is found in the hinged-open conformation. Furthermore, the characteristic locking effect of NADPH is not present in the D1393E mutant (Table 6.3), indicating that Asp1393 plays a role

in the accessibility of the FMN-binding domain and the regulation of electron transfer by CaM.

The S1176A and D1393E mutants were found to have a small effect on the thermodynamic parameters of the flavin cofactors (Table 6.8). The reduced states of the FAD cofactor were negatively shifted, with the FAD oxidised/semiquinone transition affected more, presumably due to the changes directly in the protein environment. Interestingly, the semiquinone state of the FMN cofactor was also destabilised, which could mean that the change in the hydrogen-bonding network in the mutants is transmitted to the FAD/FMN interface region where a slight disruption increases exposure of the FMN cofactor.

Substitution of His1032 by glutamine and serine produced two mutants that have a very different CaM-mediated effect compared to other mutants and even wild-type nNOSrd. Their CaM-free cytochrome *c* turnover rates (Table 6.1) were the same as those for D1393E nNOSrd, so the removal of the functionality of both residues causes an analogous change in the H-bonding network. In the presence of CaM, however, both H1032S and H0132Q nNOSrd are 3-fold faster than D1393E, and only slower than the wild-type enzyme by a factor of 2. This larger CaM-mediated activation effect is unique to these two reductase domain mutants and could feasibly be a result of a change in the conformational equilibrium. This is reflected in the pre-steady-state flavin reduction experiments where the activation by CaM, in both the oxidised and one-electron reduced forms, departed from the wild-type behaviour (Tables 6.6 and 6.7). The relatively fast observed ferricyanide reduction by the H1032Q and H1032S mutants (Table 6.2) can be explained by the fast hydride transfer to the oxidised enzymes which will be predominantly present in the turnover experiments with ferricyanide.

The importance of His1032 is further highlighted by the fact that neither H1032E nor H1032A nNOSrd could be expressed under the same conditions as the other mutants. Clearly the complete removal of the histidine side chain (alanine) or the introduction of acidic functionality (aspartate) causes a change in the tertiary structure of the folded protein.

A structural change that could effect the conformational equilibrium is the proximity of His1032 to Arg1229, which is responsible for a large part of the regulation between the hinged-open and hinged-closed states. If the removal of the bulky side chain of the histidine residue allowed the arginine to move closer to the other residues around

the FAD cofactor then this would cause more CaM-free hinge-opening. Furthermore, in the presence of CaM the arginine would be free from making salt-bridging electrostatic interactions and able to stabilise the FAD-active site. Although the Arg1229 residue itself could not directly perform the proton removal role, it could stabilise a water molecule in place of His1032, providing an alternative pathway to solvent.

In terms of the rate limiting step in the turnover of nNOSrd, the conformational equilibrium can still be viewed as essential in all of the FAD-active-site mutants. In S1176A nNOSrd, the rate of hydride transfer is severely decreased due to the removal of the functionality of the serine residue, but the binding of CaM still causes hinge-opening and activation of electron transfer through the enzyme. The substitutions of Asp1393 and His1032 produced mutants that appear to have activity limited by the rate of hydride transfer. However, these can be regarded as causing differing effects on the position of the conformational equilibrium. For Asp1393, this could be mediated through its proximity to Phe1395 and the CT while His1032 could cause an effect through both Asp1393 and salt-bridging Arg1229.

Chapter 7
Conclusions

Conclusions

The fundamental question on the function of nNOS addressed in this thesis is how activation occurs upon the binding of calmodulin, mediated by intracellular calcium. This activation step is centred on the reductase domain, and has been mechanistically investigated in detail.

The isolated nNOSrd characteristically transfers electrons to cytochrome *c* in the same way as it does to the oxygenase domain of holo-nNOS. This exhibits a 10-fold enhancement in the rate of electron transfer upon binding CaM. The CaM-free experiment was shown to be ionic-strength dependent, with less suppression of activity when salt concentration was increased. This leads to the conclusion that the CaM-mediated activation step must be ionic-strength dependent.

To further investigate the mechanism of activation, the hydride transfer event from NADPH to FAD was studied by pre-steady-state experiments. This is the first step in the turnover of cytochrome *c* and was found to be differently regulated in the oxidised enzyme compared to the one-electron reduced enzyme. CaM-binding affected both forms, but to a greater extent the physiologically relevant one-electron reduced enzyme. This contains the semiquinone state of the FMN cofactor, the presence of which has a large effect on the neighbouring FAD cofactor where the hydride transfer takes place. A conformational change takes place upon oxidation of the FMN semiquinone, confirmed by the ionic-strength dependency and small magnitude of kinetic isotope effects for the hydride transfer reactions. The binding of CaM has the same, but larger, effect as increasing the ionic strength and so must affect the same equilibrium, between the "hinged-closed" and "hinged-open" forms. It is the hinged-open form which must be accessed for fast hydride transfer, so the interconversion between two states becomes rate-determining in turnover experiments. In the oxidised form the equilibrium position is such that the fully closed form is unable to be produced, and CaM binding leads to a predominance of a more open form.

Thermodynamic analysis of the flavin cofactors in CaM-free nNOSrd was repeated using OTTLE potentiometry. This technique allows the measurement of current in

the cell to provide an accurate equilibrium point for electron transfer to the redox cofactors. The experimental data here highlighted again the lack of an effect of the binding of CaM on the midpoint reduction potentials of either flavin cofactor bound to nNOSrd.

The crystal structure of nNOSrd shows that the FAD and FMN cofactors are held in close contact, stabilised by electrostatic contacts between the FMN-binding domain and the other subdomains. This interface region is perturbed by the oxidation of the FMN semiquinone, which forms contacts with the protein structure. The salt bridge formed between Arg1229 and Glu762 is another key part of the interface and the significance of the salt bridge was investigated by the substitution of Arg1229 with glutamate. The resulting charge reversal R1229E mutant had a severe effect on the rate of steady-state cytochrome *c* reduction, which was inhibited by increasing concentration of the electron acceptor, while CaM binding increased the inhibition effect and decreased the observed rate of reduction.

The hydride transfer step to R1229E nNOSrd did not exhibit any CaM-mediated regulation, and was extremely rapid in both the oxidised and one-electron reduced forms. The subsequent electron transfer from FAD to FMN can be observed in the same stopped-flow experiments, and was severely slowed compared to the rates observed for the wild-type enzyme. The addition of ferrous cytochrome *c* to these experiments blocked the interflavin electron transfer step in the R1229E mutant.

The final step in the cytochrome *c* turnover experiment is an electron transfer from hydroquinone FMN to the heme, and this was investigated under pre-steady-state conditions using R1229E nNOSrd. A similar experiment with the wild-type enzyme previously revealed that it was "locked" by the addition of NADPH, preventing access of the FMN cofactor to cytochrome *c*, but this was completely abolished for the R1229E mutant. The FMN cofactor is always accessible in solution, to the same extent as CaM-bound activated wild-type nNOSrd and even the isolated FMN-binding domain.

The accessibility of the flavin cofactors in R1229E nNOSrd was also assessed by the use of OTTLE potentiometry. The value for the first reduction of the FMN cofactor

(oxidised/semiquinone) reflects its stabilisation by the presence of other sections of protein structure, and was seen to be destabilised in the mutant compared to the wild-type enzyme. The nature of the OTTLE cell setup could be used to allow further investigations on the separation of the FAD and FMN cofactors by spectroscopy such as EPR and ENDOR.

Clearly, the effects on the conformational equilibrium in this mutant form of nNOSrd mean that the hinged-closed form is inaccessible and the interflavin electron transfer step is disfavoured. This is why substrate inhibition is observed during cytochrome *c* turnover, with the possible added effect of the cytochrome *c* protein binding in the space in the interface. The inhibited form of the mutant enzyme, with cytochrome *c* and CaM bound, was subjected to crystallisation assays where the rationale was that the mobility of the FMN-binding domain may be lessened compared to the CaM-bound activated wild-type enzyme. Initial screening of conditions, however, proved unsuccessful but further investigation here may lead to the discovery of a CaM-bound nNOSrd structure.

Steady-state ferricyanide reduction by nNOSrd occurs differently to cytochrome *c* reduction, in that electrons can be transferred to ferricyanide from the FAD cofactor in addition to the FMN. For the wild-type enzyme, the rate of reduction was enhanced by CaM binding, but the rates were well in excess of those observed for cytochrome *c* reduction. This can be rationalised by the ability of the ferricyanide ion to oxidise the FMN semiquinone state, and the subsequent faster hydride transfer reactions of the oxidised enzyme form. CaM still activates the oxidised enzyme, and so activates ferricyanide reduction.
For the R1229E mutant, the rate of ferricyanide reduction was decreased compared to wild-type nNOSrd and was unaffected by the binding of CaM. Although the ferricyanide ion now has complete access to the open form of the enzyme, there will be a charge repulsion near to the site it must occupy to receive an electron from the FAD cofactor. Furthermore, the decreased rate of interflavin electron transfer in R1229E nNOSrd also makes the FMN cofactor an unfavourable location.

The R1229E holo-nNOS mutant was assayed to ascertain whether the removal of the salt bridge could activate electron transfer to the oxygenase domain. This was found

not to be the case, because the mutant exhibited a lack of CaM-free NO synthase activity and was slowed relative to wild-type nNOS in the presence of CaM. This lesser efficiency can be ascribed to the inaccessibility of the hinged-closed form to accept electrons from the FAD cofactor, and the increased exposure of both flavins to oxygen which increased the decoupling of the reaction.

In addition to its salt-bridging interaction, Arg1229 forms part of a well conserved network of residues around the FAD cofactor. These residues have been shown to also be important in nNOSrd catalysis. Ser1176 H-bonds to the FAD cofactor and removal of this functionality in the S1176A mutant severely limited the cytochrome *c* turnover rate. There was still a CaM-mediated activation effect that was also observed in the hydride transfer reactions. S1176A nNOSrd was regulated by CaM, in the oxidised and one-electron reduced forms, in the same way as the wild-type enzyme, indicating that Ser1176 has a role in hydride transfer.

Asp1393 H-bonds to Ser1176 but also to the nicotinamide moiety of NADPH, so it has a more complex effect on the regulation of nNOSrd. The D1393E mutant had a slower, but CaM-activated, cytochrome *c* reduction rate but was regulated by CaM differently to the wild-type enzyme in pre-steady-state reduction experiments. In addition to affecting the hydride transfer step, Asp1393 plays a role in the subsequent electron transfer events.

The role of His1032 is the least-well characterised in related flavoproteins, and the H1032S and H1032Q mutants were found to be regulated by CaM differently to the wild-type activation step. The binding of CaM has a larger effect on the steady-state cytochrome *c* reduction rates of these mutants which has not been observed for other single residue substitutions. Coupled with differences in the pre-steady-state experiments, this indicates a structural change between the hinged-closed and hinged-open conformations. It is interesting to speculate that Arg1229 could be part of this structural change when it is released from its electrostatic interaction bridging the domains. Clearly, crystallographic work on the substitutions at His1032 would reveal the nature of the interactions around the FAD cofactor and its possible facilitation of proton removal.

To re-address the main question of CaM-mediated activation, the hinged-open and hinged-closed states can be assigned different steps in the catalytic cycle of nNOSrd. FAD to FMN interflavin electron transfer must occur in the hinged-closed form, while electron transfer from FMN to heme must occur in the hinged-closed form, as alluded to in the previous discovery of the NADPH-dependent locked conformation. The productive binding of NADPH to allow the transfer of hydride to FAD depends on the movement of an aromatic residue, which can now be seen to be coupled to the adoption of the hinged-open form. The equilibrium between the two conformations is controlled by the binding of CaM to the enzyme. In the absence of CaM, hydride transfer is slowed and electrons are not released. Once CaM is bound, the mobile FMN-binding domain can move between the hinged-open and hinged-closed forms, facilitating electron transfer through nNOS.

References

1. Raju T.N. (2000), The Nobel chronicles. 1998: Robert Francis Furchgott (b 1911), Louis J Ignarro (b 1941), and Ferid Murad (b 1936), *Lancet*, **356**, 346

2. Furchgott, R.F. (1999), Endothelium-derived relaxing factor: discovery, early studies, and identification as nitric oxide (Nobel lecture), *Angew. Chem. Int. Ed.*, **38**, 1870-1880

3. Ignarro, L.J. (1999), Nitric oxide: a unique endogenous signalling molecule in vascular biology (Nobel lecture), *Angew. Chem. Int. Ed.*, **38**, 1882-1892

4. Arnold, W.P, Mittal, C.K., Katsuki, S., Murad, F. (1977), Nitric oxide activates guanylate cyclase and increases guanosine 3',5'-monophosphate levels in various tissue preparations, *Proc. Natl. Acad. Sci. USA.*, **74**, 3203-3207

5. Gruetter, C.A., Barry, B.K., McNamara, D.B., Gruetter, D.Y., Kadowtiz, P.J., Ignarro, L.J. (1979), Relaxation of bovine coronary artery and activation of coronary arterial guanylate cyclase by nitric oxide, nitroprusside and a carcinogenic nitrosoamine, *J. Cyclic Nucleotide Res.*, **5**, 211-224

6. Ignarro, L.J., Wood, K.S., Wolin, M.S. (1982), Activation of purified soluble guanylate cyclase by protoporphyrin IX, *Proc. Natl. Acad. Sci. USA.*, **79**, 2870-2783

7. Wolin M.S., Wood K.S., Ignarro L.J. (1982), Guanylate cyclase from bovine lung. A kinetic analysis of the regulation of the purified soluble enzyme by protoporphyrin IX, heme, and nitrosyl-heme, *J. Biol. Chem.*, **257**, 13312-13320

8. Murad, F. (1999), Discovery of some of the biological effects of nitric oxide and its role in cell signalling (Nobel lecture), *Angew. Chem. Int. Ed.*, **38**, 1856-1868

9. Deguchi, T., Yoshioka, M. (1982), L-arginine identified as an endogenous activator for soluble guanylate cyclase from neuroblastoma cells, *J. Biol. Chem.*, **257**, 10147-10151

10. Hibbs, J., Traintor, R. (1987), Macrophage cytotoxicity. Role for L-arginine deaminase and imino nitrogen activation to nitrate, *Science*, **235**, 473-476

11. Martin, W., Villani, G.M., Jothianadan, D., Furchgott, R.F. (1985), Blockade of endothelium-dependent and glyceryl trinitrate-induced relaxation of rabbit aorta by certain ferrous hemoproteins, *J. Pharmacol. Exp. Ther.*, **233**, 679-685

12. Wolin, M.S., Cherry, P.D., Rodenburg, J.M., Messina, E.J., Kaley, G. (1990), Methylene blue inhibits vasodilation of skeletal muscle arterioles to ACh and nitric oxide via the extracellular generation of superoxide anion, *J. Pharmacol. Exp. Ther.*, **254**, 872-876

13. Gryglewski, R.J., Moncada, S., Palmer, R.M.J. (1986), Bioassay of prostacyclin and endothelium-derived relaxing factor (EDRF) from porcine aortic endothelial cells, *Br. J. Pharmacol.*, **87**, 685-694

14. Furchgott, R.F., in: Vanhoutte, P.M. (Ed) (1988), Studies on relaxation of rabbit aorta by sodium nitrite: the basis for the proposal that the acid-activatable inhibitory factor from retractor penis is inorganic nitrite and the endothelium-derived relaxing factor is nitric oxide, *Vasodilation: Vascular Smooth Muscle, Peptides and Endothelium*, Raven Press, New York, 401-414

15. Ignarro, L.J., Byrns, R.E., Wood, K.S., in: Vanhoutte, P.M. (Ed) (1988), Biochemical and pharmacological properties of endothelium-derived relaxing factor and its similarity to nitric oxide radical, *Vasodilation: Vascular Smooth Muscle, Peptides and Endothelium*, Raven Press, New York, 427-435

16. Schmidt, H.H.H.W and Walter, U. (1994), NO at work, *Cell*, **78**, 919-925

17. Mann, B.E., Motterlini, R. (2007), CO and NO in medicine, *Chem. Comm.*, **41**, 4197-4208

18. Palmer, R.M.J., Ashton, D.S., Moncada, S. (1988), Vascular endothelial cells synthesise nitric oxide from L-arginine, *Nature*, **333**, 664-666

19. Marletta, M.A. (1994), Nitric oxide synthase: aspects concerning structure and catalysis, *Cell*, **78**, 927-930

20. Stuehr, D.J. (1999), Mammalian nitric oxide synthases, *Biochim. Biophys. Acta.*, **1411**, 217-230

21. Bredt, D., Snyder, S. (1990), Isolation of nitric oxide synthase, a calmodulin-requiring enzyme, *Proc. Natl. Acad. Sci. USA.*, **87**, 682-685

22. Schmidt, H.H.H.W., Pollock, J., Nakane, M., Gorsky, L., Fostermann, U., Heller, M., Murad, F. (1991), Purification of soluble isoform of guanylyl-cyclase-activating-factor synthase, *Proc. Natl. Acad. Sci. USA.*, **88**, 365 -369

23. Pollock, J.S., Fostermann, U., Mitchell, J.A., Warner, T.D., Schmidt, H.H.H.W., Nakane, M., Murad, F. (1991), Purification and characterisation of particulate EDRF synthase from cultured and native bovine aortic endothelial cells, *Proc. Natl. Acad. Sci. USA.*, **88**, 10480-10484

24. Stuehr, D., Cho. H., Kwon, N., Weise, M., Nathans, C. (1991), Purification and characterisation of cytokine-induced macrophage nitric oxide synthase, *Proc. Natl. Acad. Sci. USA.*, **88**, 7773-7777

25. Alderton, W.K., Cooper, C.E., Knowles, R.G. (2001), Nitric oxide synthases: structure, function and inhibition, *Biochem. J.*, **357**, 593-615

26. Nathan, C, Xie, Q.-W. (1994), Nitric oxide synthases: roles, tolls and controls, *Cell*, **78**, 915-918

27. Moncada, S., Higgs, A. (1993), The L-arginine-nitric oxide pathway, *N. Engl. J. Med.*, **329**, 2002-2012

28. Masters, B.S.S. (1994), Nitric Oxide Synthase – why so complex, *Anuu. Rev. Nutr.,* **14**, 131-145

29. Masters, B.S.S, in: Ignarro L.J. (Ed) (2000), Structural variations to accommodate functional themes of the isoforms of NO synthases, *Nitric oxide, biology and pathobiology*, Academic Press, New York, 91-104

30. Abu-Soud, H.M., Stuehr, D.J. (1993), Nitric-oxide synthases reveal a role for calmodulin in controlling electron transfer, *Proc. Natl. Acad. Sci. USA.,* **90**, 10769-10772

31. Bredt, D.S., Hwang, P.M., Glatt, C.E., Lowenstein, C., Reed, R.R., Snyder, S.H. (1991), Cloned and expressed nitric oxide synthase structurally resembles cytochrome P-450 reductase, *Nature*, **351**, 714-718

32. Brenman, J.E., Chao, D.S., Gee, S.H., McGee, A.W., Craven, S.E., Santillano, D.R., Wu, Z., Huang, F., Xia, H., Peters, M.F., Froehner, S.C., Bredt, D.S. (1996), Interaction of nitric oxide synthase with the postsynaptic density protein PSD-95 and α_1-syntrophin mediated by PDZ domains, *Cell*, **84**, 757-767

33. Crane, B.R., Rosenfeld, R.J., Arvai, A.S., Ghosh, D.K., Ghosh, S., Tainer, J.A., Stuehr, D.J., Getzoff, E.D. (1999), N-terminal domain swapping and metal ion binding in nitric oxide synthase dimerisation, *EMBO J.*, **18**, 6271-6281

34. Siddhanta, U., Presta, A., Fan, B.C., Wolan, D., Rosseau, D.L., Stuehr, D.J. (1998), Domain swapping in inducible nitric oxide synthase – electron transfer occurs mainly between flavin and heme groups located on adjacent subunits in the dimer, *J. Biol. Chem*., **273**, 18950-18958

35. Sagami, I., Daff, S., Shimizu, T. (2001), Intrasubunit and intersubunit electron transfer in neuronal nitric-oxide synthase: effect of calmodulin on heterodimer catalysis, *J. Biol. Chem*, **276**, 30036-30042

36. Roman, L.J., Martasek, P., Masters, B.S.S. (2002), Intrinsic and extrinsic modulation of nitric oxide synthase activity, *Chem. Rev.,* **102**, 1179-1189

37. Nishida, C.R., Ortiz De Montellano, P.R. (1998), Electron transfer and catalytic activity of nitric oxide synthases. Chimeric constructs of the neuronal, inducible, and endothelial isoforms, *J. Biol. Chem.*, **273**, 5566-5571

38. Sagami, I., Sato, Y., Noguchi, T., Miyajima, M., Rozhkova, E., Daff, S., Shimizu, T. (2002), Electron transfer in nitric-oxide synthase, *Coord. Chem. Rev.*, **226**, 179-186

39. Presta, A., Weber-Main, A.M., Stankovic, M.T., Stuehr, D.J. (1998), Comparative effects of substrates and pterin cofactor on the heme midpoint potential in inducible and neuronal nitric oxide synthases, *J. Amer. Chem. Soc.*, **120**, 9460-9465

40. Li, D., Kabir, M., Stuehr, D.J., Rousseau, D.L., Yeh, S-R. (2007), Substrate and isoform-specific dioxygen complexes of nitric oxide synthase, *J. Amer. Chem. Soc.*, **129**, 6943-6951

41. Stuehr, D.J., Santolini, J., Wang, Z., Wei, C., Adak, S. (2004), Update on mechanism and catalytic regulation in the NO synthases, *J. Biol. Chem.,* **279**, 36167-36170

42. Wei, C-C., Wang, Z-Q., Durra, D., Hemann, C., Hille, R., Garcin, E.D., Getzoff, E.D., Stuehr, D.J. (2005), The three nitric-oxide synthases differ in their kinetics of tetrahydrobiopterin radical formation, heme-dioxy reduction, and arginine hydroxylation, *J. Biol. Chem.*, **280**, 8929-8935

43. Ost, T.W.B., Daff, S. (2005), Thermodynamic and kinetic analysis of the nitrosyl, carbonyl, and dioxy heme complexes of neuronal nitric oxide synthase, *J. Biol. Chem.*, **280**, 965-973

44. Santolini, J., Adak, S., Curran, C.M.L., Stuehr, D.J. (2001), A kinetic simulation model that describes catalysis and regulation in nitric-oxide synthase, *J. Biol. Chem.*, **276**, 1233-1243

45. Santolini, J., Meade, A.L., Stuehr, D.J. (2001), Differences in three kinetic parameters underpin the unique catalytic profiles of nitric-oxide synthases I, II, and III, *J. Biol. Chem.*, **276**, 48887-48898

46. Adak, S., Santonlini, J., Tikunova, S., Wang, Q., Johnson, J.D., Stuehr, D.J. (2001), Neuronal nitric oxide synthase mutant (Ser1412-Asp) demonstrates surprising connections between heme reduction, NO complex formation, and catalysis, *J. Biol. Chem.,* **276**, 1244-1252

47. Crane, B.R., Arvai, A.S., Ghosh D.K., Wu, C., Getzoff, E.D., Stuehr, D.J., Tainer, J.A. (1998), Structure of nitric oxide synthase oxygenase dimer with pterin and substrate, *Science*, **279**, 2121-2126

48. Raman, C.S., Li, H., Martasek, P., Kral, V., Masters, B.S.S., Poulos, T.L. (1998), Crystal structure of constitutive endothelial nitric oxide synthase: A paradigm for pterin function involving a novel metal center, *Cell*, **95**, 939-950

49. Fischmann, T.O., Hruza, A., Niu, X.D., Fossetta, J.D., Lunn, C.A., Dolphin, E., Prongay, A.J., Reichert, P., Lundell, D.J., Narula, S.K., Weber, P.C. (1999), Structural characterisation of nitric oxide synthase isoforms reveals striking active site conservation, *Nat. Struct. Biol*, **6**, 233-242

50. Li, H., Shimizu, H., Flinspach, M., Jamal, J., Yang, W., Xian, M., Cai, T., Wen, E.Z., Jia, Q., Wang, P.G., Poulos, T.L. (2002), The novel binding mode of N-alkyl-N-hydroxyguanidine to neuronal nitric oxide synthase provides mechanistic insights into NO biosynthesis, *Biochemistry*, **41**, 13868-13875

51. Wang, Z-Q., Wei, C-C., Santolini, J., Panda, K., Wang, Q., Stuehr, D.J. (2005), A tryptophan that modulates tetrahydrobiopterin-dependent electron transfer in nitric oxide synthase regulates enzyme catalysis by additional mechanisms, *Biochemistry*, **44**, 4676-4690

52. Li, H., Igarashi, J., Jamal, J., Yang, W., Poulos, T.L. (2006) Structural studies of constitutive nitric oxide synthases with diatomic ligands bound, *J. Biol. Inorg. Chem.*, **11**, 753-768

53. Nagano, S., Poulos, T.L. (2005), Crystallographic study on the dioxygen complex of wild-type and mutant cytochrome P 450cam: Implications for the dioxygen activation mechanism, *J. Biol. Chem.*, **280**, 31659-31663

54. Lad, L., Koshkin, A., de Montellano, P.R., Poulos, T.L. (2005), Crystal structures of the G139A, G139A-NO and G143H mutants of human heme oxygenase-1. A finely tuned hydrogen-bonding network controls oxygenase versus peroxidase activity, *J. Biol. Inorg. Chem.*, **10**, 138-146

55. Shimizu T., Tateishi T., Hatano M., Fujii-Kuriyama Y. (1991), Probing the role of lysines and arginines in the catalytic function of cytochrome P450d by site-directed mutagenesis. Interaction with NADPH-cytochrome P450 reductase, *J. Biol. Chem.*, **266**, 3372-3375.

56. Shimanuki, T., Sato, H., Daff, S., Sagami, I., Shimizu, T. (1999), Crucial role of Lys423 in the electron transfer of neuronal nitric oxide synthase, *J. Biol. Chem.,* **274**, 26956-26961

57. Massey, V. (1995), Introduction: flavoprotein structure and mechanism, *FASEB J.*, **9**, 473-475

58. Singer, T.P., Ramsay, R.R. (1995), Monoamine oxidases: old friends hold many surprises, *FASEB J.*, **9**, 605-610

59. Fernandez, H.H., Chen, J.J. (2007), Monamine oxidase inhibitors: current and emerging agents for parkinson disease, *Clinical Neuropharmacology*, **30**, 150-168.

60. Entsch, B., Van Berkel, W.J.H. (1995), Structure and mechanism of para-hydroxybenzoate hydroxylase, *FASEB J.,* **9**, 476-483

61. Entsch, B., Cole, L.J., Ballou, D.P. (2005), Protein dynamics and electrostatics in the function of p-hydroxybenzoate hydroxylase, *Arch. Biochem. Biophys.*, **433**, 297-311

62. Mansoorabadi, S.O., Thibodeaux, C.J., Liu, H. (2007), The diverse roles of flavin coenzymes – nature's most versatile thespians, *J. Organic. Chem.*, **72**, 6329-6342

63. De Colibus, L., Mattevi, A. (2006), New frontiers in structural flavoenzymology, *Curr. Opin. Struct. Biol.*, **16**, 722-728

64. Chapman, S.K., Reid, G.A., Bell, C., Short, D., Daff, S. (1996), Flavocytochrome b_2 : an ideal model system for studying protein-mediated electron transfer, *Biochem. Soc. Trans*., **24**, 73-77

65. Reid G.A., Miles C.S., Moysey R.K., Pankhurst K.L., Chapman S.K. (2000), Catalysis in fumarate reductase, *Biochim. Biophys. Acta*., **1459**, 310-315.

66. Chapman, S. K., Welsh, F., Moysey, R., Mowat, C., Doherty, M. K., Turner, K. L., Munro, A. W., Reid, G. A. (1999), Flavocytochromes : transceivers and relays in biological electron transfer, *Biochem. Soc. Trans*., **27**, 185-189.

67. Masters, B.S.S. (2005), The journey from NADPH-cytochrome P450 oxidoreductase to nitric oxide synthases, *Biochem. Biophys. Res. Comm.*, **338**, 507-519

68. Porter, T.D., Kasper, C.B. (1986), NADPH-cytochrome P-450 oxidoreductase: flavin mononucleotide and flavin adenine dinucleotide domains evolved from different flavoproteins, *Biochemistry*, **25**, 1682-1687

69. Wang, M., Roberts, D.L., Paschke, R., Shea, T.M., Masters, B.S.S., Kim, J. P. (1997), Three-dimensional structure of NADPH-cytochrome P450 reductase: prototype for FMN- and FAD- containing enzymes, *Proc. Natl. Acad. Sci. USA.*, **94**, 8411-8416

70. Watenpaugh, D.K., Sieker, L.C., Jensen, L.H. (1973), The binding of riboflavin-5'-phosphate in a flavoprotein: flavodoxin at 2.0Å resolution, *Proc. Natl. Acad. Sci. USA.*, **70**, 3857-3860

71. Karplus, P.A., Daniels, M.J., Herriott, J.R. (1991), Atomic structure of ferredoxin-$NADP^+$ reductase : prototype for a structurally novel flavoenzyme family, *Science*, **251**, 60-66

72. Bredt, D.S., Snyder, S.H. (1994), Nitric oxide: A physiologic messenger molecule, *Annu. Rev. Biochem.*, **63**, 175-195

73. Zhang, J., Martasek, P., Paschke, R., Shea, T., Masters, B.S.S., Kim, J. P. (2001), Crystal Structure of the FAD/NADPH-binding domains of rat neuronal nitric oxide synthase, *J. Biol. Chem.*, **276**, 37506-37513

74. Garcin, E.D. Bruns, C.M. Lloyd, S.J. Hosfield, D.J. Tiso, M. Gacchui, R. Stuehr, D.J. Tainer, J.A. Getzoff, E.D. (2004) Structural basis for isozyme-specific regulation of electron transfer in nitric oxide synthase, *J. Biol. Chem*, **279**, 37918-37927

75. Roman, L.J., Sheta, E.A., Martasek, P., Gross, S.S., Lui, Q., Masters, B.S.S. (1995), High-level expression of functional rat neuronal nitric oxide synthase in *Escherichia coli*, *Proc. Natl. Acad. Sci. USA.,* **92**, 8428-8432

76. Gachhui, R., Presta, A., Bentley, D.F., Abu-Soud, H.M., McArthur, R., Brudvig, G., Ghosh, D.K., Stuehr, D.J. (1996), Characterisation of the reductase domain of rat neuronal nitric oxide synthase generated in the methylotrophic yeast *Pichia pastoris*, *J. Biol. Chem.*, **271**, 20594-20602

77. Newton, D.C., Montgomery, H.J., Guillemette, J.G. (1998), The reductase domain of the human inducible nitric oxide synthase is fully active in the absence of bound calmodulin, *Arch. Biochem. Biophys.,* **359**, 249-257

78. Abu-Soud, H.M., Yoho, L.L., Stuehr, D.J. (1994), Calmodulin controls neuronal nitric-oxide synthase by a dual mechanism. Activation of intra- and interdomain electron transfer, *J. Biol. Chem.*, **269**, 32047-32050

79. Adak, S., Ghosh, S., Abu-Soud, H.M., Stuehr, D.J. (1999), Role of reductase domain cluster 1 acidic residues in neuronal nitric-oxide synthase, *J. Biol. Chem.*, **274**, 22313-22320

80. Konas, D.W., Takaya, N., Sharma, M., Stuehr, D.J. (2006), Role of Asp1393 in catalysis, flavin reduction, NADP(H) binding, FAD thermodynamics, and regulation of the nNOS flavoprotein, *Biochemistry*, **45**, 12596-12609

81. Panda, K., Haque, M.M., Garcin-Hosfield, E.D., Durra, D., Getzoff, E.D., Stuehr, D.J. (2006), Surface charge interactions of the FMN module govern catalysis by nitric-oxide synthase, *J. Biol. Chem.*, **281**, 36819-36827

82. Ghosh, D.K., Holliday, M.A., Thomas, C., Weinberg, J.B., Smith, S.M.E., Salerno, J.C. (2006), NOS output state; design and properties of nitric-oxide synthase oxygenase/FMN domain constructs, *J. Biol. Chem.,* **281**, 14173-14183

83. Feng, C., Tollin, G., Holliday, M.A., Thomas, C., Salerno, J.C., Enemark, J.H., Ghosh, D.K. (2006), Intraprotein electron transfer in a two-domain construct of neuronal nitric oxide synthase: the output state in nitric oxide formation, *Biochemistry*, **45**, 6354-6362

84. Feng, C., Tollin, G., Hazzard, J.T., Nahm, N. J.,Guillemette, J.G., Salerno, J.C., Ghosh, D.K. (2007), Direct measurement by laser flash photolysis of intraprotein electron transfer in a rat neuronal nitric oxide synthase, *J. Amer. Chem. Soc.*, **129**, 5621-5629

85. Alberty, R. A., (2004), Standard apparent reduction potentials of biochemical half reactions and thermodynamic data on the species involved, *Biophys. Chem*., **111**, 115-122.

86. Noble, M.A., Munro, A.W., Rivers, S.L., Robledo, L., Daff, S.N., Yellowlees, L.J., Shimizu, T., Sagami, I., Guillemette, J.G., Chapman, S.K. (1999), Potentiometric analysis of the flavin cofactors of neuronal nitric oxide synthase, *Biochemistry*, **38**, 16413-16418

87. Gao, Y.T., Smith, S.M.E., Weinberg, J.B., Montgomery, H.J., Newman, E., Guillemette, J.G., Ghosh, D.K., Roman, L.J., Martasek, P., Salerno, J.C. (2004), Thermodynamics of oxidation-reduction reactions in mammalian nitric-oxide synthase isoforms, *J. Biol. Chem.*, **279**, 18759-18766

88. Garnaud, P.E., Koetsier, M, Ost, T.W.B., Daff, S. (2004), Redox properties of the isolated flavin mononucleotide- and flavin adenine dinucleotide-binding domains of neuronal nitric oxide synthase, *Biochemistry*, **43**, 11035-11044

89. Daff, S. (2003), Calmodulin-dependent regulation of mammalian nitric oxide synthase, *Biochem. Soc. Trans.,* **31**, 502-505

90. Guan, Z-W., Iyanagi, T. (2003), Electron transfer is activated by calmodulin in the flavin domain of human neuronal nitric oxide synthase, *Arch. Biochem. Biophys.*, **412**, 65-76

91. Pearson, R.B., Wettenhall, R.E.H., Means, A.R., Hartshorne, D.J., Kemp, B.E. (1988), Autoregulation of enzymes by pseudosubstrate prototopes: myosin light chain kinase, *Science*, **241,** 970-973

92. Cruzalegui, F.H., Kapiloff, M.S., Morfin, J.P., Kemp, B.E., Rosenfeld, M.G., Means, A.R. (1992), Regulation of intrasteric inhibition of the multifunctional calcium/calmodulin-dependent protein kinase, *Proc. Natl. Acad. Sci. USA.*, **89**, 12127-12131

93. Perrino, B.A., Ng, L.Y., Soderling, T.R. (1995), Calcium regulation of calcineurin phosphatase activity by its B subunit and calmodulin. Role of the autoinhibitory domain, *J. Biol. Chem.*, **270**, 340-346

94. Chattopadhyaya, R., Meador, W.E., Means, A.R., Quiocho, F.A. (1992), Calmodulin structure refined at 1.7Å resolution, *J. Mol. Biol.*, **228**, 1177-1192

95. Aoyagi, M., Arvai, A.S., Tainer, J.A., Getzoff, E.D. (2003), Structural basis for endothelial nitric oxide synthase binding to calmodulin, *EMBO J.*, **22**, 766-775

96. Stevens-Truss, R., Beckingham, K., Marletta, M.A. (1997), Calcium binding sites of calmodulin and electron transfer by neuronal nitric oxide synthase, *Biochemistry*, **36**, 12337-12345

97. Spratt, D.E., Taiakina, V., Palmer, M., Guillemette, J.G. (2007), Differential binding of calmodulin domains to constitutive and inducible nitric oxide synthase enzymes, *Biochemistry*, **46**, 8288-8300

98. Salerno, J.C., Harris, D.E., Irizarry, K., Patel, B., Morales, A.J., Smith, S.M.E., Martasek, P., Roman, L.J., Masters, B.S.S., Jones, C.L., Weismann, B.A., Lane, P., Liu, Q., Gross, S.S. (1997), An autoinhibitory control element defines calcium-regulated isoforms of nitric oxide synthase, *J. Biol. Chem.,* **272**, 29769-29777

99. Sheta, E.A., McMillan, K., Masters, B.S.S. (1994), Evidence for a bidomain structure of constitutive cerebellar nitric oxide synthase, *J. Biol. Chem*, **269**, 15147-15153

100. Lane, P., Gross, S.S. (2000), The autoinhibitory control element and calmodulin conspire to provide physiological modulation of endothelial and neuronal nitric oxide synthase activity, *Acta. Physiol. Scand.*, **68**, 53-63

101. Nishida, C.R., Ortiz de Montellano, P.R. (1999), Autoinhibition of endothelial nitric-oxide synthase. Identification of an electron transfer control element, *J. Biol. Chem.*, 274, 14692-14698

102. Daff, S., Sagami, I., Shimizu, T. (1999), The 42-amino acid insert in the FMN domain of neuronal nitric oxide synthase exerts control over Ca^{2+}/Calmodulin electron transfer, *J. Biol. Chem.*, **274**, 30589-30595

103. Nishida, C.R., Ortiz De Montellano, P.R. (2001), Control of electron transfer in nitric-oxide synthases: swapping of autoinhibitory elements among nitric-oxide synthase isoforms, *J. Biol. Chem.*, **276**, 20116-20124

104. Roman, L.J., Miller, R.T., De la Garza, M.A., Kim, J-J.P., Masters, B.S.S. (2000), The C terminus of mouse macrophage inducible nitric-oxide synthase attenuates electron flow through the flavin domain, *J. Biol Chem*., **275**, 21914-21919

105. Roman, L.J., Martasek, P., Miller, R.T., Harris, D.E., de la Garza, M.A., Shea, T.M., Kim, J-J. P., Masters, B.S.S. (2000), The C termini of constitutive nitric oxide synthases control electron flow through the flavin and heme domains and affect modulation by calmodulin, *J. Biol. Chem.*, **275**, 29225-29232

106. Jachymova, M., Martasek, P., Panda, S., Roman, L.J., Panda, M., Shea, T.M., Ishimura, Y., Kim, J-J.P., Masters, B.S.S. (2005), Recruitment of governing elements for electron transfer in the nitric oxide synthase family, *Proc. Natl. Acad. Sci. USA.,* **102**, 15833-15838

107. Roman, L.J., McLain, J., Masters, B.S.S. (2003), Chimeric enzymes of cytochrome P450 oxidoreductase and neuronal nitric-oxide synthase reductase domain reveal structural and functional differences, *J. Biol. Chem.*, **278**, 25700-25707

108. Roman, L.J., Masters, B.S.S. (2006), Electron transfer by neuronal nitric oxide synthase is regulated by concerted interaction of calmodulin and two intrinsic regulatory elements, *J. Biol. Chem.,* **281**, 23111-23118

109. Tiso, M., Tejero, J., Panda, K., Aulak, K.S., Stuehr, D.J. (2007), Versatile regulation of neuronal nitric oxide synthase by specific regions of its C-terminal tail, *Biochemistry*, **46**, 14418-14428

110. Dimmeler, S., Fleming, I., Fisslthaler, B., Hermann, C., Busse, R., Zeiher, A.M. (1999), Activation of nitric oxide synthase in endothelial cells by Akt-dependent phosphorylation, *Nature*, **399**, 601-605

111. Fulton, D., Gratton, J-P., McCabe, T.J., Fontana, J., Fujio, Y., Walsh, K., Franke, T.F., Papapetropoulos, A., Sessa, W.C. (1999), Regulation of endothelium-derived nitric oxide production by the protein kinase Akt, *Nature*, **399**, 597-601

112. McCabe, T.J., Fulton, D., Roman, L.J., Sessa, W.C. (2000), Enhanced electron flux and reduced calmodulin dissociation may explain "calcium independent" eNOS activation by phosphorylation, *J. Biol. Chem.*, **275**, 6123-6128

113. Lane, P., Gross, S.S. (2002), Disabling a C-terminal autoinhibitory control element in endothelial nitric-oxide synthase by phosphorylation provides a molecular explanation for activation of vascular NO synthesis by diverse physiological stimuli, *J. Biol. Chem.*, **277**, 19087-19094

114. Komeima, K., Hayashi, Y., Naito, Y., Watanabe, Y. (2000), Inhibition of neuronal nitric-oxide synthase by calcium/calmodulin-dependent protein kinase IIα through Ser847 phosphorylation in NG108-15 neuronal cells, *J. Biol. Chem.*, **275**, 28139-28143

115. Chen, Z.-P., Mitchelhill, K.I., Michell, B.J., Stapleton, D., Rodriguez-Crespo, I., Witters, L.A., Power, D.A., Ortiz de Montellano, P.R., Kemp, B.E. (1999), AMP-activated protein kinase phosphorylation of endothelial NO synthase, *FEBS Lett.*, **443**, 285-289

116. Knudsen, G.M., Nishida, C.R., Mooney, S.D., Ortiz de Montellano, P.R. (2003), nitric-oxide synthase (NOS) reductase domain models suggest a new control element in endothelial NOS that attenuates calmodulin-dependent activity, *J. Biol. Chem.*, **278**, 13814-13824

117. Jones, R.J., Smith. S.M.E., Gao, Y.T., DeMay, B.S., Mann, K.J., Salerno, K.M., Salerno, J.C. (2004), The function of the small insertion in the hinge subdomain in the control of constitutive mammalian nitric-oxide synthases, *J. Biol. Chem.*, **279**, 36876-36883

118. Haque, M.M., Panda, K., Tejero, J., Aulak, K.S., Fadlalla, M.A., Mustovich, A.T., Stuehr, D.J. (2007), A connecting hinge represses the activity of endothelial nitric oxide synthase, *Proc. Natl. Acad. Sci. USA.*, **104**, 9254-9259

119. Craig, D.H., Chapman, S.K., Daff, S. (2002), Calmodulin activates electron transfer through neuronal nitric oxide synthase reductase domain by releasing an NAPDH-dependent conformational lock, *J. Biol. Chem.*, **277**, 33987-33994

120. Garnaud, P-E.F. (2006), Calmodulin activation of the reductase domain of mammalian neuronal nitric oxide synthase, PhD Thesis, University of Edinburgh

121. Jones, R. J.,Gao, Y.T., Simone, T.M., Salerno, J.C., Smith, S.M.E. (2006), NADPH analog binding to constitutive nitric oxide activates electron transfer and NO synthesis, *Nitric Oxide*, **14**, 228-237

122. Tejero, J., Perez-Dorado, I., Maya, C., Martinez-Julvez, M., Sanz-Aparico, J., Gomez-Moreno, C., Hermoso, J.A., Medina, M. (2005), C-terminal tyrosine of ferredoxin-$NADP^+$-reductase in hydride transfer processes with $NAD(P)^+/H$, *Biochemistry*, **44**, 13477-13490

123. Martinez-Julvez, M., Tejero, J., Peregrina, J.R., Nogues, I., Frago, S., Gomez-Moreno, C., Medina, M. (2005), Towards a new interaction enzyme:coenzyme, *Biophys. Chem.*, **115**, 219-224

124. Tiso, M., Konas, D.W., Panda, K., Garcin, E.D., Sharma, M., Getzoff, E.D., Stuehr, D.J. (2005), C-terminal residue Arg1400 enables NADPH to regulate electron transfer in neuronal nitric oxide synthase, *J. Biol. Chem.,* **280**, 39208-39219

125. Deng Z., Aliverti A., Zanetti G., Arakaki A.K., Ottado J., Orellano E.G., Calcaterra N.B., Ceccarelli E.A., Carrillo N., Karplus P.A. (1999), A productive $NADP^+$ binding mode of ferredoxin-$NADP^+$ reductase revealed by protein engineering and crystallographic studies, *Nat. Struct. Biol*., **6**, 847-853.

126. Hubbard, P. A., Shen, A.L., Paschke, R., Kasper, C.B., Kim, J-J. P. (2001), NADPH-cytochrome P450 oxidoreductase. Structural basis for hydride and electron transfer, *J. Biol. Chem.*, **276**, 29163-29170

127. Adak, S., Sharma, M., Meade, A.L., Stuehr, D.J. (2002), A conserved flavin-shielding residue regulates NO synthase electron transfer and nicotinamide coenzyme specificity, *Proc. Natl. Acad. Sci. USA.*, **99**, 13516-13521

128. Konas, D.W., Zhu, K., Sharma, M., Adak, K.S., Brudvig, G.W., Stuehr, D.J. (2004), The FAD-shielding residue Phe1395 regulates neuronal nitric-oxide synthase catalysis by controlling $NADP^+$ affinity and a conformational equilibrium within the flavoprotein domain, *J. Biol. Chem.,* **279**, 35412-35425

129. Panda, S.P., Gao, Y.T., Roman, L.J., Martasek, P., Salerno, J.C., Masters, B.S.S. (2006), The role of a conserved serine residue within hydrogen bonding distance of FAD in redox properties and the modulation of catalysis by Ca^{2+}/Calmodulin of constitutive nitric-oxide synthases, *J. Biol. Chem.*, **281**, 34246-34257

130. Panda, K., Adak, S., Konas, D., Sharma, M., Stuehr, D.J. (2004), A conserved aspartate (Asp-1393) regulates NADPH reduction of neuronal nitric oxide synthase, *J. Biol. Chem.*, **279**, 18323-18333

131. Shen, A.L., Kasper, C.B. (1995), Role of acidic residues in the interaction of NADPH-cytochrome P450 oxidoreductase and cytochrome *c*, *J. Biol. Chem.,* **270**, 27475-27480

132. Goloubinoff, P., Gatenby, A.A., Lorimer, G.H. (1989), GroE heat-shock proteins promote assembly of foreign prokaryotic ribulose bisphosphate carboxylase oligomers in Escherichia coli, *Nature (London)*, **337**, 44-47

133. Pollock, V.V., Barber, M.J. (2001), Kinetic and mechanistic properties of biotin sulfoxide reductase, *Biochemistry*, **40**, 1430-1440.

134. Palmer T. (1995), Understanding Enzymes, 4th Ed., Ellis Horwood Ltd.

135. Hazzard, J.T., Cusanovich, M.A., Tainer, J.A., Getzoff, E.D., Tollin, G. (1986), Kinetic studies of reduction of a 1:1 cytochrome c-flavodoxin complex by free flavin semiquinones and rubredoxin, *Biochemistry*, **25**, 3318-3328

136. Gibson, Q.H. (1969), Rapid mixing: stopped flow, *Meth. Enzymol*, **16**, 187-228

137. Knight, K., Scrutton, N.S. (2002), Stopped-flow kinetic studies of electron transfer in the reductase domain of neuronal nitric oxide synthase: re-evaluation of the kinetic mechanism reveals new enzyme intermediates and variation with cytochrome P450 reductase, *Biochem. J.*, **367**, 19-30

138. Dutton, P.L. (1978), Redox potentiometry: determination of midpoint potentials of oxidation-reduction components of biological electron-transfer systems, *Meth. Enzymol.*, **54**, 411-435

139. Schrammel, A., Gorren, A.C.F., Stuehr, D.J., Schmidt, K., Mayer, B. (1998), Isoform-specific effects of salts on nitric oxide synthase activity, *Biochem. Biophys. Acta.,* **1387**, 257-263

140. Wolthers, K.R., Schimerlik, M.I. (2002), Neuronal nitric oxide synthase: substrate and solvent kinetic isotope effects on the steady-state kinetic parameters for the reduction of 2,6-dichloroindolphenol and cytochrome c^{3+}, *Biochemistry*, **41**, 196-204

141. Cleland, W.W. (2007), Use of isotope effects to determine enzyme mechanisms, *J. Label. Compd. Radiopharm.*, **50**, 1006-1015

142. Dunford, A.J., Rigby, S.E.J., Hay, S., Munro, A.W., Scrutton, N.S. (2007), Conformational and thermodynamic control of electron transfer in neuronal nitric oxide synthase, *Biochemistry*, **46**, 5018-5029

143. Watterson, D.M., Sharief, F., Vanaman, T.C. (1980), The complete amino acid sequence of the Ca^{2+}-dependent modulator protein (calmodulin) of bovine brain, *J. Biol. Chem.*, **255**, 962–975

Appendix I

Representations of nNOS structure

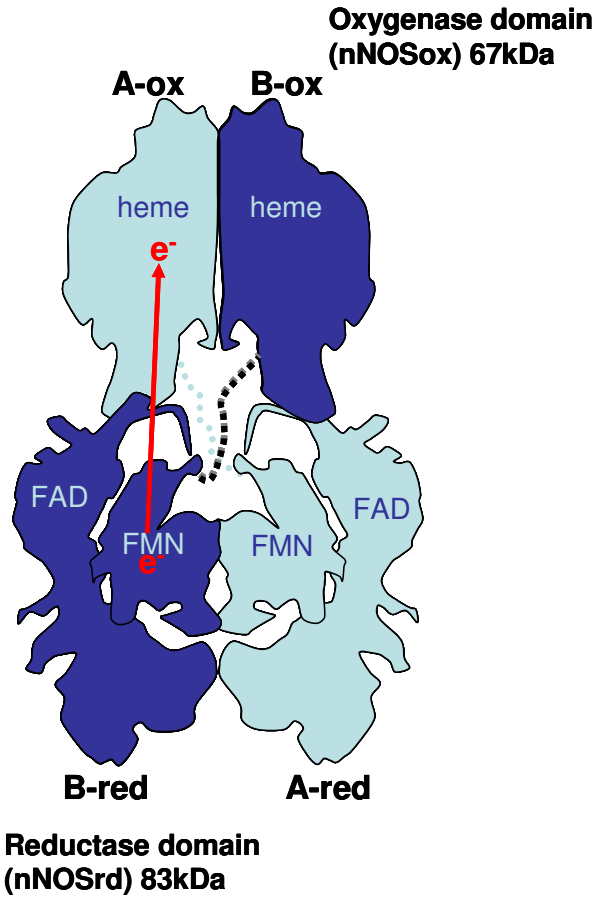

Possible dimeric structure of nNOS, based on crystal structures of nNOSoxy (PDB code 1OM4) and nNOSrd (1TLL). Electrons are transferred from the reductase domain of one monomer to the oxygenase domain of the adjacent monomer.

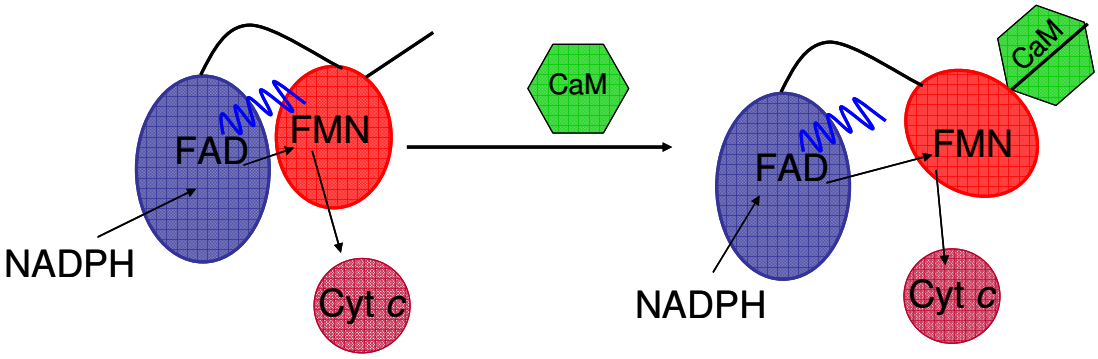

Calmodulin activation of nNOSrd. Binding of CaM releases the reductase domain from a conformational lock, allowing the FMN to transfer electrons to the oxygenase domain or artificial electron acceptors such as cytochrome *c*.

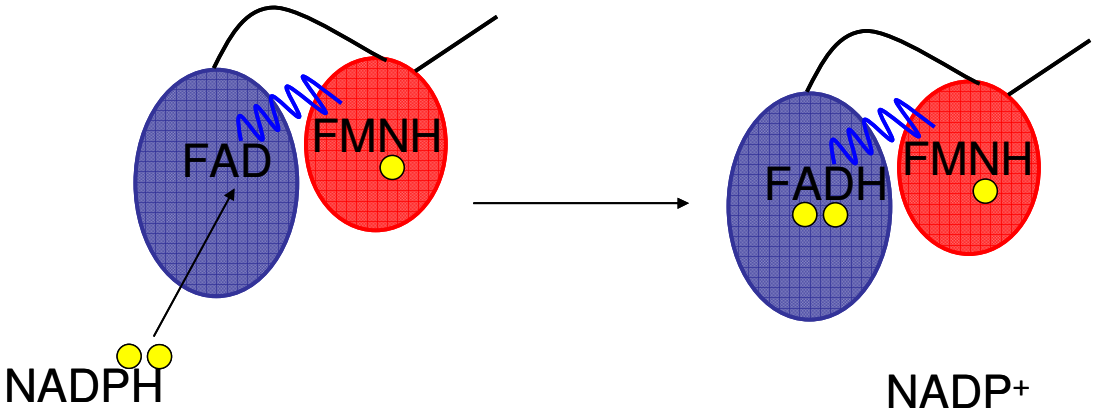

Stopped flow reduction of one-electron reduced nNOSrd

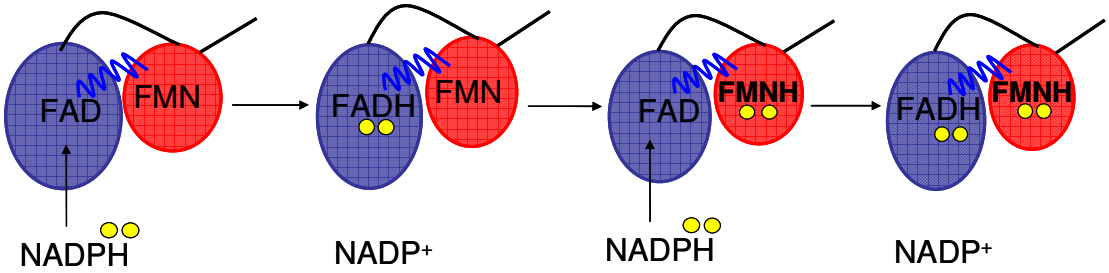

Stopped flow reduction of fully oxidised reduced nNOSrd

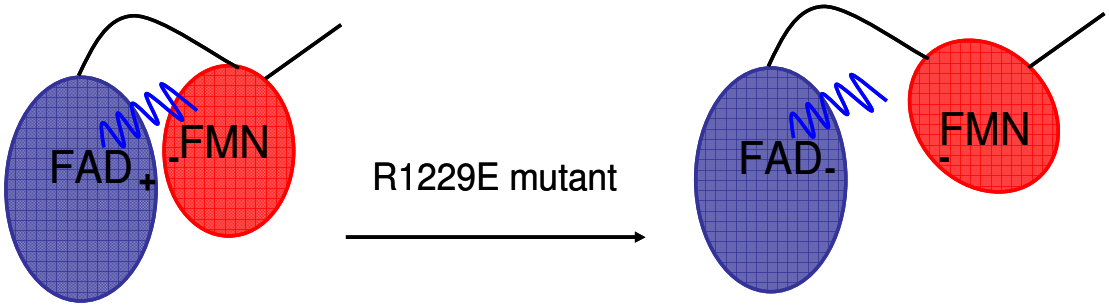

Breaking the salt bridge at Arg1229 introduces an electrostatic repulsion and likely destabilised interaction between the FMN- and FAD- binding domains

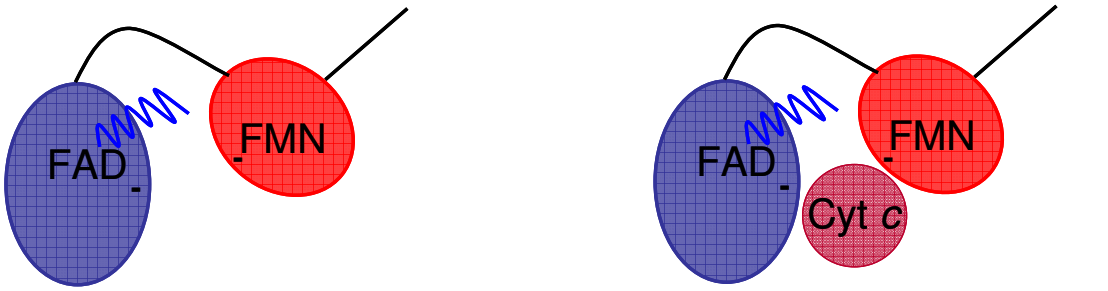

Electron transfer is inhibited in R1229E nNOSrd (left) and the separation introduces the possibility of cytochrome *c* binding in an unproductive conformation to inhibit binding (right)

Appendix II

Derivation of equations

Michaelis-Menten kinetics

Equation 1 shows the basis of simple Michaelis-Menten kinetics. E is the enzyme, S the substrate, P the product, and ES the complex produced between enzyme and substrate binding together. The equation relies on a number of assumptions; that the substrate binding is rapid and reversible, that k_2 is slow and rate-determining, and that investigations are restricted to the initial period of the reaction [134].

$$E + S \underset{k_{-1}}{\overset{k_1}{\rightleftharpoons}} ES \xrightarrow{k_2} E + P \qquad \textbf{Equation 1}$$

Based upon these assumptions, equation 2 is obtained, where v is equal to the overall rate, $[E_0]$ is the total concentration of the enzyme and [S] is the concentration of free substrate. K_S is the dissociation constant of ES and is defined in equation 3.

$$v = \frac{k_2[E_0][S]}{[S] + K_S} \qquad \textbf{Equation 2} \qquad K_S = \frac{[E][S]}{[ES]} \qquad \textbf{Equation 3}$$

When the substrate concentration is very high, the entire enzyme is present as the enzyme-substrate complex and the limiting velocity V_{max} is reached. Under these conditions, equations 4 and 5 are applied.

$$v = \frac{V_{max}[S]}{[S] + K_S} \qquad \textbf{Equation 4} \qquad V_{max} = k_2[E_0] \qquad \textbf{Equation 5}$$

Defining the Michaelis constant, K_m, as the value of [S] that gives an initial velocity equal to half of the maximal velocity, the equation can be simplified further to equation 6. In limiting cases, the Michaelis constant is a measurement of how well the substrate binds to the enzyme. The equilibrium assumption is regarded as being a special case of the more general steady-state assumption, where k_1 is much greater than k_2.

$$v = \frac{V_{max}[S]}{[S] + K_m} \qquad \textbf{Equation 6}$$

A Michaelis-Menten plot is obtained by determining the first-order rate constants at a range of substrate concentrations. Fitting these data to equation 6 produces the Michaelis parameters k_{cat}, and K_m. The maximal rate of reaction under saturating conditions, k_{cat}, is the same as k_2 in equation 1 and is determined by extrapolation. The catalytic efficient of the enzyme is a second-order rate constant and defined in this case as k_{cat}/K_m.

Inhibition kinetics

The effect of an inhibitor, I, on the enzymatic reaction is shown in Equation 7. ESI is a dead-end complex formed when the inhibitor binds to the ES complex. K_i is the inhibitor constant and is defined in equation 8.

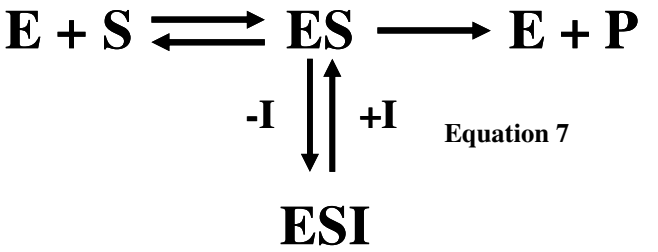

Equation 7

$$K_i = \frac{[ES][I]}{[ESI]} \qquad \textbf{Equation 8}$$

Arranging these in the same manner as equation 4 gives equation 9, for general uncompetitive inhibition. If the substrate is identical to the inhibitor then equation 10 is attained.

$$v = \frac{V_{max}[S]}{[S]\left(\frac{1 + [I]}{K_i}\right) + K_m} \quad \text{Equation 9}$$

$$v = \frac{V_{max}[S]}{[S]\left(\frac{1 + [S]}{K_i}\right) + K_m} \quad \text{Equation 10}$$

In the case of more severe inhibition, where the inhibitor binds to the enzyme only, equation 11 can be utilised. This is based on the Michaelis-Menten assumption, equation 6, where V_{min} is the velocity reached when all of the enzyme molecules are bound to the inhibitor.

$$v = V_{max} - \left(\frac{V_{min}[S]}{K_i + [S]}\right) \quad \text{Equation 11}$$

Debye-Huckel theory

The activity of an ion in solution can be determined by means of the concentration and the activity coefficient, γ. The activity of a species A, Act_A, is shown in Equation 12, where it is equal to the concentration of species A multiplied by the activity coefficient.

$$Act_A = [A]\gamma \quad \text{Equation 12}$$

The Debye-Huckel equation enables the determination of the activity coefficient of an ion in an aqueous solution of known ionic strength according to equation 13, where A is a temperature- and solvent- dependent constant, z_i is the integer charge of the ion and I is the ionic strength of the aqueous solution.

$$\log \gamma = -Az_i^2\sqrt{I} \quad \textbf{Equation 13}$$

By combining equation 13 with the Bronsted relation, equation 14 represents the Debye-Bronsted equation. k_2 is the second order rate constant and k_0 is the second order rate constant at I=0. A plot of log k_2 vs. $\sqrt{I}$ generates a straight line allowing the calculation of the charges involved in the reaction between two species.

$$\log k_2 = \log k_0 + 2Az_+z_-\sqrt{I} \quad \textbf{Equation 14}$$

Appendix III
Meetings attended

Gordon Research Conference (GRC) on Nitric oxide

22-27 May 2005, Il Cioco, Barga, Italy – poster presented

5th, 6th and 7th UK NO Forums

December 2004, Edinburgh – attendee

December 2005, London – poster presented

December 2006, Hatfield – oral presentation given

Biological and Biophysical section meeting, Firbush point field centre, Perthshire

April 2005 – attendee

April 2006 – poster presented

April 2007 – oral presentation given, awarded joint 1st in the section

9th and 10th Redox enzymes meeting, Firbush point field centre, Perthshire

June 2005 – attendee

June 2006 – attendee